Investigation of Inelastic Reactions in Deuteron Proton Collisions Between $T_d = 437$ and 559 MeV Using the PROMICE/WASA Detector at CELSIUS.

DISSERTATION

zur Erlangung des Doktorgrades
des Fachbereichs Physik
der Universität Hamburg

vorgelegt von

Jan Greiff
aus Hamburg

Hamburg 1999

Gutachter der Dissertation: Prof. Dr. W. Scobel
Prof. Dr. D. Vogt

Gutachter der Disputation: Prof. Dr. W. Scobel
Prof. Dr. K. Wick

Datum der Disputation: 16.09.1999

Dekan des Fachbereichs Physik und
Vorsitzender des Promotionsausschusses: Prof. Dr. F.-W. Büßer

Abstract

This work describes an experiment and its analysis aiming at a decomposition of contributions from different production mechanisms for $dp \to dN\pi$ reactions within the energy region of $T_d = 437 - 559\,\mathrm{MeV}$ (in terms of maximum pion momenta: $0.32 < \eta = p_{\pi,max}^{c.m.}/m_\pi c < 0.86$).

The experiment has been performed at the CELSIUS storage ring in Uppsala (Sweden) using the PROMICE/WASA detector setup, with its ability to detect and reconstruct charged particles under forward angles and γ's from e.g. π^o decays with a central calorimeter. Particles, which have not been detected have been reconstructed via missing mass.

The application of a (cooled) deuteron beam in conjunction with an internal H_2 cluster-jet target allowed to study regions of phase space where quasi-free $pN \to d\pi$ production mechanisms, as predicted by [MN 93], become visible.

This was of particular importance, since recently precise measurements on the reaction $pd \to pd\pi^o$ have been published for the first time in the near threshold region of $T_p = 208.4 - 294.6\,\mathrm{MeV}$ $(0.10 < \eta < 0.96)$ [Roh 94]. The results of [Roh 94] were indicating production mechanisms with all nucleons participating in the interaction, contradicting the predictions of [MN 93].

The results given in this thesis confirm the assumption of three nucleon mechanisms in [Roh 94] at lower energies close to the three nucleon threshold. On the other hand they show also a dominance for an underlying quasifree $pN \to d\pi$-process at the higher energies close to the two nucleon threshold. As a consequence the cross sections given in this work differ at the higher energies from those in [Roh 94], which is understood in terms of a different coverage of phase space.

In addition to the examination of the $dp \to dN\pi$ channels it has been possible to extract data for the four body channel $dp \to ppp\pi^-$.

For the 'Bremsstrahlungs'-reaction $dp \to dp\gamma$ data sets will be shown, which have never been measured before within this energy region. The analysis for $dp \to dp\gamma$ showed again contributions from quasi-free $np \to d\gamma$ but similar to the pion production process models have to be included, where all three nucleons participate in the production mechanism.

Zusammenfassung

Im Rahmen dieser Arbeit wird ein Experiment beschrieben, welches darauf abzielte, die Anteile unterschiedlicher Pion-Produktionsmechanismen in $dp \to dN\pi$ Reaktionen im Energiebereich von $T_d = 437 - 559\,\mathrm{MeV}$ zu untersuchen. Der Energiebereich entspricht maximalen Pionimpulsen von $0.32 < \eta = p_{\pi,max}^{c.m.}/m_\pi c < 0.86$ im Schwerpunktsystem.

Das Experiment wurde unter Verwendung des PROMICE/WASA Detektors am CELSIUS Speicherring in Uppsala (Schweden) durchgeführt. Es machte von den besonderen Fähigkeiten des Detektors Gebrauch, geladene Teilchen unter Vorwärtswinkeln zu detektieren. Der Detektor lieferte Energien, Energieverluste und Winkel der auftreffenden Teilchen. Nicht beobachtete Teilchen wurden über die 'missing mass' identifiziert. γ's, die zum Beispiel beim Zerfall des neutralen π^o entstehen, konnten zusätzlich mit einem Zentralkalorimeter bestimmt werden.

Die Anwendung eines gekühlten Deuteronen-Strahls in Verbindung mit einem internen H_2 Cluster-Jet-Target erlaubte Regionen des Phasenraumes zu studieren, in denen quasifreie $pN \to d\pi$ Produktionsmechanismen, wie sie von [MN 93] vorhergesagt wurden, sichtbar werden.

Dies war von besonderer Relevanz vor dem Hintergrund, daß zuvor genaue Messungen der $pd \to pd\pi^o$ Reaktion im Bereich nahe der Schwelle, d.h. in der Energieregion von $T_p = 208.4 - 294.6\,\mathrm{MeV}$ $(0.10 < \eta < 0.96)$ [Roh 94] veröffentlicht wurden. Die Ergebnisse dieser Messungen deuteten auf andere Produktionsmechanismen hin, welche die Teilnahme aller drei Nukleonen am Reaktionsmechanismus implizit voraussetzten und den quasifreien Annahmen von [MN 93] widersprachen.

Die Ergebnisse dieser Arbeit bestätigen die Annahme solcher Drei-Nukleon-Prozesse bei niedrigen Energien, d.h. nahe der Drei Nukleon Schwelle, aber sie zeigen auch eine zunehmende Dominanz des quasifreien $pN \to d\pi$ Prozesses bei höheren Energien nahe der Zwei Nukleon Schwelle. Dies hat zur Konsequenz, daß bei höheren Energien die gemessenen totalen Wirkungsquerschnitte von denen in [Roh 94] abweichen, zumal in beiden Experimenten verschiedene Bereiche des Phasenraumes abgedeckt wurden.

Zusätzlich zu den $dp \to dN\pi$ Reaktionen war es im Rahmen dieser Arbeit auch möglich, für den Vierteilchenkanal $dp \to ppp\pi^-$ Daten zu extrahieren.

Für die 'Bremsstrahlungs'-Reaktion $dp \to dp\gamma$ werden ebenfalls Daten gezeigt, die nie zuvor in diesem Energiebereich gemessen wurden. Die Analyse der $dp \to dp\gamma$-Daten zeigte ebenfalls deutliche Beiträge eines quasifreien $np \to d\gamma$ Prozesses. Ähnlich wie bei der Pion-Produktion müssen aber auch Modelle zur Beschreibung der Daten hinzugezogen werden, die die Teilnahme aller drei Nukleonen am Reaktionsprozeß voraussetzen.

Contents

List of Figures

List of Tables

Chapter 1

Introduction

Since 1935 when Yukawa [Yuk 35] suggested that particles with intermediate masses (compared to electrons and protons) could be responsible for the interaction between neutrons and protons, mesons have become *the* exchange quantums for the strong interactions, somehow in analogy to the role, which photons play in quantum electrodynamics. However, the understanding and the description of the strong nuclear interaction turned out to be more difficult than it was e.g. for the electromagnetic interaction. Now, more than fifty years after the discovery of the pion [Occ 47], there is still need for good experimental data to improve the understanding of these elementary forces.

The production of *real* mesons requires a high momentum transfer and it is therefore suited to probe the nucleon nucleon interaction at small distances. As a result the production of mesons in nucleon nucleon and nucleon nucleus collisions in intermediate energies has attracted much attention during the past decades. The data base on meson production in nucleon nucleon collisions has improved significantly, especially for pions, the lightest members in the meson family. The availability of a new generation of accelerator storage rings with 'cooled' particle beams, which is equivalent to a small momentum spread of the beam, now allows to study these reactions very close to the production threshold.

At these energies the theoretical treatment is easier, because the spectrum of accessible angular momentum states is limited and therefore only a few partial waves contribute. On the other hand the experiments are the more difficult the closer one gets to the threshold. One has to deal with very small cross sections, with larger relative uncertainties for the excess energies and with particles, which are emitted under small angles in the laboratory frame, where internal experiments have difficulties to detect them.

While the pion production in $NN \rightarrow NN\pi$ reactions, especially in proton-proton collisions, has been a focus of research, the pion production within the three nucleon system has not been of central interest. This changes now however for two reasons.

- First of all progress in the nucleon nucleon pion production requires also to increase the quality of the data on neutron induced reactions. The use of neutron beams has the disadvantage of relatively poor intensity and energy resolution, which prevents to look at the near threshold regions and free neutron targets do not exist. The use of deuterium as a target, however may solve this problem.

- The second point of interest is to examine the effects of a multinuclear environment on the pion production process and the three nucleon system with a deuteron in the initial state is the easiest one to understand, since the properties of the deuteron are known with a good accuracy.

These two points above are strongly related and any progress on one of them might influence the other especially in the near threshold regions.

It is the main aim of the experiment described in this thesis to improve the understanding of the pion production process in deuteron-proton collisions, with a special focus on $dp \rightarrow dp\pi^o$ within the deuteron kinetic energy range of 437 to 559 MeV.

The first and up to this work only attempt to examine this reaction within the near threshold region has been performed in 1991 at the IUCF cooler ring in Indiana [Roh 93],[Roh 94]. It yielded excellent results very close to threshold, but suffered from a limited acceptance at energies of more than 30 MeV above threshold (i.e. $\eta > 0.5$, compare equation 1.1). Therefore it was not possible to give reliable results concerning absolute cross sections and the fractions of the competing reaction mechanisms. For the energy region of $\eta > 0.5$ significant contributions from a pure $pn \rightarrow d\pi^o$ process have been predicted according to the only detailed calculations, which have been published so far for this reaction and energy region [MN 93].

This thesis therefore focuses on closing the gap between the experimental data in [Roh 94] and the theoretical predictions in [MN 93] and it is therefore quite natural, that these two works will be referred to frequently throughout the next 120 pages.

The following sections of this chapter will summarize the present experimental situation and the theoretical understanding of single pion production. After a short overview on nucleon nucleon single pion production the three nucleon system will be reviewed and a more detailed summary of [Roh 94] and [MN 93] will be given.

1.1 Pion Production in the 2-Nucleon System

Pion production in nucleon nucleon collisions has been a field of interest in nuclear physics for some decades now. The precise knowledge of the reaction cross sections for NN single pion production is an indispensable input for the understanding of NN interactions above the pion production threshold.

A list of the possible single pion production channels is given in table 1.1 together with their threshold beam energies. It is common to use the isospin invariance in strong interactions to reduce the ten reaction cross sections to the four independent cross sections σ_{11},σ_{10}^{d},σ_{10}^{np} and σ_{01}, where the indices i, f in σ_{if} denote the initial and final state isospins of the nucleons, respectively. The four cross sections can then be added incoherently to reproduce the observable $NN\pi$ cross sections ([Ros 54],[Ver 82]). It has to be noted, that the Coulomb interaction and the difference in the particle masses have an isospin breaking effect, which is however usually below the accuracy of the experimental data. Its most obvious effect is seen in the different threshold energies $E_{thr.}$.

Therefore in view of a comparison of the cross sections, the laboratory beam energy is not well suited as a parameter, especially in the near threshold region. Instead the cross sections are more conveniently plotted as a function of the maximum pion momentum in the center of mass system. The universal threshold parameter η is therefore, with c set equal to 1, defined as

$$\eta = \frac{p^{\pi}_{c.m.max.}}{m_{\pi}} \tag{1.1}$$

A second approach to express the energy dependence of cross sections is to parameterize it as a function of the excess energy Q in the center of mass system.

channel	$T_{N,thr.}$ [MeV]	
$pp \rightarrow d\pi^+$	287.52	$\sigma_{10}(d)$
$pp \rightarrow pp\pi^o$	279.66	σ_{11}
$pp \rightarrow pn\pi^+$	287.52	$\sigma_{10}(np) + \sigma_{11}$
$pn \rightarrow d\pi^o$	274.69	$\frac{1}{2}\sigma_{10}(d)$
$pn \rightarrow pp\pi^-$	286.53	$\frac{1}{2}(\sigma_{11} + \sigma_{01})$
$pn \rightarrow pn\pi^o$	279.72	$\frac{1}{2}(\sigma_{10}(np) + \sigma_{01})$
$pn \rightarrow nn\pi^+$	292.64	$\frac{1}{2}(\sigma_{11} + \sigma_{01})$
$nn \rightarrow d\pi^-$	281.95	$\sigma_{10}(d)$
$nn \rightarrow nn\pi^o$	279.64	σ_{11}
$nn \rightarrow np\pi^-$	286.72	$\sigma_{10}(np) + \sigma_{11}$

Table 1.1: *Single pion production channels in NN interactions and the threshold beam energies. Throughout this work the notation* $N_1N_2 \rightarrow X$ *defines a reaction in the* N_2 *rest frame, where* N_1 *is always the beam nucleon (either proton p or neutron n) and* N_2 *is defined as the target nucleon, if not explicitly stated otherwise.*

Figure 1.1: *The* $NN \rightarrow NN\pi$ *cross sections for projectile energies* T_N *below 1.5GeV [Ver 82].*

$$Q_{c.m.} = \sqrt{s} - \sum_i m_i, \tag{1.2}$$

where $\sqrt{s}$ is the total invariant mass and m_i denotes the mass of the ith outgoing particle. η is then proportional to $\sqrt{Q_{c.m.}}$. Following [MN 93] η will be used throughout this thesis. The energy region $\eta < 1$ is usually defined as the near threshold region.

1.1.1 The Experimental Situation

The progress in the understanding of the meson production has always been connected to the development of both accelerator and detector technique. Early experiments with bubble chambers and low intensity beams revealed already the typical features of the reactions. The use of new target systems, progress in detector development (like e.g. the application of high resolution drift chambers, scintillator calorimeters, time of flight measurements etc.) and last but not least the availability of particle beams with increased maximum intensities has led to a rapid increase of knowledge on the experimental side. Since the 1970‘s the so called meson factories like TRIUMF[1], LAMPF[2], PSI[3] , or SATURNE[4] have yielded elastic and inelastic NN and πN scattering up to about 1 GeV laboratory energies.

Today the cooler rings at IUCF[5], CELSIUS[6] and COSY[7] with their improved beam qualities allow measurements closer to threshold and in case of the IUCF (and COSY) also the determination of polarization observables at these energies. CELSIUS and COSY also continue on the investigation of heavier meson and multi pion production.

As shown in figure 1.2 the most complete data samples for the single pion production processes exist for the $Np \to d\pi$ channels (e.g. [Hut 91], [Hei 96], [Dro 96]), for $pp \to pp\pi^o$ (e.g. [Mey 92], [Bon 95], [Mey 98]) and for $pp \to pn\pi^+$ (e.g. [Dae 95], [Fla 98], [Har 97]). For $np \to pp\pi^-$ the experimental situation is very poor close to threshold. However [Dun 98] have recently published three differential cross sections and in the near future also results closer to threshold can be expected from CELSIUS, giving hopefully access to the σ_{01} partial cross section. Recently also progress has been made in the study of polarization observables, which is necessary to clearly distinguish higher partial waves at higher energies (e.g. [Mey 98c]).

1.1.2 The Theoretical Situation

The theoretical description of pion production processes in nucleon nucleon processes has always been connected to the availability of experimental data and therefore most publications were referring to the $pp \to pp\pi^o$, $pp \to d\pi^+$ or $pp \to pn\pi^+$ channels.

In the past the pion production process was mainly considered a process, where the pion is produced by either nucleon and emitted directly or rescattered by the second nucleon (e.g. [Kol 66]) (figure 1.3 a,b). In the early 90‘s the production process was reviewed when precise measurements of the total $pp \to pp\pi^o$ cross section close to threshold [Mey 90] showed, that

---

[1] Vancouver, Canada

[2] Los Alamos, USA

[3] Villigen, Switzerland

[4] Saclay, France

[5] Bloomington, USA

[6] The Svedberg Laboratory, Uppsala, Sweden

[7] Jülich, Germany

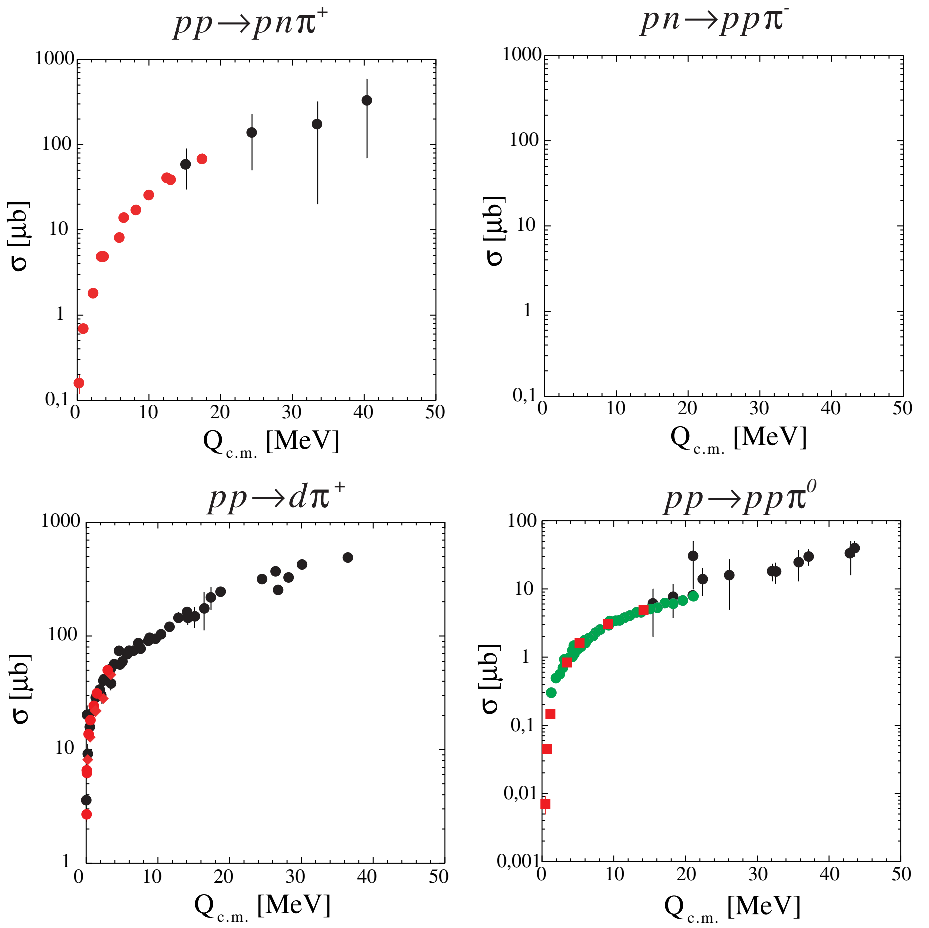

Figure 1.2: *The Experimental situation for some of the pion production channels in nucleon nucleon interaction in the near threshold region [Joha 99].*

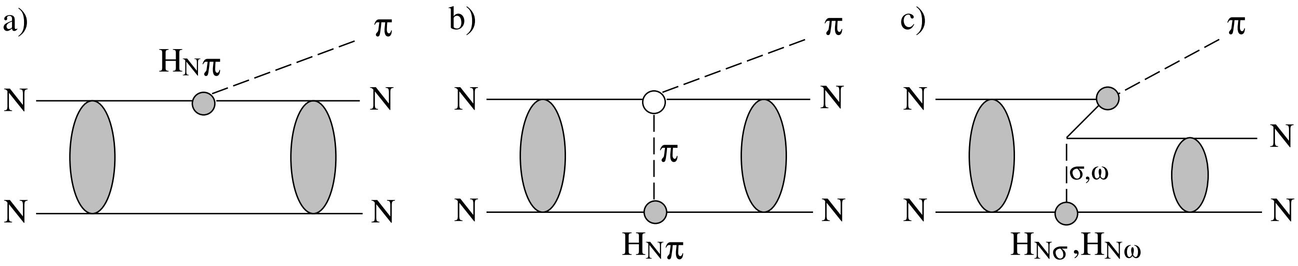

Figure 1.3: *Some diagrams for the $NN \to NN\pi$ production mechanisms proposed from theory: (a) direct production, (b) pion production with pion rescattering on the second nucleon; (c) pion production via heavy meson exchange (HME). The ellipses indicate initial and final state interactions.*

the theory failed to describe the magnitude of the cross section by about a factor of 5 (e.g. [Mil 91], [Nis 92]).

Since then different models have been developed, which try to reproduce the total cross sections.

The first one assumes, that a short range heavy meson exchange (HME) is responsible for the higher cross sections (e.g. [Lee 93], [Hor 94]). This additional, relativistic mechanism is represented by a so called z-graph, where the exchanged heavy meson couples to a proton-antiproton pair. The virtual antiproton combines then with the incident proton at the pion vertex (figure 1.3c).

A second approach, which includes off-shell πN-rescattering (e.g. [Her 95](without HME), [Han 95](with HME)), is also able to solve the previous discrepancy in the cross section magnitude.

Additional investigations using Chiral Perturbation Theory are also under way (e.g. [Coh 96], [Par 96], [Sat 97]), but the present calculations still underestimate the data by large factors.

In addition to the models described above the strong influence of the Δ-resonance has to be taken into account. It is clearly visible in the σ_{10} and σ_{11} cross sections at energies, where pion-p-wave contributions come into play. Nevertheless its influence is also discussed for s-wave pions close to threshold. If these pions are produced from a Δ-decay into a p-wave πN system and the pion suffers an s-wave rescattering on the second nucleon, this might affect also the s-wave pion production (e.g. [Nis 95], [Han 98]).

All these models have improved the theoretical description of the experimental data, but the discussions about the nature of the pion production process have not been settled up to now.

A recent review about the experimental and theoretical situation can also be found in [Mey 98b].

1.2 Pion Production in the Proton Deuteron System

The pion production in collisions between the proton and the deuteron is experimentally very similar to the NN case. However, the threshold energies for meson production are much lower than for the two nucleon case, because the additional nucleon is in principle able to participate in the momentum transfer.

In addition to the two and three body final states, which can also be found in NN collisions, the proton deuteron system allows also four body final states. In total seven different reaction channels with single pion production can be expected, which are listed in table 1.2.

1.2.1 The Experimental Situation

First experiments looking at the pion production in collisions between a beam-proton and a target-deuteron have been already published in the 1950‘s. [Hal 53] have performed a first measurement to extract relative cross sections for π^o production in proton nucleus collisions at a proton beam energy of 340 MeV. They have detected only one γ, which was expected to originate from the π^o decay.

[Pro 57] and [Dun 60] have tried to extract the $pn \rightarrow X\pi^o$ total cross sections from two inclusive measurements of $pp \rightarrow X\pi^o$ and $pd \rightarrow X\pi^o$ also by detecting only the γ‘s.

In 1974 [Bab 74] have performed a bubble chamber experiment, where they found 77 events of $pd \rightarrow pd\pi^o$ and 113 events of $pd \rightarrow nd\pi^+$ at a proton-beam energy of 1.1 GeV .

channel	$T_{p,thr.}$ [MeV]	$T_{d,thr.}$ [MeV]
$dp \to {}^3\mathrm{He}\pi^0$	198.7	397.1
$dp \to {}^3\mathrm{H}\pi^+$	206.8	413.4
$dp \to dp\pi^0$	207.4	414.5
$dp \to ppn\pi^0$	210.9	421.5
$dp \to ppp\pi^-$	216.1	431.9
$dp \to dn\pi^+$	216.6	433.0
$dp \to pnn\pi^+$	220.1	440.0
$dp \to {}^3\mathrm{He}\gamma$	0.0	0.0
$dp \to dp\gamma$	0.0	0.0
$dp \to ppn$	3.3	6.7
$dp \to ppn\gamma$	3.3	6.7

Table 1.2: *Single pion production channels in dp interactions and the threshold beam energies for proton and deuteron beams. The other inelastic channels are also given.*

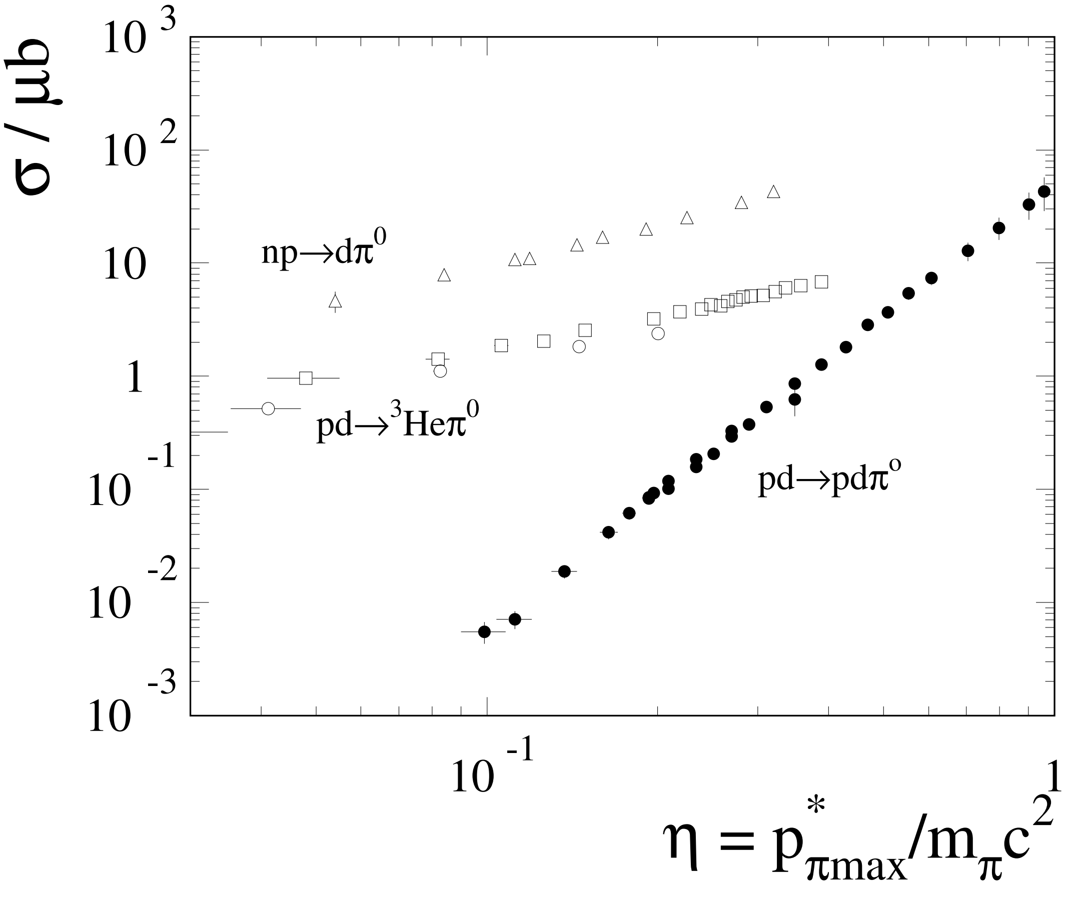

Figure 1.4: *The experimental situation for the pion production channels in proton deuteron interaction close to threshold ($\eta < 1$). Total cross sections exist for $pd \to {}^3\mathrm{He}\pi^0$ (○[Pic 92]; □[Nik96]) and for $pd \to pd\pi^o$ (● [Roh 94]). The $np \to d\pi^o$ cross section (△[Hut 91]) is also shown for later comparison with $pd \to pd\pi^o$.*

Since the late seventies the number and quality of pd experiments has then improved and the following review is given with respect to the different final states.

Two Body Final States

Among the two body final states the $pd \to {}^3\mathrm{H}\pi^+$ reaction has only been examined to measure the branching ratio compared to $pd \to {}^3\mathrm{He}\pi^0$ ([Cre 60],[Har 60],[Sil 85]). For $nd \to {}^3\mathrm{He}\pi^-$ there exists only one measurement of differential cross sections between 400 and 580 MeV [Fra 80].

However, the largest fraction of the available data has been acquired for the two body final state $pd \to {}^3\mathrm{He}\pi^0$. Some differential cross sections and analyzing powers have been published at energies in the Δ-region between 300 and 800 MeV ($\eta > 1$) ([Car 78], [Low81], [Sil 85], [Cam 87], [Bou 88]). [Bou 88] has shown the only measurement of this reaction using a deuteron beam.

The most complete data sample for $pd \to {}^3\mathrm{He}\pi^0$ in the near threshold region ($\eta < 1$) has recently been published by [Nik96], but it shows a small discrepancy to a previous measurement [Pic 92]. These data points are also shown in figure 1.4.

Three Body Final States

For the three body final state $dn\pi^+$ there exist only two published measurements from LAMPF. [Hog 78] have given fivefold differential cross sections at 585 MeV using a coplanar two arm spectrometer and a similar setup has been used for a second measurement at 800 MeV [Lo79]. While [Duc 78] include different production mechanisms with single and double scattering amplitudes to describe the 585 MeV data, [Lo79] claim, that the reaction basically proceeds through a quasifree process $pp \to d\pi^+$.

For the reaction $pd \to pd\pi^o$ there exists a fifth order differential cross section at $T_p = 585\,\mathrm{MeV}$ [Hog 77]. However, the main reference for this channel is an IUCF measurement [Roh 94] (see also figure 1.4), which provides total $pd \to pd\pi^o$-cross sections from threshold up to 295 MeV. It will be described in more detail on the next pages.

Four Body Final States

The only four body reaction for which data has been published is $pd \to ppp\pi^-$. [Dak 82] have performed a bubble chamber experiment in the energy region of 500 to 1000 MeV to extract also the $pn \to pp\pi^-$ cross sections and to look for possible dibaryonic resonances. [Pon 89] have measured analyzing powers at a beam energy of 400 MeV and recently [Dun 98] have published three differential cross sections at 353, 403 and 440 MeV .

To summarize the experimental situation one can say, that only for $pd \to {}^3\mathrm{He}\pi^0$ and $pd \to pd\pi^o$ good data samples in the near threshold region exist.

1.3 Motivation for this Experiment

A previous Experimental Setup to measure $pd \to pd\pi^o$

In 1991 a precise measurement of the reaction $pd \to pd\pi^o$ has been performed at the Cooler Ring of the Indiana University Cyclotron Facility (IUCF) ([Roh 93],[Roh 94]), aiming to measure total cross sections in the near threshold region of $\eta < 0.5$.

The experiment has used an electron-cooled proton beam and an internal windowless deuterium gas-jet target. The detector setup was able to identify the charged particles and measure their energy, time-of-flight and angle, if emitted into a forward cone at angles between 2^o and 11^o or 4^o and 19^o, depending on the alignment of the detector. Protons with kinetic energies between 18 and 120 MeV and deuterons between 25 and 160 MeV have been stopped in a forward calorimeter. The lower energy limit for the particle detection was caused by dead material in front of the calorimeter. The π^o has then been reconstructed by the missing mass of the kinematically complete proton and deuteron.

Close to threshold the experiment covered up to 65 percent of the available phase space. However, at larger energies ($0.5 < \eta < 1.0$) the limited angular range of the forward detector caused a rapidly decreasing acceptance. In addition the low energy limit for particle-detection generated difficulties in the description of the reaction mechanism. It made the experiment quite insensitive to pd-reactions whenever the production mechanism is mainly based upon a *quasi-free* pn-reaction. This is important to notice, because at beam energies far above the threshold ($\eta > 0.85$) the initial proton within the deuteron can be emitted isotropically with small energies according to the target deuteron wave function and has therefore in most cases not been detected.

Since the detector did not cover the whole phase space, the subsequent analysis of the data and the determination of the total cross sections turned out to be sensitive to the models, which have been used to describe the population of all final states in phase space.

Similar to previous treatments of e.g. $NN \to NN\pi$ reactions [Roh 94] assumed, that the distributions of the outgoing particles can be parameterized in terms of a partial wave expansion. This approach separates the final state wave function into two independent angular momentum states Ll, where L is the angular momentum in the pd-subsystem and l that of the π^o with respect to the pd-pair. A fit of the experimentally obtained angular and energy distributions showed, that close to threshold only the lowest partial wave combination Ss (L=0,l=0) contributes, whereas at higher energies also higher angular momentum states up to Pd (L=1,l=2) had to be included to describe the data. This was not very surprising, since a similar behavior was also found for the nucleon nucleon reactions.

A more detailed description of these parameterizations is later on given in section 4.3. Here it is sufficient to note, that this phenomenological approach somehow treats the deuteron as a fundamental particle, similar to e.g. the protons in the reaction $pp \to pp\pi^o$ and that it does not explicitly take into account its composition of a weakly bound proton and neutron.

A different approach to treat the deuteron only as a quasifree two nucleon target has also been suggested as described now.

The Quasifree Reaction Model for $pd \to pd\pi^o$

Meyer and Niskanen [MN 93] have evaluated the total cross section for pion production in the reaction $pd \to pd\pi^o$ under the assumption that it is entirely due to the quasi-free elementary $pn \to d\pi^o$-process, where the initial beam-proton interacts with the neutron of the initial target-

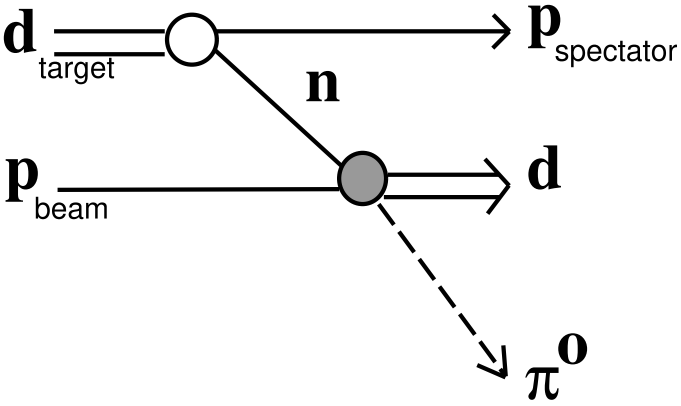

Figure 1.5: *The spectator model from [MN 93]. The two vertices denote the deuteron wave function (white) and the free* $np \to d\pi^o$ *reaction (grey).*

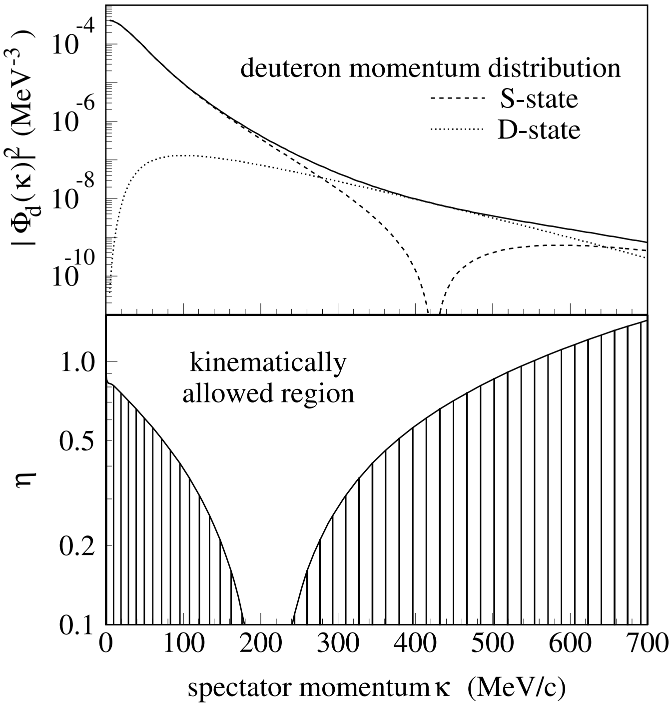

Figure 1.6: *The square of the deuteron wave function in momentum space as a function of the spectator momentum (top). The region, which can contribute to a quasi-free* $dp \to dN\pi$ *production is shown as a function of* η *(bottom). Its upper limit is given by energy and momentum conservation within the overall system and its lower limit is given by the minimum invariant mass within the two nucleon system* $pN \to d\pi$ *[Roh 94]. The energy at which the pion production with zero spectator momentum becomes possible is sometimes referred to as the* two-nucleon threshold *or* quasifree threshold

deuteron and forms the outgoing deuteron and the pion. The proton within the initial deuteron acts only as a spectator and does not participate in the production process.

Their *spectator model* will be described in more detail in section 4.3; it needs mainly two ingredients. The first ingredient is the nucleon momentum distribution within the deuteron, obtained through a Fourier decomposition of the deuteron wave function, and the second is the free $pn \rightarrow d\pi^o$ cross section. It has been parameterized based upon experimental results from [Hut 91] for the near threshold region.

According to their model the total cross sections for $pd \rightarrow pd\pi^o$ can be predicted. For values of $\eta > 1$ they approach the input cross sections for $pn \rightarrow d\pi^o$ but they should be strongly suppressed close to the threshold. This suppression is due to the limited range of momenta within the deuteron, being accessible for the pion production process (compare figure 1.6). At threshold all particles move with the same velocity in the forward direction, yielding a spectator momentum of $\approx 200\,\mathrm{MeV}/c$. At this value the momentum density distribution Φ_d^2 in the deuteron is a factor 10^3 lower than for a nucleon at rest and this should reduce the cross section as compared to $pn \rightarrow d\pi^o$ accordingly.

Theory versus Experiment

Indeed are the total cross sections in [Roh 94] orders of magnitude below the ones for $pn \rightarrow d\pi^o$, but nevertheless they are by a factor of up to five larger than the predictions from [MN 93] according to their model (compare figure 1.7).

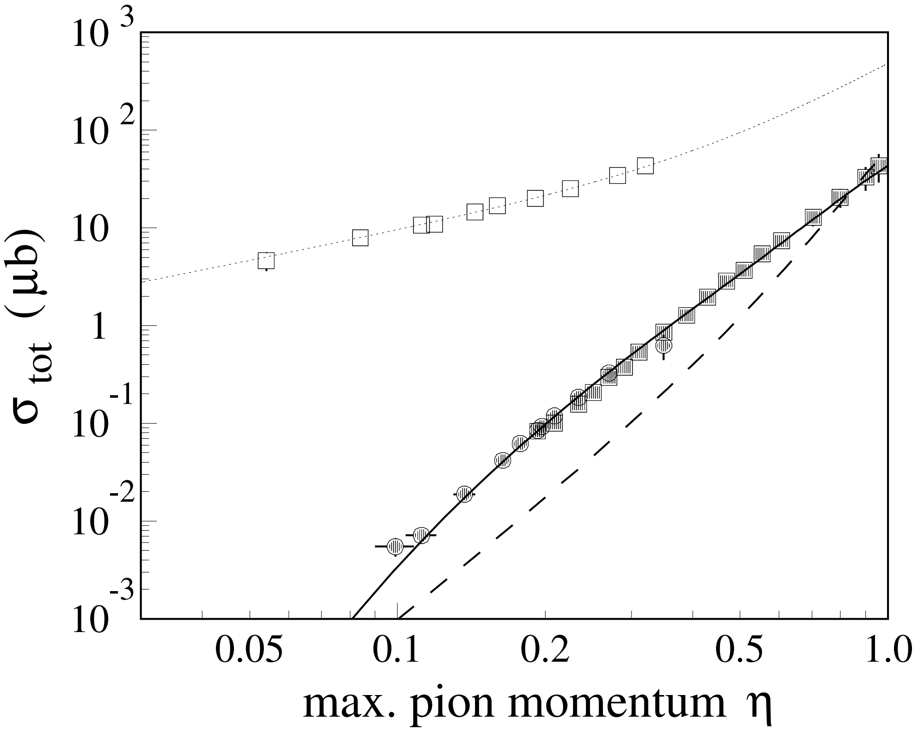

Figure 1.7: *The total cross sections for $pd \rightarrow pd\pi^o$(filled symbols) obtained from [Roh 94] in comparison to predictions from [MN 93]. The dashed line shows the calculation based upon the quasifree model without inclusion of pd-final state interaction. The solid line illustrates the energy dependence with the final state interaction included, but with an arbitrary normalization to the experimental data. The open symbols show the $pn \rightarrow d\pi^o$ cross sections and their parameterization (dotted), which has been included into the quasifree model calculation.*

This discrepancy can be due to (*i*) contributions of other, more complicated production mechanisms, where all nucleons are involved, or to (*ii*) the effects of the final state interaction (FSI) between the proton and the deuteron in the exit channel.

The analysis in [Roh 94] succeeded to describe the angular and energy distributions of the outgoing protons and deuterons using only the partial wave expansion if Ss,Ps,Pp and Pd partial waves are included, but *without* contributions from the quasi-free process.

[MN 93] claimed, that all discrepancies are solved, if the final state interaction (FSI) is properly taken into account. Indeed did the introduction of a significant final state interaction describe the relative energy dependence of the total cross section quite well, because it had an increasing effect closer to threshold, where all outgoing particles have small relative momenta with respect to each other. However, it is then also of arbitrary normalization and looses its predictive power for the absolute magnitude of the cross sections. In addition it failed completely in the description of the energy distributions of the outgoing protons and deuterons, both with and without inclusion of FSI, which indicated that the assumption of a pure quasifree mechanism was wrong.

On the other hand showed the simultaneous measurement of the reaction $pd \to nd\pi^+$, which is expected to be related to $pd \to pd\pi^o$ by isospin-invariance, at the higher energies the typical features of an underlying quasifree $pp \to d\pi^+$-process as predicted by [MN 93], supporting their theory.

This discrepancy may have been caused by the limited detector acceptance and this can be best illustrated by showing the Dalitz-plots given in [Roh 94] (figure 1.8). In the first line the Monte Carlo (MC) simulated acceptance in phase space is demonstrated, if the detector acceptance is included in the analysis. Assuming the quasifree model from [MN 93], as shown in the second line, the acceptance for $pd \to pd\pi^o$ is only good within a region of phase space which is *not* favored by this production mechanism. The acceptance for $pd \to nd\pi^+$ samples a complementary region of phase space, where the quasifree model is significant and indeed the experimental data at the bottom seem to support the assumption of this process. The third line shows the assumed partial wave parameterization, which has been obtained by a best fit to the experimental distributions for $pd \to pd\pi^o$. For this model the acceptance for $pd \to pd\pi^o$ and $pd \to nd\pi^+$ is opposite to that for the quasifree model: The acceptance for $pd \to pd\pi^o$ is considerably higher, but for $pd \to nd\pi^+$ it has decreased significantly.

It must be suspected, that under these experimental conditions it was quite difficult to extract good results concerning the cross sections and the production mechanisms of $pd \to Nd\pi$ reactions. As a consequence [Roh 94] concluded after a detailed discussion of the acceptance problems, that the Indiana experiment yielded reliable total cross sections in the region $0.1 < \eta < 0.5$, for which it was designed, but for $\eta > 0.5$ the systematical uncertainties due to the limited detector acceptance were substantial.

For $0.1 < \eta < 0.5$ the quasifree model from [MN 93] was not needed to describe the experimental data and it failed to describe the magnitude of the cross sections. Above $\eta = 0.5$ the experimental data did not allow to quantify quasifree $pn \to d\pi^o$ contributions within the $pd \to pd\pi^o$ mechanisms.

As a result a supplementary measurement was suggested, which should cover a much larger acceptance in phase space within the energy range of $0.5 < \eta < 1.0$. This experiment should then be able to distinguish between pure quasifree $pn \to d\pi^o$ reactions and other mechanisms where all nucleons participate in the pion production mechanism.

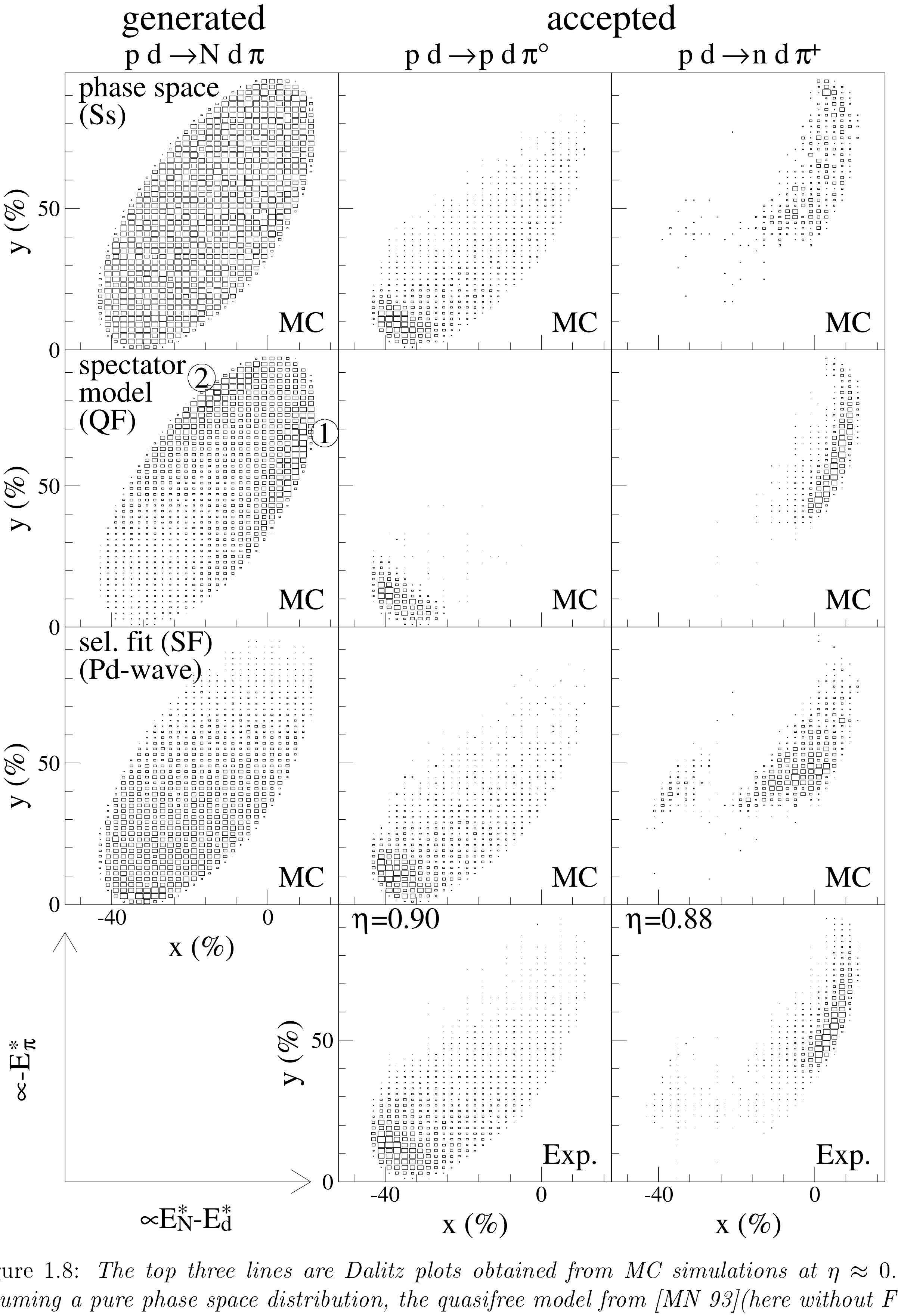

Figure 1.8: *The top three lines are Dalitz plots obtained from MC simulations at $\eta \approx 0.89$, assuming a pure phase space distribution, the quasifree model from [MN 93](here without FSI) and the partial wave parameterization used for the description of the data in [Roh 94]. In the center(right) column are the simulated distributions of $pd \rightarrow pd\pi^o$ ($pd \rightarrow nd\pi^+$) events including the IUCF-detector acceptance. The line at the bottom shows the experimental IUCF-data.*

1.4 Requirements to the Experimental Setup

In the previous section it was demonstrated that an experiment to examine $pd \to pd\pi^o$ above $\eta = 0.5$ must be able to detect or reconstruct an assumed spectator proton with a good acceptance. This proton will have a small relative momentum with respect to the neutron of the deuteron and it will be emitted more or less isotropically in the initial deuteron rest frame. To comply with this situation there are three different ways of progress:

- Using a proton beam in connection with a deuteron target, the first idea is of course to extend the detector setup for a direct measurement of the spectator proton with a large acceptance. However, since most of the protons have small energies of only a few MeV, this requires an equipment without dead material in front of the detectors, low energy thresholds and a good energy resolution, which covers a large solid angle. In practice this can only be achieved with silicon detectors placed inside the evacuated target chamber or behind extremely thin windows to reduce the effects of absorption to a minimum. The experimental difficulties of such a setup are substantial.
- The second approach is to abandon the option of a direct detection of the spectator proton. A kinematically complete measurement then has to identify and reconstruct the two γ's from the π^o-decay instead. This requires a massive calorimeter for the detection of the high energetic γ's with large angular coverage. Usually the resolution of such a setup also limits the accuracy to which the spectator proton momentum can be reconstructed.
- Another possibility is to take advantage of *inverse kinematics*. By using a *deuteron beam* in connection with a *hydrogen target* the spectator protons are boosted into a forward cone with approximately half of the deuteron-beam momentum. Although in internal experiments the very forward going protons are lost within the beam pipe, the detection of a larger fraction is possible even with a detector covering only forward angles. Since the protons will then have energies in the order of 100 MeV or more, the effects of dead material like for example target chamber windows in front of the detectors can be tolerated to some extent.

All these experimental setups require the identification and reconstruction of the outgoing deuterons to clearly separate $pd \to pd\pi^o$ from $pd \to ppn\pi^o$.

In 1995 an experiment was proposed at the The Svedberg Laboratory in Uppsala/Sweden, which intended to make use of the unique feature of the CELSIUS facility to accelerate and store deuterons to examine $dp \to dp\pi^o$ using inverse kinematics [Sco 95]. The PROMICE/WASA detector offered the possibility of detecting the outgoing protons and deuterons under forward angles and did also allow to detect some γ's from the π^o decays. This experiment was then performed in 1996 and 1997 and it is the topic of the next chapters.

Chapter 2

The Experimental Setup

2.1 TSL and CELSIUS

The CELSIUS[1] accelerator is located at the The Svedberg Laboratory (TSL) [TSL 95],[TSL 98] in Uppsala[Ada 92]. It is the main swedish national facility for accelerator based research and provides resources for scientists from Sweden and other, mainly european, countries.

An overview of the TSL accelerator facilities is given in figure 2.1. The Gustav Werner Cyclotron (GWC) [Hol 92] is the source for protons, deuterons and heavier ions, which can be injected into the CELSIUS ring [Rei 97], but it provides also beams for a broad program of research projects in physics and biology as well as a proton beam for medical cancer treatment.

Circumference	81.8 m
Maximum kinetic energy	
for protons	1360 MeV
Maximum kinetic energy	
for cooled protons	550 MeV
Maximum kinetic energy	
for ions with Q/A=1/2	470 MeV/A
Relative momentum spread $\Delta p/p$	
without cooling	$2 \cdot 10^{-3}$
with cooling	$2 \cdot 10^{-4}$
typical intensity in CELSIUS	
for protons	$1 \cdot 10^{11}$
for deuterons	$1 \cdot 10^{10}$

Table 2.1: *Some properties of the CELSIUS accelerator ([Rei 97], [Häg 97]).*

A selection of parameters for CELSIUS is given in table 2.1. Usually CELSIUS operates with unpolarized protons, which can be accelerated up to an energy of $T_p = 1360$ MeV, allowing

---

[1] The name CELSIUS stands for **C**ooling with **EL**ectrons and **S**toring of **I**ons from the **U**ppsala **S**ynchrocylotron. It has been chosen to commemorate Anders Celsius (1701-1744) who lived and worked in Uppsala within the early 18th century.

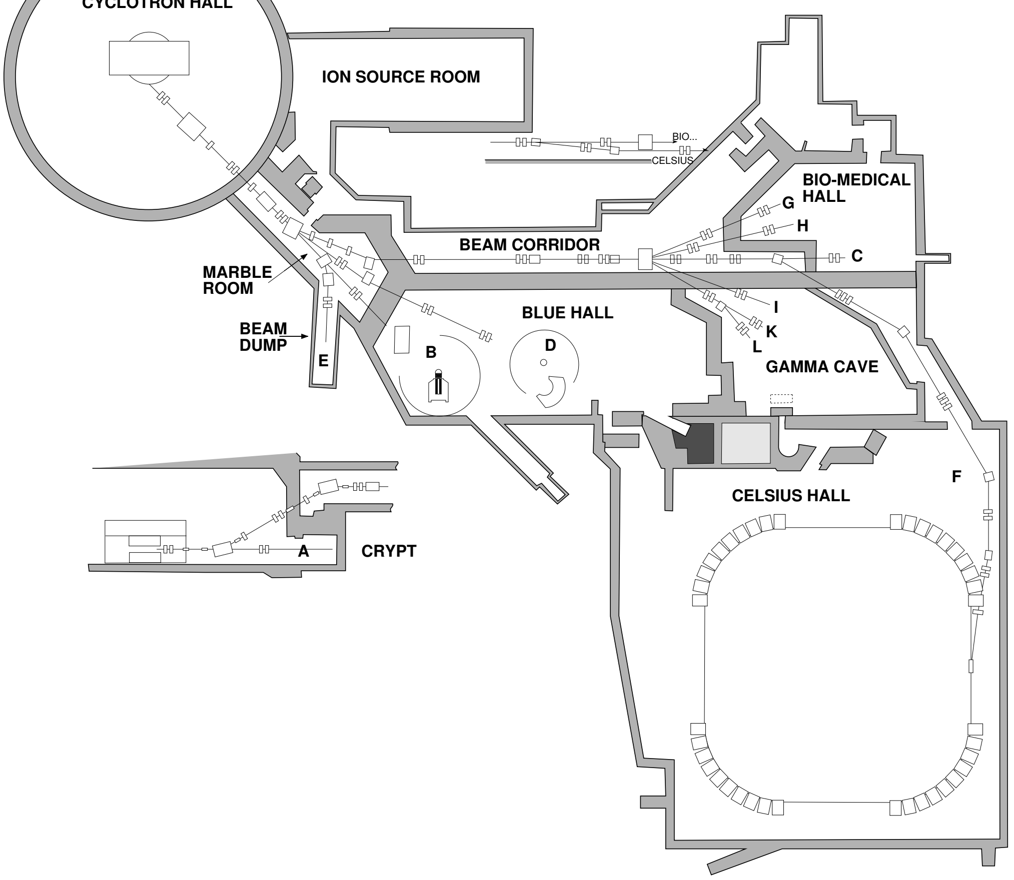

Figure 2.1: *Top view of the The Svedberg Laboratory accelerator facilities*

to study single and multi pion production as well as η production mechanisms. In addition CELSIUS is able to store and accelerate heavier ions from deuterons up to ${}^{40}Ar^{18+}$. As discussed before the ability of CELSIUS to provide deuteron beams has been crucial for this experiment and the following description of the accelerator and detectors is given with respect to the experimental conditions during our beam times in September 1996 and April 1997.

After a stripping injection process the deuterons from the GWC were accelerated within CELSIUS to the final energies between $T_d = 437$ and 559 MeV. The process of injection and acceleration, also called *ramping*, usually took up to 30 seconds and another 30 seconds were needed at the end of each accelerator *cycle* to let the magnetic fields return to the injection levels. To achieve a duty cycle of 80-90 percent the deuterons were stored for an interval of 240 to 540 seconds after reaching the nominal energy. This part of the accelerator cycle is usually called the *flat top*. The life time of the beam was usually at least one order of magnitude longer than the cycle length, which resulted in stable counting rates during the cycles.

CELSIUS offers also the possibility of *electron cooling* [Sed 93], which has been used in this

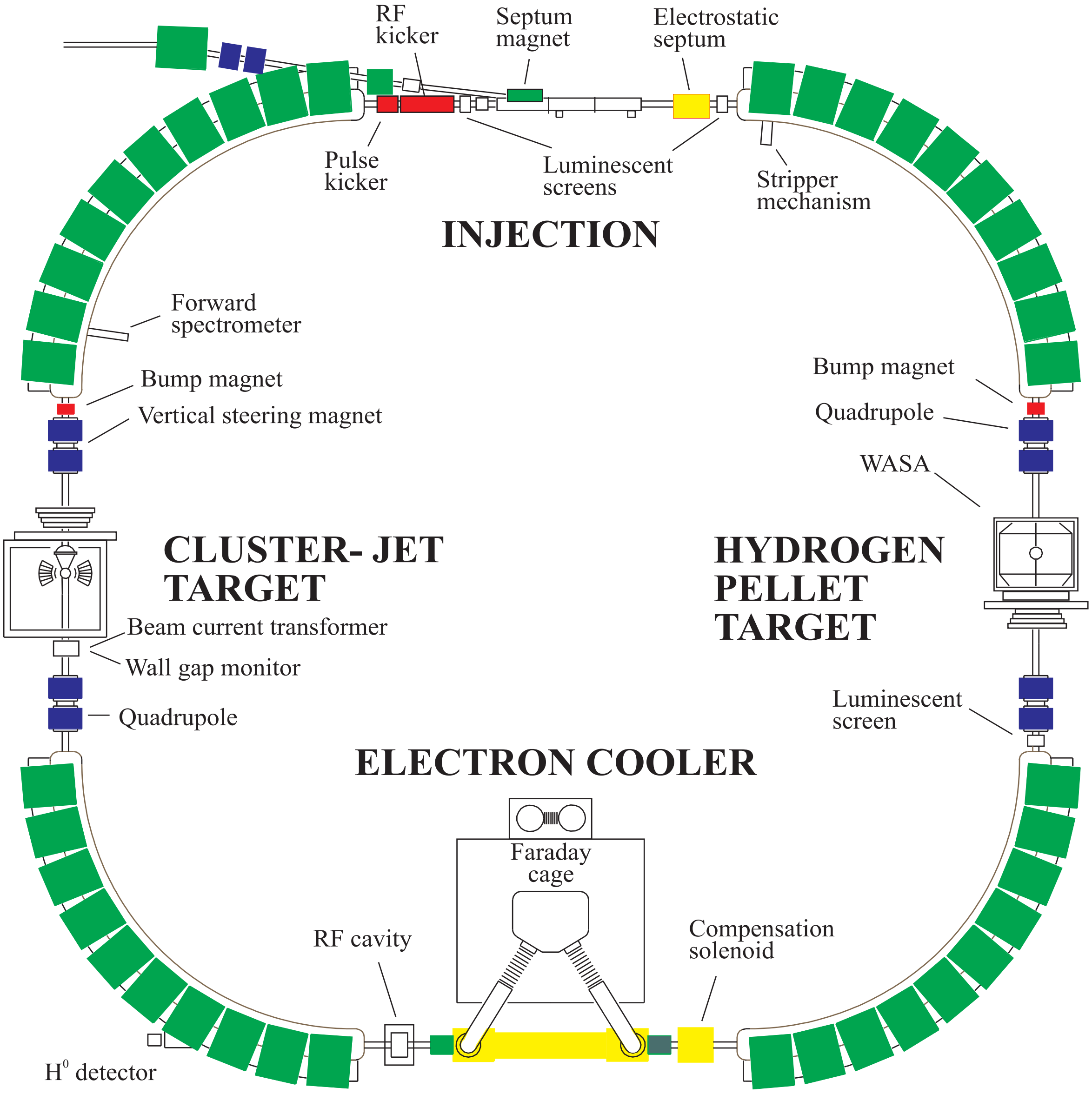

Figure 2.2: *Top view of the CELSIUS accelerator*

experiment at the two lowest energies of $T_d = 437$ and 454 MeV to decrease the momentum spread of the beam as well as its transverse dimensions.

As shown in figure 2.2 two of the four straight sections of CELSIUS are occupied with the beam injection and the electron cooler. The remaining two sections contain two experimental sites. The PROMICE/WASA[2]-detector has been located at the cluster-jet target position and is currently rebuilt as a 4π-detector at the pellet-target position on the opposite side of the ring (see also the outlook in section 5.2). The new 4π detector is now usually called WASA. The following description however refers only to the old PROMICE/WASA setup, which has been used during the beam times in September 1996 and April 1997.

---

[2] **PR**oduction **O**f **M**esons **I**nside **CELSIUS** / **W**ide **A**ngle **S**hower **A**pparatus

2.2 The PROMICE/WASA Experiment

An overview of the PROMICE/WASA detector setup is shown in figure 2.3. The whole detector setup has been developed as a multi purpose experiment to examine different reactions with single and double π-production as well as η-production and Bremsstrahlungs reactions. Its ability to identify particles and to measure their momenta allowed a full reconstruction of the event kinematics within the given detector acceptance.

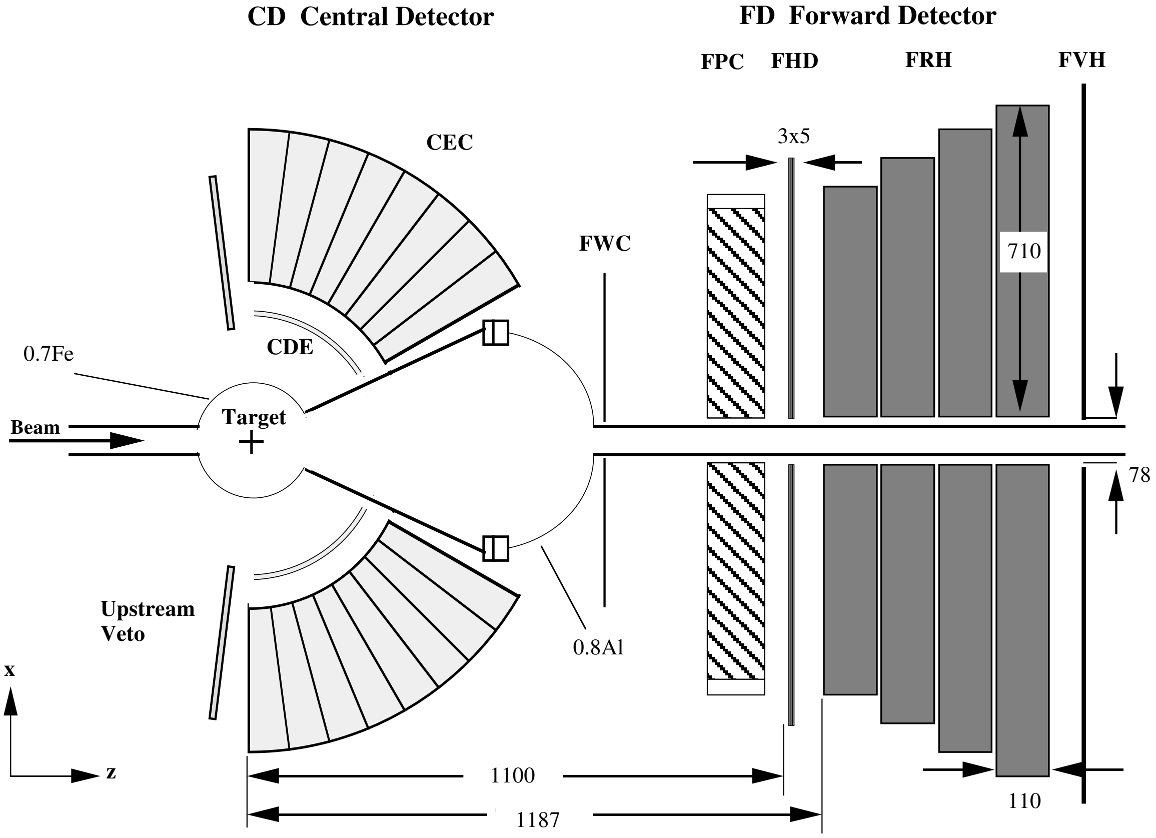

Figure 2.3: *A view of the PROMICE/WASA setup, cut in the horizontal plane. It can be divided into a Central Detector (CD) part and a Forward Detector (FD) part. In our experimental setup the layout of the target chamber differs from this drawing (compare figure 2.5).*

The experiment can be divided into the target system, a central detector part and a forward detector part. While the Forward Detector (FD) has been designed to measure only charged particles the Central Detector (CD) was able to detect neutral and charged particles. In the past, however, it was mainly used to detect γ's from neutral meson decays.

For the PROMICE/WASA detector a right handed orthogonal coordinate system is defined with the origin at the nominal vertex position. The x and z axis are in the CELSIUS plane as indicated in figure 2.3 so that z points along the beam axis and x points outward of the ring. y is then oriented antiparallel to the target beam. The angles given within this Thesis are usually defined with respect to the assumed average vertex position. The polar angle Θ is defined with respect to the beam axis and the azimuthal angle Φ with respect to the x-axis counted counterclockwise, if seen along the beam direction.

The detector parts will be described in more detail now. A tabulated selection of the detector parameters is also given in appendix A.

2.2.1 The Target System

The cluster-jet target system [Eks 97], which has been used in connection with the PROMICE/ WASA setup is able to provide a variety of gaseous targets ranging from H_2 to Xe, but for this experiment only H_2 has been used.

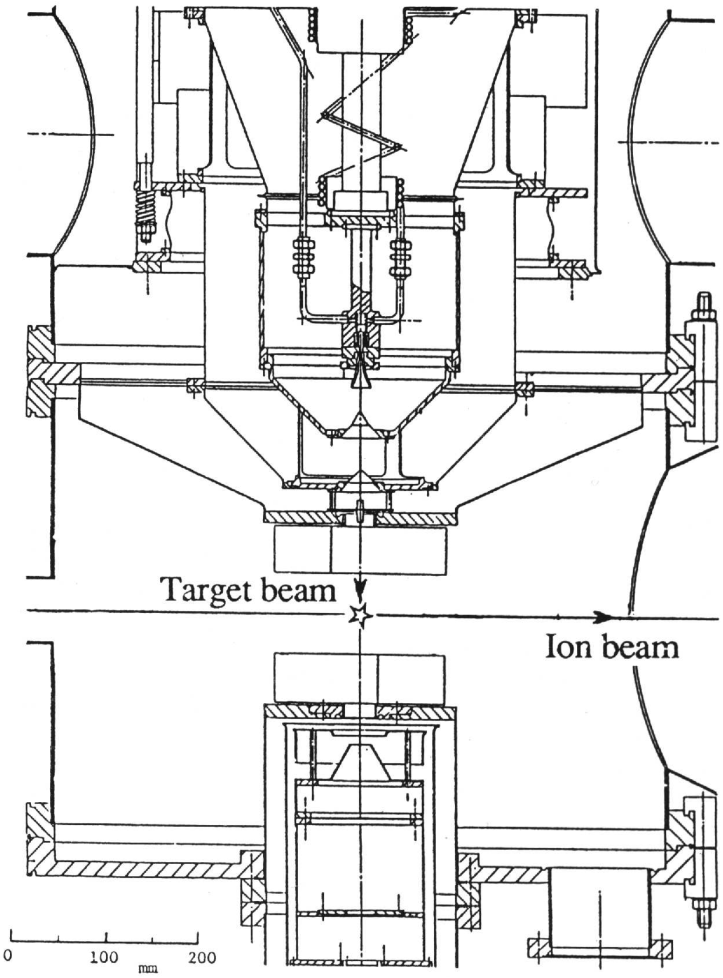

Figure 2.4: *Side view of the Cluster Jet Target system*

Figure 2.4 shows the central part of the cluster jet target. The upper part contains the differentially pumped beam source. Next one can see the interaction region and the cryogenic target beam dump in the lower part. For the target beam production the gas is pressed by a few atmospheres through a nozzle, which is usually cooled down to 20-30 K by a two stage cryogenerator. Under these pressure-temperature conditions close to the phasetransition to liquid a cluster beam is formed, which then passes a skimmer and a set of collimators, resulting in a beam with a well defined intensity profile. At the intersection with the CELSIUS beam the cross section of the target beam is oval shaped with a length of 10.5 mm along the circulating CELSIUS beam and 6.5 mm across. The target thickness is then in the order of $1.3 \cdot 10^{14}$atoms/cm^2. The target system can operate for periods of one to two days before the cryogenic beam dump has to be regenerated [Eks 97].

The whole target system is connected to the scattering chamber shown in figure 2.5. This chamber has been designed to fulfill the requirements of the PROMICE/WASA experiment as well as demands from other experiments using the cluster jet target in connection with internal silicon detectors or external magnet spectrometers.

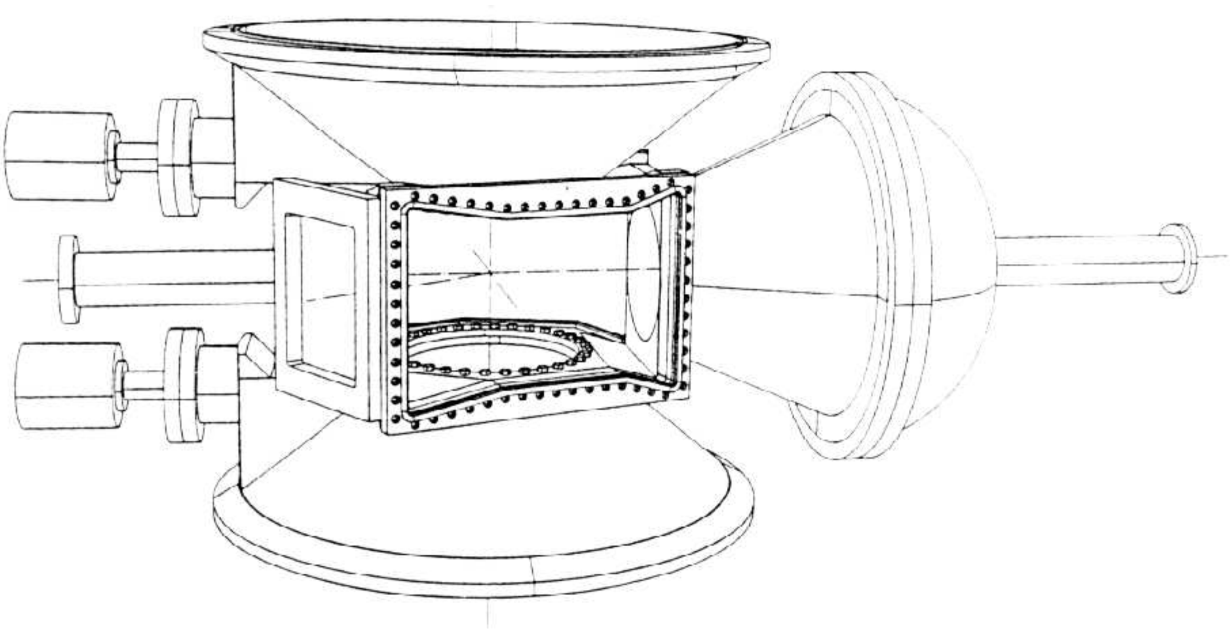

Figure 2.5: *Schematic view of the central scattering chamber, installed at the cluster-jet target system to accommodate internal as well as external detector configurations. [TSL 98]*

Its main parameter is the forward cone with a 0.8 mm thin, hemispherical aluminium window, which allows scattering angles between 3^o and 25^o. It contains two support bars under the horizontal and vertical angles, which limit the acceptance within this region.

The two sides of the scattering chamber facing the Central Detector contain a central window of 0.5 mm stainless steel each. These windows stop protons with an energy of less than 11 MeV. This fact had to be taken into account in connection with the design of our luminosity detectors, which were placed outside of the vacuum directly in front of this window [Koc 97].

2.2.2 The Forward Detector (FD)

The main purpose of the Forward Detector was to measure the angle and kinetic energy of charged particles, emitted into the forward cone. It allowed also different methods to identify these particles. In this thesis the fraction of the Forward Detector covering angles from 4^o to 22^o has been used for analysis.

The Forward Detector has been structured in several detector layers, which are shown in figure 2.3. These layers contained a Window Counter (FWC), a tracker (FPC), a scintillator hodoscope (FHD), a calorimeter (FRH) and a downstream veto (FVH).

Window Counters

Directly in front of the target chamber cone a Window Counter (FWC) has been located, which consisted of four segments of 3mm thin plastic scintillator. It served only as trigger on charged particles. The four segments did not cover the horizontal and vertical areas at which the support bars were located in the forward cone of the target chamber.

Tracker

Behind the Window Counters two frames of straw chambers, the so called Forward Proportional Chambers (FPC , sometimes also referred to as *Tracker*) were placed. Each of the two frames contained four layers of straws based on the operating principle of drift chambers working in proportional mode [Dyr 97]. They were mounted around the beam pipe, rotated by 90^o with respect to each other. Therefore they allowed to reconstruct the x- and y-hit position of a track within a forward cone extending from 4^o to 28^o and they have been the main reference for the reconstruction of the particle angle.

Forward Hodoscope

Behind the tracker a set of three layers of 5 mm thin plastic scintillators was placed. This detector is called the Forward Hodoscope (FHD) or sometimes also the Jülich Hodoscope[3].

As shown in figure 2.6 this detector consisted of two layers of 24 elements shaped like Archimedes spirals with opposite directions (FHD 1 and FHD 2) and one layer of 48 radial shaped elements (FHD 3). The combination of the three overlapping layers gives a matrix of 1104 triangular pixels covering comparable azimuthal and polar angles. Before the installation of the tracker this hodoscope has been used to reconstruct the particle angles, but nowadays its position information is only relevant in the track reconstruction procedures as an additional constraint to eliminate ambiguities.

The FHD has also been used for trigger purposes to determine charged particle multiplicities and its third layer FHD 3 gave the energy information that is utilized within the E/dE particle identification procedures, which will be described in more detail in section 3.4.

---

[3] with respect to the Forschungszentrum Jülich in Germany where it was manufactured

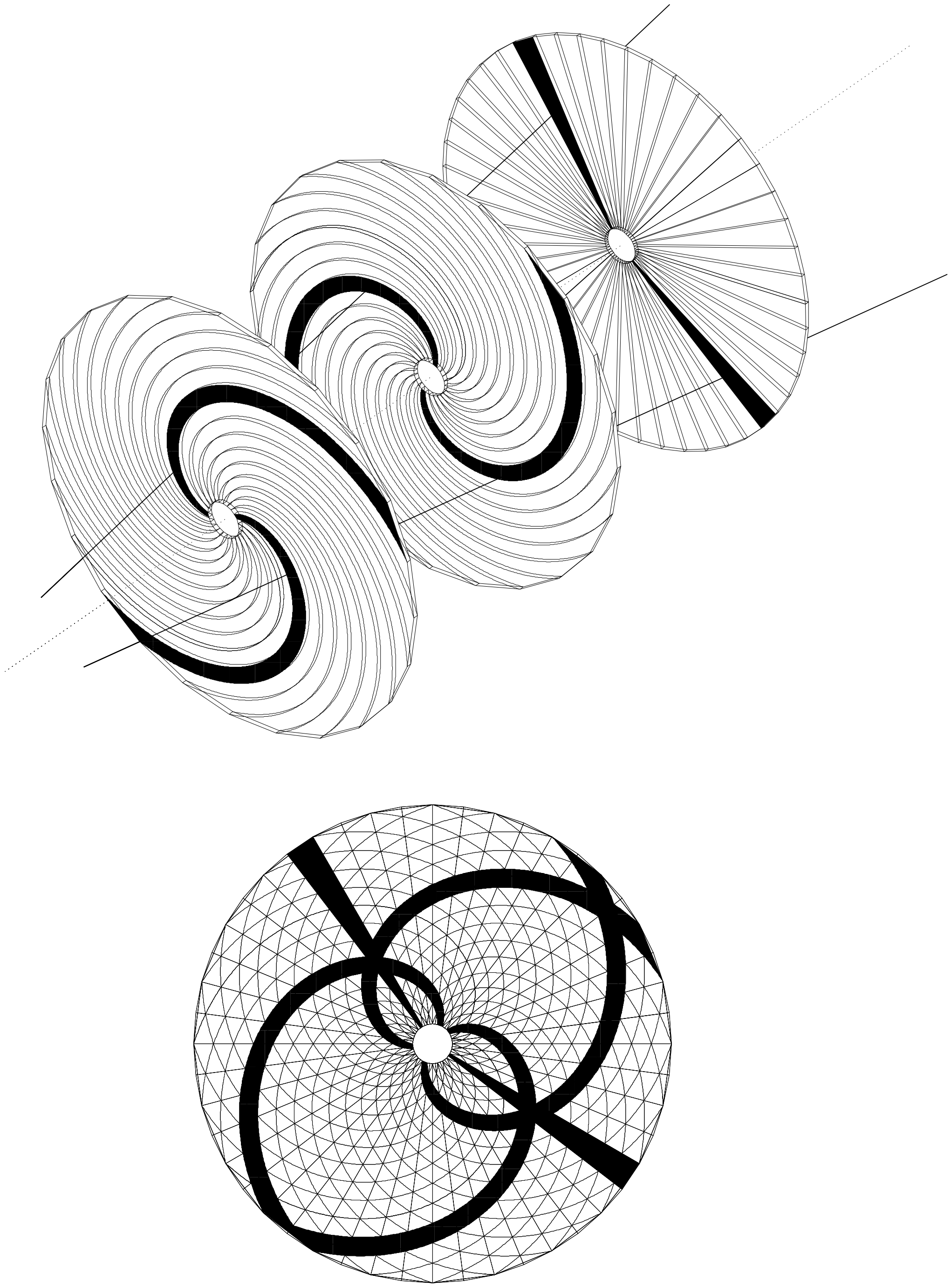

Figure 2.6: *The Forward Hodoscope Detector(FHD) (also called Jülich Hodoscope). The figure shows the pattern information obtained if two charged particles hit the detector. In contrast to the upper part of the figure the three layers of the detector are in reality placed directly on top of each other with a distance of less than 1 mm in between.*

Range Hodoscope

The Forward Range Hodoscope (FRH) shown in figure 2.7 consisted of four planes of plastic scintillator, which have been used to determine the total energies of the charged particles.

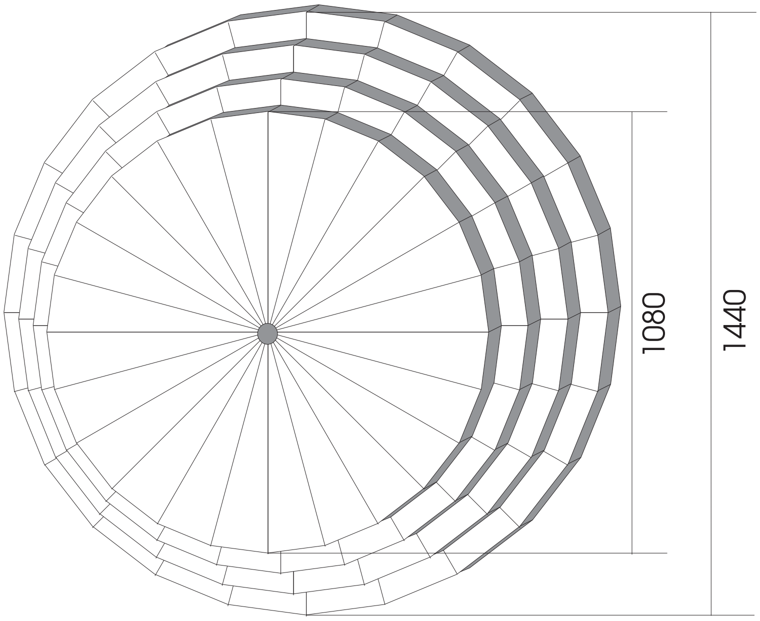

Figure 2.7: *The Forward Range Hodoscope (FRH). Each of the four layers consists of 24 elements*

Each plane itself consisted of twentyfour 11 cm thick blocks, which in total were able to stop protons with kinetic energies of up to 300 MeV and deuterons of up to 400 MeV. The elements were oriented in such a way, that one element of the FRH was covered by two adjacent elements in the third plane of FHD. This gave the possibility to use the energy information for particle identification. In addition to the conventional ADC and TDC readout all elements of the FRH were also monitored with a long range TDC to look for delayed pulses from the decay of charged pions, which have hit the Forward Detector. This will be described in more detail in section 3.4.3.

Downstream Veto

Behind the FRH a Veto Hodoscope (FVH) has been installed [Bro 95], which consisted of twelve horizontally arranged plastic scintillator bars of 2cm thickness with double sided readout. They have been used in our experiment to veto the trigger for suppression of particles punching through the FRH, which could not occur with particles from the reactions of interest.

2.2.3 The Central Detector (CD)

The Central Detector consisted of two modules of electromagnetic calorimeters (CECR and CECL), both equipped with sets of scintillator veto counters to distinguish charged from neutral particles [Sch 95]. Its main purpose has been to detect high energetic γ's from π^o or η decays. In addition the veto-counters have also been used to detect charged particles like e.g. elastically scattered protons for luminosity determination ([Sch 95],[Häg 97],[Dyr 97]).

Each module contained an array of 7 by 8 CsI crystals as shown in figure 2.8. In our setup these modules covered polar angles between $\approx 30^o$ and 90^o and azimuthal angles of more than $\pm 25^o$ with respect to the horizontal plane [Sch 95]. This angular range was reduced, if the outer crystals have to be removed from the trigger or during the offline analysis to avoid energy leakage effects at the outer rim of the calorimeter.

The veto counters in front of the CsI crystals included two layers of 4.5 mm thick plastic scintillators with 20 elements placed horizontally and 28 elements placed vertically (CFB)[TSL 98].

In addition the Central Detector was equipped with four scintillators to veto charged particles coming from the region upstream of the target, which were produced e.g. by the beam halo interacting with the beam tube. It is shown in figure 2.3.

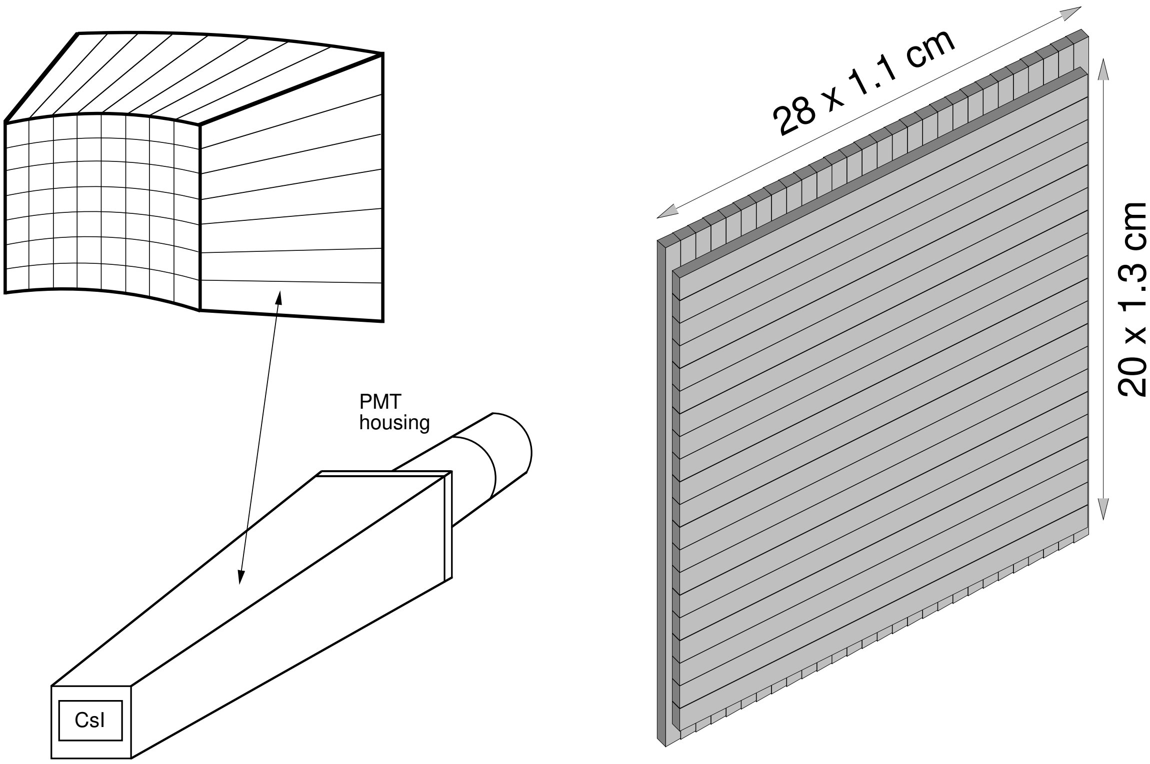

Figure 2.8: *One of the Central Detector CsI calorimeters. It consisted of 56 elements. In front of each module an array of* 28×20 *scintillatorbars were placed for the detection of charged particles (CFB). The figure is not to scale.*

2.2.4 The Trigger and Data Acquisition System

The PROMICE/WASA detector contained about 450 detector channels using ADCs and about 1500 channels for position and time measurements using TDCs. All detector signals were transmitted from the CELSIUS hall to a counting room via 43 m long BNC cables. The complete electronics of the trigger and data acquisition system were housed in the counting room.

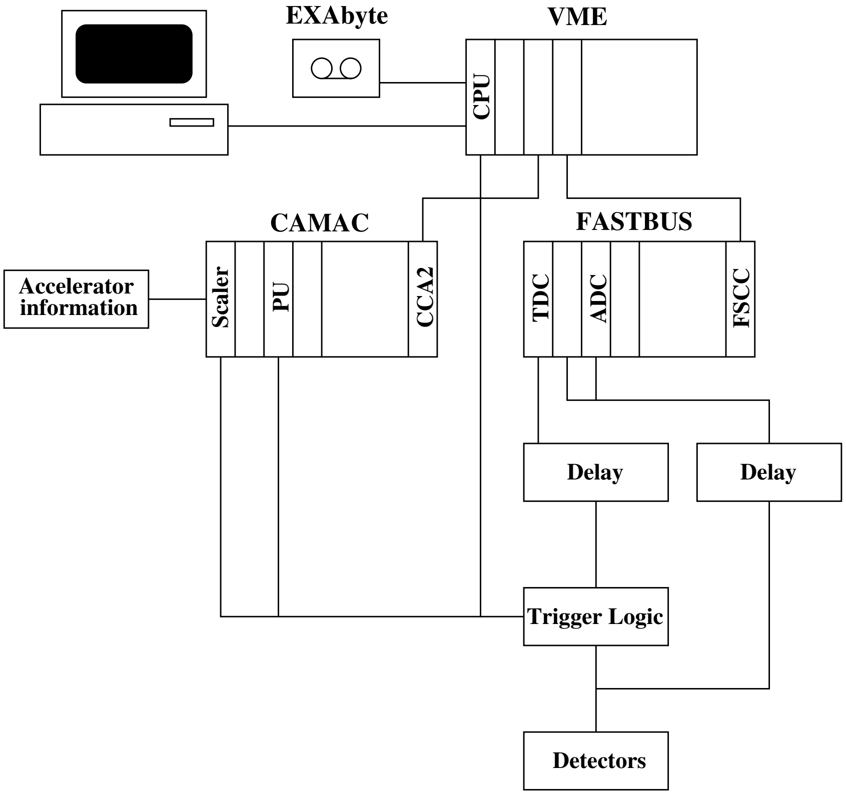

Figure 2.9: *Layout of the PROMICE data acquisition system [Häg 97]*

The Data Acquisition System

The PROMICE/WASA data acquisition system (DAS) was built around the VME-based VALET-Plus system developed at CERN ([Gus94],[CERN Val], [TSL 95]). Its general setup is shown in figure 2.9.

The obtained data was transferred from CAMAC and FASTBUS front-end-electronics to the VALET processor via VME interfaces. The Valet system then wrote the data to an 8*mm*-Exabyte tape for later offline analysis, while in parallel two PC's were monitoring the VME traffic and also the conduct of the experiment with a portion of the event flow. One of them was acting for online monitoring of the detector channels and one has been used for a first online event reconstruction. A VAX/VMS based system has been operating to control the high voltages of the detector photomultipliers. During the April 97 beam time the old VALET FIC8320-processor unit has been replaced by a new PowerPC unit, which was controlled by a WindowsNT workstation [TSL 98].

The incoming signals from the scintillating detectors and from the Si luminosity counters were split into two branches using passive voltage dividers. One branch, after being fed into discriminators, was used for processing with the trigger logic and for time-measurement. The second branch was connected to the charge sensitive FASTBUS ADCs for later energy reconstruction of the signals.

The Trigger System

The total event rate within the PROMICE/WASA experiment was in the order of 10^5 events per second. When operating with a deadtime of about 50 percent, the data acquisition system was able to process about $500 kByte/s$. This is equivalent to about $250 events/s$ with an average event length of $2kByte$ each. To bring down the incoming event rate to a manageable level a *hardware-trigger* had to be formed.

Throughout this work a trigger means always a set of coincidence requirements based upon certain hit patterns of the combined detector components. The hardware-trigger was based upon logical combinations of the discriminated detector signals[4]. All signals from the scintillators and silicon-detectors could be included into the trigger as long as their discriminated signals fell together within a time window of 100 ns width.

The hardware-trigger system was divided into two levels. The *primary trigger* was based upon the combination of signals from different elements of the same single detectors. For example a very simple trigger (**T1**) was based upon the condition of at least 1 element hit in two layers of FHD (compare figure 3.6). This trigger has been set for all events with at least one charged track in the Forward Detector. Another primary trigger has been set under the condition of at least one hit in one of the silicon luminosity counters (**HLU**). These primary trigger signals have then been combined to *secondary triggers* like e.g. **T1HLU**, which is equivalent to a coincidence between the silicon detectors and the Forward Detector.

Events fulfilling the secondary trigger conditions could then activate the data acquisition system and generate the gate signals for the ADCs and the stop signals for the TDCs. The ADC gates were open for $200ns$ for the plastic scintillators and for $2\mu s$ for the CsI crystals and the silicon detectors. Since the event rates were very different for different secondary triggers, prescalers, adjustable in powers of 2, were used to include triggers with high rates and to scale event classes of interest to comparable rates.

The trigger signal rates were also monitored with scalers during the online acquisition to check detector stability and deadtimes.

---

[4] Similar conditions have also been set during the offline analysis procedure after applying pedestal subtraction and threshold conditions. This is then sometimes called a *software-trigger*

2.3 Luminosity Determination

The total cross sections σ_{tot} of a reaction are usually defined via

$$\sigma_{tot} = \frac{N_{exp}}{L\epsilon} \tag{2.1}$$

with

N_{exp} : Number of experimentally observed events
ϵ : Detection efficiency
L : Time integrated luminosity

The luminosity is then defined as

$$L = \frac{dN_P}{dt} \cdot \frac{N_T}{F} \tag{2.2}$$

with

dN_P/dt : Number of incoming projectiles per time interval dt
N_T/F : Averaged target areal density

Since it was not possible in this experiment to measure the target density and beam intensity directly with a good accuracy, the luminosity had to be determined with a simultaneous measurement of differential elastic *dp* scattering. For this reaction precise results from [Roh 94],[Roh 98] have been available as reference.

The simultaneous measurement had also the advantage, that the dead times of the data acquisition system canceled out.

Reference Data

[Roh 94],[Roh 98] have determined the differential cross sections for elastic *pd* scattering within the energy range of $T_p = 200 - 295\,\mathrm{MeV}$ at proton laboratory scattering angles between 7^o and 19^o. The data was based on a simultaneous measurement of elastic *pp* and *pd* scattering and normalized the *pd* yield to the known *pp* cross section.

The differential cross sections for the elastic *pd* scattering were then fitted with the empirical expression of

$$\begin{aligned}\frac{\mathrm{d}\sigma_{\mathrm{pd,fit}}}{\mathrm{d}\Omega_{\mathrm{lab}}}(\theta) &= \mathrm{A}\left(1-\mathrm{B\,T_p}+\mathrm{C\,T_p}^2\right)\left(1-\frac{\mathrm{D}-\mathrm{E\,T_p}^2}{1-\mathrm{e}^{-\tilde{\theta}/\mathrm{H}}}\left\{\tilde{\theta}-\mathrm{K}\,\tilde{\theta}^3\right\}\right) && (2.3)\\ \text{with } \tilde{\theta} &= \theta-(\mathrm{F}+\mathrm{G}\sqrt{\mathrm{T_p}}) && (2.4)\end{aligned}$$

where the values of the nine parameters are:

A = 72.4 mb/sr	F = 22.7 deg
B = 5.16 GeV^{-1}	G = –0.99 deg/$\sqrt{\text{MeV}}$
C = 11.79 GeV^{-2}	H = 0.179 deg
D = 7.18 10^{-2} deg^{-1}	K = 1.16 10^{-3} deg^{-2}
E = 4.87 10^{-3} GeV^{-2} deg^{-1}	

The systematical experimental error of the given values was in the order of 3% plus an additional 5-8% uncertainty due to the uncertainties in the reference for the elastic *pp* cross sections.

The Experimental Setup

Elastic *dp* scattering occurs only for small momentum transfers with significant cross sections. Events with larger momentum transfers favor the breakup reaction $dp \rightarrow ppn$. Therefore the experimental setup was laid out for events with the deuteron hitting the Forward Detector and the recoiling protons being emitted under large angles with low energies.

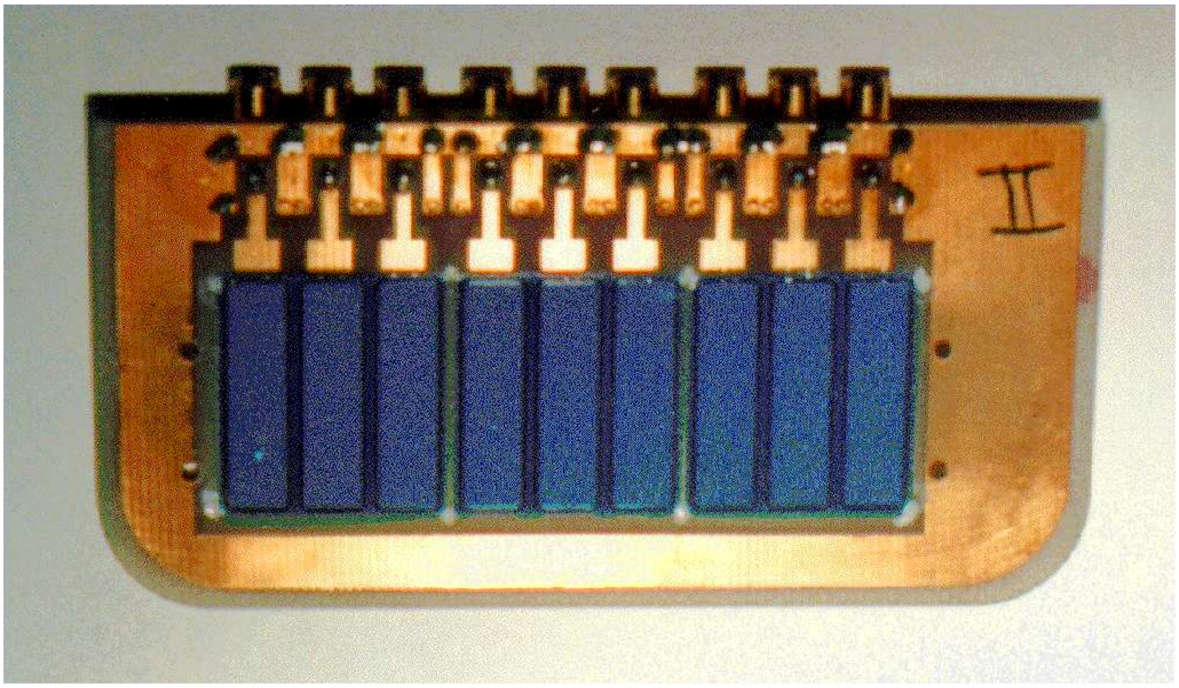

Figure 2.10: *A photograph [Koc 97] of one silicon detector module containing 9 elements with an active volume of* 5mm × 20mm × 300μm.

For this purpose two sets of silicon detectors (HLU)[5] have been developed [Koc 97], which have been placed outside of the vacuum directly in front of the central target chamber window (see figure 2.11). Each set contained 9 silicon elements of 5mm × 20mm × 0.3mm (see figure 2.10) covering proton scattering angles between 68^o and 84^o. The detectors have been read out with standard preamplifiers[6] that gave a signal which was split into two branches. On the first

---

[5] The naming convention defines that HLUL is the module located at positive x-values (compare figure 2.3) and HLUR is the module located at negative x-values. The numbering is oriented along the beam-axis.

[6] CANBERRA 970D

branch a fast trigger signal[7] was generated, which was only in the order of 25 ns slower than the corresponding trigger signal obtained with the Forward Detector photomultipliers. Within the second branch a slower signal has been formed[8], which had to fit into a 2μs gate of the ADCs.

To avoid ground loops the detectors were electrically isolated and shielded in an aluminium box with an aluminium foil window in front of the detectors. Due to the vacuum pumping system the target chamber was vibrating with a frequency of approximately 800 Hz and so were the detectors, because they were attached to the target chamber. These vibrations showed up in the signals and had to be eliminated from the trigger-branch using a high pass filter.

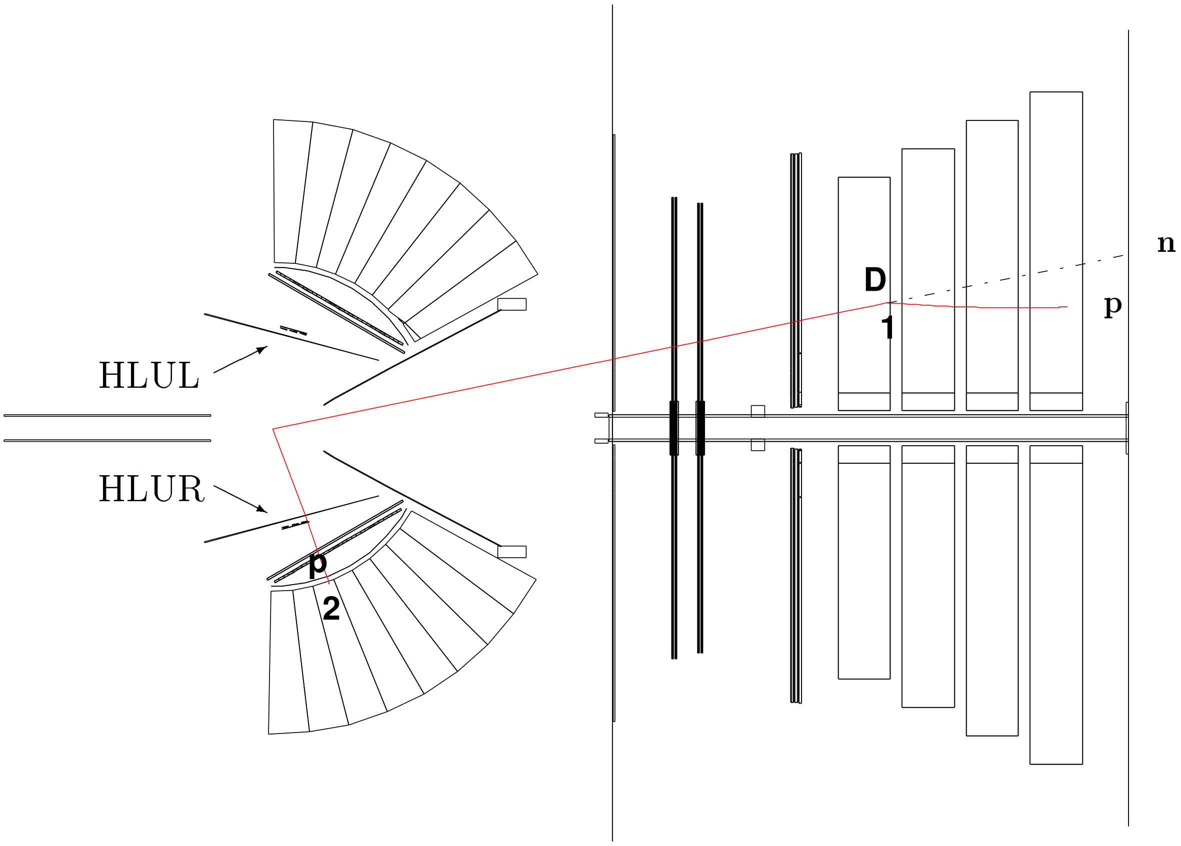

Figure 2.11: *A $dp \to dp$ event at $T_d = 559\,MeV$ obtained using the Monte Carlo Package WMC. The deuteron (1) hits the Forward Detector (where it breaks up into a proton and neutron) and the proton (2) is detected with one of the Silicon Detectors (HLU), sitting in front of the target chamber window. The forward cone of the target chamber is not drawn here, but nevertheless included in the Monte Carlo simulation.*

Considering the effects of absorption and angular straggling of the low energetic protons within the 0.5 mm steel target chamber window, it would of course have been better to place the detectors *inside* of the vacuum chamber. This solution has been discussed, since the silicon

---

[7] using Le Croy 612 fast amplifiers

[8] amplified by EMETRON ELA 1003 amplifiers

detectors in use were not only designed as luminosity counters but also as prototypes for a detector setup to identify and reconstruct spectator protons in *pd* reactions[9]. However, the limited amount of time available for the production and testing of the silicon detectors and readout electronics prevented such a solution. As a consequence only those three to four out of nine elements of each module have been analysed for the luminosity determination, for which the effects of the target chamber window were negligible according to Monte Carlo Simulations.

The experimental setup is described in more detail in [Koc 97] and the procedure applied to extract the luminosity at PROMICE/WASA will be described now.

Applied Procedures

Events with a hit from a charged particle in the Forward Detector and a hit in one of the silicon detectors were selected with the hardware trigger T1HLU. For each element of the silicon detectors the polar angles of the coincident Forward Detector-hits were fitted with a Gaussian function to obtain the scattering angle Θ_d (see also figure 2.12) of the candidates for elastically scattered deuterons.

To obtain the number of *elastic dp* events the background from non-elastic reactions had to be considered. The bulk of it originated from the breakup-reaction $dp \to ppn$ and followed mainly a quasi-free elastic $pp \to pp$ kinematic; so the application of a cut on the coplanarity of the elastic *dp* kinematics was not sufficient for their removal. The background has therefore been parameterized with a second degree polynomial (P2) obtained through a 'G+P2'-fit under the Gauss peak (G) of the deuteron azimuthal angle using PAW [CERN 93e] (see also figure 2.12). It has then been subtracted from the spectra and the number of elastically scattered deuterons has been obtained by integrating them over scattering angles from 5.5^o to 14.25^o.

While the scattering angle has been defined by the detection of the deuteron in the Forward Detector, the opening angle has been given by the geometric acceptance of the silicon detectors for the detected protons. $\Delta\Omega_p$ has therefore been calculated from their active area of 1cm^2 and their alignment with respect to the vertex.

The integrated luminosity is then

$$L = \left[\frac{d\sigma_{dp}(\theta_d, T_d)}{d\Omega_p}\right]^{-1} \cdot N_{exp}(T_d, \theta_d, \Delta\Omega_p) \cdot \Delta\Omega_p^{-1} \cdot \epsilon^{-1} \tag{2.5}$$

and the differential cross section

$$\frac{d\sigma_{dp}(\theta_d, T_d)}{d\Omega_p} \tag{2.6}$$

has been obtained from a Lorentz-transformation of equation 2.4.

The detection efficiency ϵ has been assumed to be 1. A careful examination of the silicon detectors using α-particles from a collimated ^{241}Am-source under vacuum conditions did not indicate any inefficiencies [Koc 97]. Silicon detector elements for which visible effects of the target chamber window were expected due to GEANT Monte Carlo simulations have been excluded from the analysis. The efficiency of the Forward Detector for a detection of one charged particle using the T1 trigger has been determined previously to be very close to 1 (e.g. [Häg 97]). Any inefficiency of this trigger would also later on cancel out in the calculation of the inelastic cross sections, because this trigger-condition was also part of the more sophisticated triggers for the inelastic reactions.

---

[9] This detector was then realized one year later inside the target chamber [TSL 98]

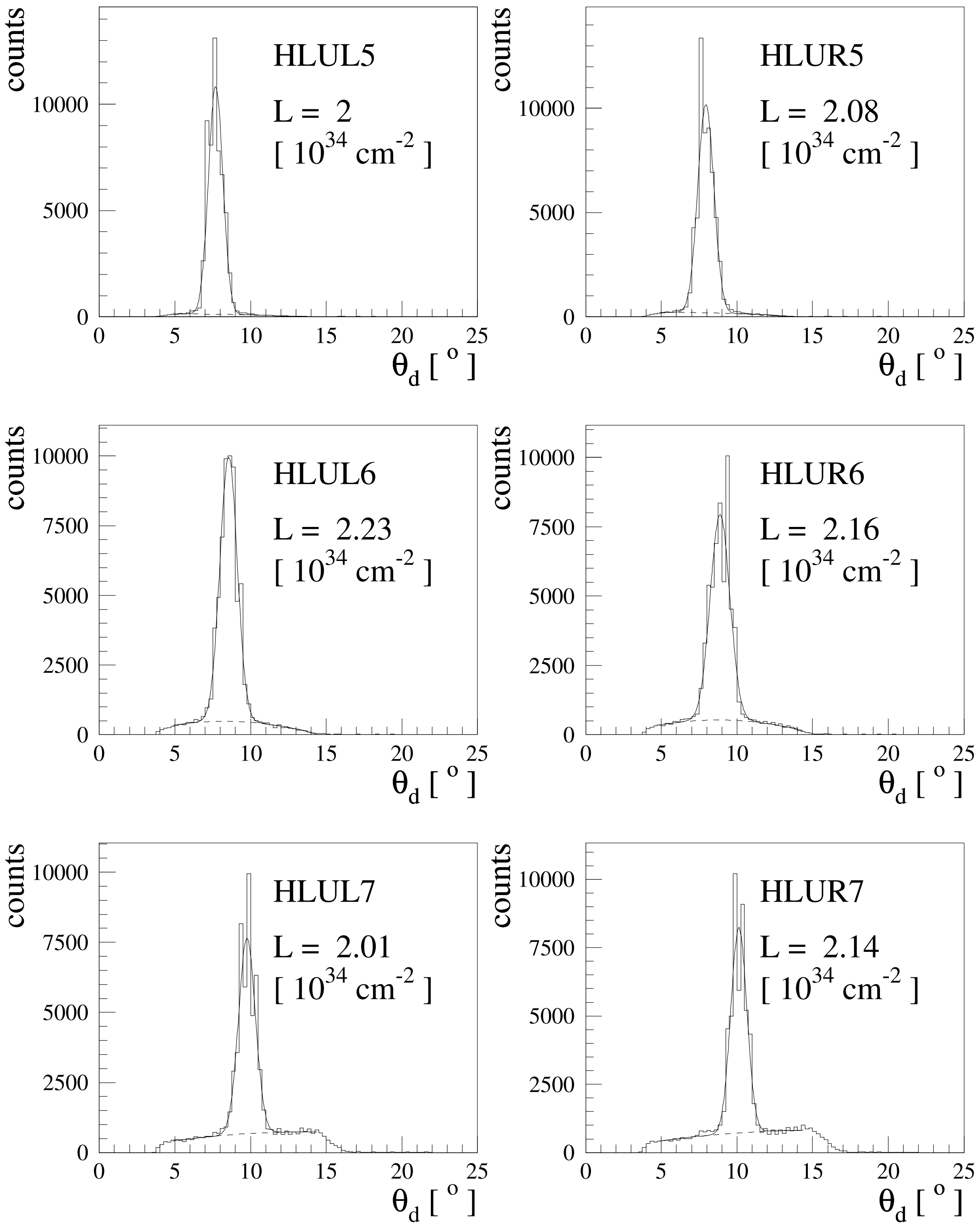

Figure 2.12: *Deuteron angular distributions for events with coincident hits in the Silicon Luminosity Detectors (HLU) at* $T_d = 455$ *MeV. During the April 1997 run period the luminosity has been determined with six elements, three on each side of the PROMICE-detector. The parameterization for the background subtraction is plotted as a dashed line.*

Nevertheless, for the April 97 run period the luminosities obtained with the different elements of the silicon modules differ by about five percent with respect to the averaged value as shown for example in figure 2.12. During the first run period in September 1996 the deviations were in the order of 15 percent. It was not possible to extract the origin of these variations and therefore systematical errors of 5 % and 15 % were assumed for the two run periods in addition to the 8% percent uncertainty of the reference data for elastic *pd* scattering.

2.4 Run Summary

In total 30 shifts (8 hours each) of beam time have been available for this experiment. The shifts were divided into two experimental run periods of 15 shifts each, the first one in September 1996 and the second one in April 1997. Both runs were scheduled at the end of a three week period of measurements with the PROMICE/WASA-detector and in both cases the first two weeks were mainly dedicated to the examination of π- and η- production processes in proton proton collisions at different energies ([Bro 99],[Dyr 97],[Joh 99]). Some of the data sets that have been recorded during these first weeks were used in this thesis for the detector calibration and for various cross checks of the detector performance.

The preparation of the CELSIUS-beam usually took in the order of one shift for each new energy and this limited the number of energy points that have been selected for examination. As a result in total six energies have been measured, three during each run period. The clean beam conditions, which have been observed during the runs have also led to the decision not to perform a subthreshold measurement but to double the period of data taking at the lowest energy of $T_d = 437$ MeV instead. A run summary is given in table 2.2 and 2.3.

For all runs a number of different event types has been recorded in parallel with special hardware triggers, that have been set due to the different requirements. In addition to the main triggers for the physics events, triggers have been set for the luminosity determination, for the online and offline monitoring of the detector stability and during the first runs of the experimental periods also for calibration purposes.

A list of the used triggers is given now.

Selected Triggers

- The main physics trigger **PTWJ12V** was set to select events with two charged particles being stopped in the Forward Detector .

  This trigger required a coincidence of two hits in the Window Counters (FWC), two hits in FHD1, two hits in FHD2 and no hit in the downstream veto FVH. At the energy of $T_d = 455\,\mathrm{MeV}$ the last layer of the Range Hodoscope (FRH4) and at the lowest energy of $T_d = 437\,\mathrm{MeV}$ the last two layers (FRH3 and FRH4) have been included in the downstream veto condition.

  The veto condition has been chosen to reject background events from the breakup reaction $dp \to ppn$ and to reduce the count rates accordingly. The protons of this reaction often have energies large enough to punch through the whole Forward Detector. Deuterons, protons and π^+ from the reactions $dp \to dp\pi^o$, $dp \to dn\pi^+$, $dp \to ppn\pi^o$ or $dp \to ppp\pi^-$ are not affected by the veto condition. However, protons from the reaction $dp \to dp\gamma$ sometimes have energies large enough to hit also elements in the last two layers of the

T_d [MeV]	cooling	$\eta_{dp\pi^o}$	Tape Nr.	L_{int} $[10^{34}cm^2]$	Prescaling PTWJ12V $[2^n]$	Cycle Time $[s]$	Total time $[hh:mm]$
491.8	off	0.612	431		3	32 - 269	03:45
491.8	off	0.612	432		3	32 - 269	03:50
491.8	off	0.612	433		3	32 - 269	03:35
491.8	off	0.612	434		3	32 - 269	03:50
491.8	off	0.612	435		3	32 - 269	01:50
491.8	off	0.612	$\sum$	1.59			16:50
559.0	off	0.862	436		3	32 - 269	06:35
559.0	off	0.862	437		3	32 - 269	04:30
559.0	off	0.862	438		3	32 - 269	04:15
559.0	off	0.862	439		3	32 - 269	01:10
559.0	off	0.862	$\sum$	1.72			16:30
436.7	on	0.320	440		0	32 - 269	06:40
436.7	on	0.320	441		0	32 - 269	06:50
436.7	on	0.320	442		0	32 - 269	06:45
436.7	on	0.320	443		0	32 - 269	06:10
436.7	on	0.320	444		0	32 - 269	06:25
436.7	on	0.320	445		0	32 - 269	06:00
436.7	on	0.320	$\sum$	1.74			38:50

Table 2.2: *Run Summary for the September 1996 Beam Time. Runs not being included in the analysis are not shown. For the main physics trigger* **PTWJ12V** *the prescaling factors are also given. The luminosities are calculated with respect to the* recorded *event rates.*

T_d [MeV]	cooling	$\eta_{dp\pi^o}$	Tape Nr.	L_{int} $[10^{34}cm^2]$	Prescaling PTWJ12V $[2^n]$	Cycle Time $[s]$	Total time $[hh:mm]$
514.8	off	0.705	468		3	32 - 269	10:05
514.8	off	0.705	$\sum$	0.71			10:05
454.7	on	0.434	474		1	37 - 569	03:50
454.7	on	0.434	476		1	37 - 569	04:00
454.7	on	0.434	477		1	37 - 569	04:45
454.7	on	0.434	479		1	37 - 569	06:55
454.7	on	0.434	480		1	37 - 569	02:55
454.7	on	0.434	481		1	37 - 569	07:35
454.7	on	0.434	$\sum$	2.14			30:00
436.7	on	0.320	482		0	37 - 569	06:15
436.7	on	0.320	484		0	37 - 569	10:40
436.7	on	0.320	485		0	37 - 569	09:40
436.7	on	0.320	$\sum$	2.57			26:35

Table 2.3: *Run Summary for the April 1997 Beam Time. Runs not being included in the analysis are not shown.*

Range Hodoscope (FRH3 and FRH4). The trigger condition has therefore reduced the acceptance for this reaction. This will be discussed in section 4.5.

Typical count rates of this trigger were in the order of 500 to 1000 Hz. Since this was more than the data acquisition system was able to write to tape, the trigger has been prescaled by up to a factor of $2^3 = 8$. These prescaling factors are listed in the tables 2.2 and 2.3 for each run too.

- A second physics trigger **T10** has been set to look for coincidences of at least one neutral hit in each of the two CsI modules of the Central Detector (CECL and CECR). It was set to extract π^o-production events from the reactions $dp \to dp\pi^o$ and $dp \to ppn\pi^o$, where the two decay-γ's hit the Central Detector. This trigger required a minimum energy deposition of approximately 10 MeV in a group of the inner 5×6 CsI crystals of the modules [Sch 95]. The plastic scintillating detectors CFL and CFR in front of the CsI-crystals (see also figure 2.8) have been used to veto hits from charged particles.

  The trigger rate was always in the order of only a few Hz and therefore no prescaling has been applied.

  The offline analysis showed, that for this hardware-trigger the necessary trigger informations have not in all cases been recorded correctly. A reconstruction of the trigger efficiency turned out to be difficult and *no* total cross sections based upon this trigger are given within this work. Nevertheless it has been used for the calibration of the CsI modules since the total efficiency of the trigger was not important for the calibration procedure.

- The luminosity trigger **T1HLU** was set for events with one hit in the luminosity detectors in coincidence with at least one hit in the first two layers of the Jülich Hodoscope (FHD1 and FHD2) to detect events from elastic *dp* scattering with the deuteron hitting the Forward Detector and the proton hitting the Silicon Detectors [Koc 97].

  The rate of the trigger was usually in the order of 10-20 Hz. During the September 1996 beam time this trigger was not prescaled. In April 1997 it was prescaled by a factor of $2^2 = 4$.

- The light pulser clock triggered also the data acquisition system at a rate of 3 Hz. These light pulser events were used in the offline analysis to check the stability of the detector elements. They have not been prescaled.

- Four additional primary triggers have been recorded for later offline checks of the detector performance, for an examination of trigger efficiencies and for the calibration of the detector. These triggers, **T1** (at least one hit in the first layer of the Jülich Hodoscope FHD1), **T3** (at least one hit in the first layer of the Forward Range Hodoscope FRH1), **T5** (at least one hit in both layers of the Central Veto detectors CFL or CFR) and **T7** (at least one hit in one of the CsI modules CECL or CECR) have however been prescaled by large factors between 2^8 and 2^{12} since they had count rates of several kHz.

Chapter 3

Event Reconstruction

In this chapter the procedures are described, which have been used to obtain the final data sets. The reader will see that many of the steps, which lead from the raw data sample to the identified and reconstructed event, strongly depend on the comparison between real data and Monte Carlo calculations. Therefore the description of the offline analysis begins with a general description of the Monte Carlo programs including the GEANT based detector simulation WMC.

The different steps of the offline analysis will then be presented in a logical order, starting with the calibration of the different detector components, followed by the reconstruction and identification of particle tracks in the detector, the application of energy corrections and finally the identification of different event-types using the available track information.

The reader who is mainly interested in the physics of inelastic *dp*-interactions may proceed directly to chapter 4, where the obtained results are discussed in comparison with different physical models. Readers who are also interested to judge the performance of this experiment, its unique features as well as its weaknesses should continue here.

3.1 The Offline Analysis Package

The data analysis in this thesis is based upon a couple of tools, mainly originating from the WASA/PROMICE Offline Program library ([Cal 92]). The whole package is written in FORTRAN 77 and uses various parts of the CERNLIB [CERN 93].

Most components have been developed under the VMS operating system, but have lateron been transferred to various flavors of UNIX like e.g. Ultrix, OSF, Linux, SUN-OS or, like in this case, to Solaris. This analysis has been physically performed on a heterogeneous cluster of SUN workstations of the I. Institut of Experimentalphysik of the University of Hamburg, which were distributed between Hamburg and Uppsala and connected via Internet.

The general structure of the offline analysis package is outlined in figure 3.1. Its central part is the **P**ROMICE/**W**ASA event **REC**onstruction program **PWREC**, which is able to read and process both experimental data and Monte Carlo events from the **W**asa **M**onte **C**arlo program **WMC**. WMC itself simulates the effects of the PROMICE/WASA detector and needs the kinematical input from a separated event generator. The different parts of the code are described in more detail now, but since a complete description is not possible in this thesis the really interested reader has to study also the references and the documentation of the code.

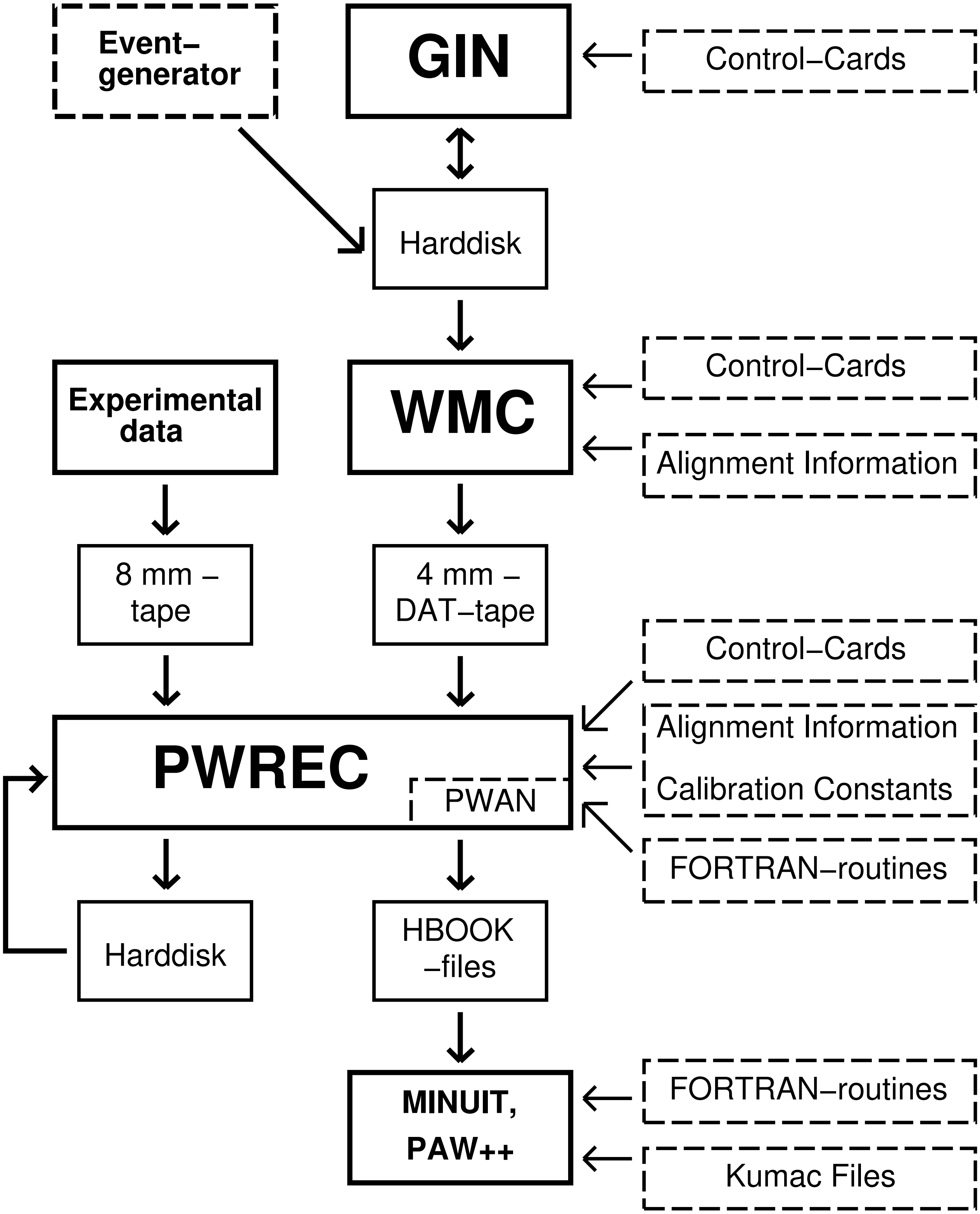

Figure 3.1: *Flow chart of the PW offline analysis programs. The dashed boxes show those parts of the analysis procedure, which have been changed significantly to fulfill the requirements for this experiment.*

3.1.1 Event Generation

For the event generation procedure only the technical aspects are described here. The physical model assumptions are discussed later in chapter 4 in connection with the obtained results.

The general principle of the procedures is, that a set of *events* is generated with the 3N components of the lab-momenta of the N outgoing primary particles, which are produced at the interaction point. These sets of momenta are also often called the *final states* of the reaction. The distribution of the final states is limited because energy and momentum conservation have to be fulfilled and all valid sets of final states populate the so called *phase space.*

According to the description in [BK 73] for the unpolarized cases the phase space integral can be defined as

$$R_N = \int \prod_{i=1}^{N} \frac{d^3 P_i}{2E_i} \delta^4 \left(P - \sum_{i=1}^{N} P_i \right), \tag{3.1}$$

where P_i define the four momenta $(E_i, \vec{p_i})$. The factors c and $\hbar$ are set to 1. Following [Roh 94] one obtains for a beam particle with lab momentum p_B and a target of mass m_T the cross section

$$\sigma = \frac{(2\pi)^4}{4 m_T p_B} \int \prod_{i=1}^{N} \frac{d^3 \vec{p_i}}{(2\pi)^3} \delta^4 \left(P_{tot} - \sum_{i=1}^{N} P_i \right) |M|^2, \tag{3.2}$$

where the transition matrix element $|M|^2$ describes the population of the available phase space. It can also be expressed in the form

$$|M|^2 = | < \Psi_f(P_1, \ldots, P_N) | T | \Psi_i > |^2 \tag{3.3}$$

with the initial and final state wave functions Ψ_i and Ψ_f and the transition operator T.

A constant $|M|^2$ means, that each volume element within the phase space is populated with the same density. This will be later on called a pure *phase space distribution*, which can in practice be generated with the routine GENBOD [CERN 93c].

Deviations from the phase space distribution reflect the reaction dynamics and have to be expressed by the definitions of $|M|^2$. These definitions of $|M|^2$ will be described in more detail in chapter 4. However, if a non-constant $|M|^2$ has to be applied on a set of events, this can in practice be done in at least two different ways and is described here for the two event generators, which have been used throughout this analysis.

GIN

The standard event generator GIN from the PROMICE/WASA library is based upon FOWL [CERN 93d] and can not only be used to generate the input for WMC but also for primary studies of the detector acceptance for different reactions. It offers the possibility to make cuts within phase space and includes some tools to simulate the effects of e.g. energy smearing, caused by the limited resolution of detectors.

If a reaction dynamic is included into the event generation procedure, GIN keeps all phase space distributed events, but gives each event an individual weight factor, which has then to be processed through the whole procedure of the detector simulation and event analysis.

GIN has been used in this thesis and in [Koc 97] as an event generator for the reactions $dp \to dp$, $pp \to pp$ and $pp \to d\pi^+$ in connection with calibration and detector studies.

Event Generator EVGEN for inelastic *dp*-reactions

The event generator EVGEN, which has been used throughout this thesis to describe the inelastic *dp*-interactions is based upon the same routines that have been applied to describe the data in [Roh 94]. It has been chosen to allow the direct comparison of the PROMICE/WASA results with those from the preceding IUCF experiment.

In case of a non phase space distribution it uses a different approach to include the weight functions into the final event distributions. For each event a random number $0 \leq R \leq 1$ is generated and only events with $R < |M|^2/|M|^2_{max}$ are accepted and kept for future processing. $|M|^2_{max}$ is the upper bound of the weight in phase space and has to be calculated from the model assumptions. Each accepted event has then a weight of 1 and can therefore be treated the same way real events are.

Both approaches, the use of weight factors and the rejection method, have their advantages and disadvantages with respect to e.g. CPU-time consumption or concerning the possibilities to add (sub-)sets of different models. However, since these differences do not affect the physical results, if they are handled correctly, they need not be discussed in detail here.

In addition to the description in [Roh 94] the used event generator has been modified to fulfill the requirements for the PROMICE/WASA experiment. Its output format has been changed to that of GIN to allow the processing with WMC. It can now also be used for the inverse kinematics case with the deuteron beam and proton target. One of the differences to the IUCF experiment is the ability of the PROMICE/WASA experiment to detect the γ's from the π^o-decay. Therefore the π^o decay has been included into the event generator using the routine JDECAY from GIN. This means also, that the decay γ's are handled as 'primary' particles because the π^o-decay occurs for all practical reasons instantaneously. In contrast the π^+-decay is not included in the event generator due to its long life time of $26ns$ and it will be later on handled as a secondary reaction by WMC.

Finally the event generator has also been extended to handle the reactions $dp \rightarrow NNN\pi$ and $dp \rightarrow dp\gamma$. This will also be described in more detail in chapter 4.

Both event generators provide sets of histograms describing the particle kinematics and write the kinematics of the generated events to disk for further processing with WMC.

3.1.2 Detector Response Simulation (WMC)

The detector simulation WMC[1] is based upon the GEANT package from CERN [CERN 93a]. It takes the detector geometry as an input from an alignment file and simulates the effects of the detector on events, which have been obtained with an event generator like GIN. In WMC both passive and active volumes are defined. Passive volumes are for example the beam-pipes or the target chamber, which influence the particle tracks, but do not give a measured information. Active volumes are for example the scintillators, which give energy or time information.

WMC takes the lab momenta of the generated events, distributes them across the vertex according to user definitions, and tracks all particles through the whole detector. The tracking routines include the simulation of energy losses, angular straggling, particle decays and different kinds of secondary interactions. These simulated effects are based upon parameterizations of known cross sections (see e.g. [Fes 85]), but their accuracy depends of course on the quality of the input data, which GEANT uses. Therefore one always has to judge and, if possible, improve the quality of the Monte Carlo description concerning different effects.

---

[1] **W**ASA **M**onte **C**arlo

For detector elements with hits, the deposited energies and hit times are recorded and stored in an output format, which is in many ways similar to the experimental data and can be read with PWREC. WMC includes for example effects from light-quenching, but it is not able to simulate non-uniformities of the scintillators or non-linearities of the photomultipliers. Therefore the corresponding corrections are not applied on Monte Carlo data during the analysis with PWREC.

In addition to the simulated detector response the output from WMC contains also the original final state momenta, which can be used to compare the efficiency of the event reconstruction procedures.

It has to be noted that the results from this experiment, similar to all other experiments in this field, depend on a reliable Monte Carlo description of the detector. Therefore cross checks have been made to control the quality of the WMC-events in comparison with experimental data. These cross checks have not only been performed for the *dp*-reactions, which have been the focus of our experimental runs, but also with other data samples from *pp* or *pd*-reactions at several different beam energies.

3.1.3 Event Reconstruction (PWREC) and Physics Analysis (PWAN)

Both, the experimental and Monte Carlo data sets, have been analysed using the PWREC routines from the WASA/PROMICE Offline Program library ([Cal 92]).

The structure of the event analysis procedure is shown in figure 3.2 in a simplified way. It can be divided into the initialization, the event loop and the final closing procedure. Similar to WMC most parts of the analysis procedures can be controlled by sets of parameters, which are structured in so called *cards*. They are read in during the initialization procedure together with all the parameters, which contain the alignment and calibration information.

For each event a loop has then to be passed. After the digital event information is read either from magnetic tape or from harddisk using EPIO [CERN 93b] it has to be decoded into a set of ADC and TDC informations. Each ADC entry together with the corresponding TDC information is later on called a *hit*. The hit information is then also translated into coordinates using the detector alignment information.

The next step is the trigger processing, where first cuts on e.g. hardware triggers or special numbers of hits in different detectors can be applied.

For events with valid trigger conditions each ADC information is then corrected for pedestals and removed, if it falls below the applied thresholds. The remaining hit ADC informations from the calorimeter parts of the detector are then translated into so called *deposited energies*. The deposited energy is in principle proportional to the amount of light, which is produced in the scintillator. It contains already corrections for the *nonuniformity* of the detectors and the different amplifications of the photomultipliers, which are also monitored by a light pulser system.

Neighboring hits in the same detectors are then combined to *clusters* and different clusters, which show some overlap if seen from the vertex position, are connected to *tracks* (see subsection 3.3).

The procedure operating with these tracks is based upon the PWAN routine ([Cal 92]), which itself is also a part of the WASA/PROMICE Offline Program library. In contrast to the other parts of PWREC it has been considerably modified and extended to fulfill the requirements of this experiment. It allows to identify the tracks, to reconstruct the *kinetic energy* of the identified particles and finally to make all the necessary cuts to identify and select the

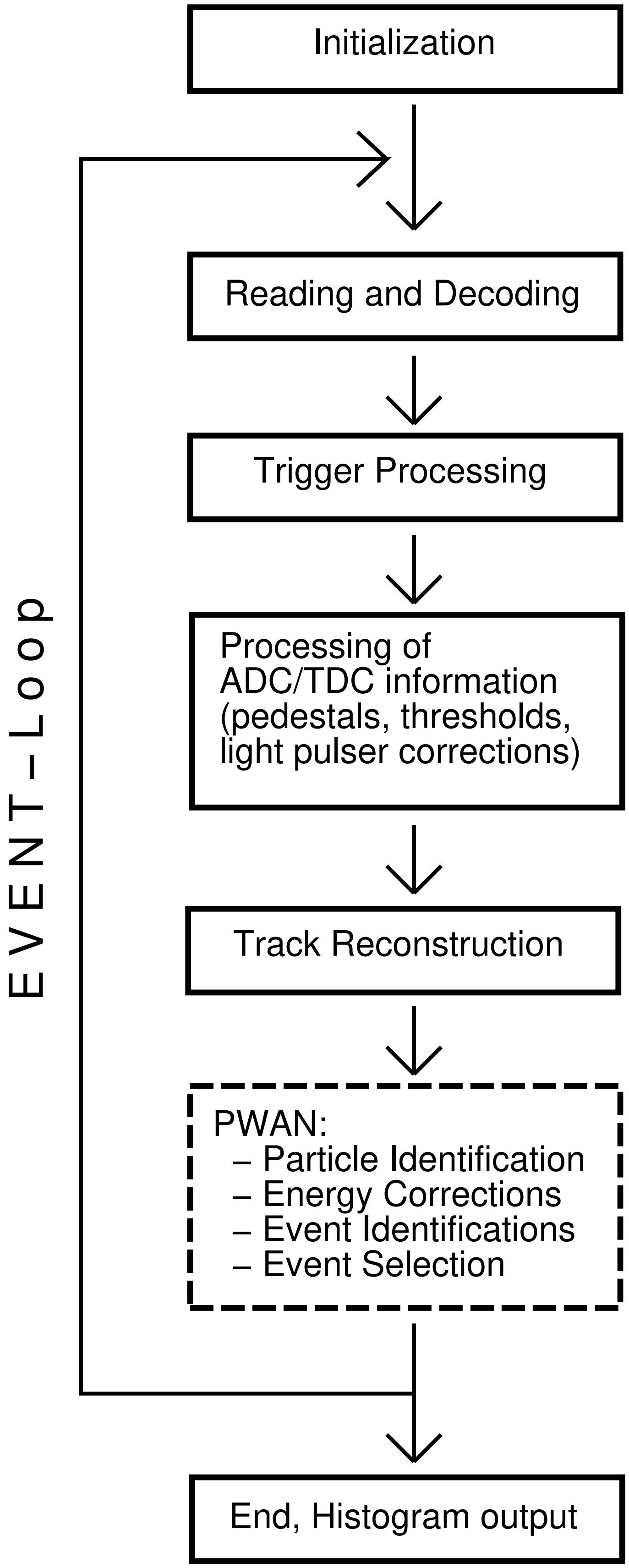

Figure 3.2: *Simplified flow chart of the applied PWREC analysis program.*

different event types.

The different steps of the calibration and analysis procedures will be described in more detail now.

3.2 Detector Calibration and Alignment

The experimental data consist of sets of digital ADC (and TDC) information, which have to be translated to corresponding energy depositions in the different detector elements. For the scintillator elements this translation is a function, parameterized by a set of *calibration constants.* These constants depend both on the position of a hit and on the amount of produced light, because they have to take into account the *non-uniformity* of the light output of the different scintillators and the *non-linearity* of the photomultiplier-tubes. Additional corrections have to be applied for different particle types. These *quenching*-effects are discussed later.

The quality of the calibration functions is crucial, because it limits the accuracy with which particles and events can be identified and reconstructed. Most of the time of the analysis has therefore been spent on the control and improvement of the calibration.

3.2.1 Calibration of the Forward Detector (FD)

The calibration of the forward detector plastic scintillators has been done using signals from elastically scattered protons. At a known beam energy the proton scattering angle and energy are correlated and therefore the ADC information from the experiment can be compared directly with the deposited energy information obtained from Monte Carlo simulations with WMC. The Monte Carlo data has to include the effects of dead material, secondary interactions and quenching.

Each scintillator element is therefore divided into several radial *bins* (given by the granularity of the FHD). For each bin a constant is extracted, describing the non-uniformity remaining after the overall parameters for amplification and non-linearity of each photomultiplier are applied. The standard calibration procedure is described in more detail in e.g. [Wat 92], [Cal 93].

The present experiment suffers a bit from the lack of elastically scattered protons from several different beam energies to include them into the data base for calibration. Due to a limited quality of the available pp data sets and due to the fact that for experimental reasons the amplification of some photomultipliers had to be changed *after* the initial calibration run, there was only one suitable data sample at a proton beam energy of $T_p = 400$ MeV available for each beam time. These 400 MeV $pp \to pp$ events have then been used to extract the amplification factors for the photomultiplier tubes while the non-uniformity constants have been partly kept from previous experimental runs. A careful analysis has shown, that the non-uniformity constants for the FRH did not change much over long periods of time, but for the FHD they had to be extracted again for each beam time.

In practice the accuracy of the different calibration constants differed for each detector element and has been examined using all available data sets like e.g. $pp \to pp$, $pp \to d\pi^+$ as well as experimental results from two pion production runs $pp \to X\pi\pi$ and $dp \to X$ at different energies. The calibration of the FRH has never caused significant problems for this analysis. In contrast the calibration of FHD 3, which is important for the E/dE particle identification, has proven to be difficult. More effort had to be made to improve it so that the systematical errors caused by the limited accuracy of the calibration were small in comparison to others which are described in section 3.4.

No serious attempt has been made to obtain good calibration constants for the two spiral planes of FHD and it has only been checked that the signals from these elements were well above thresholds.

3.2.2 Calibration of the Central Detector (CD)

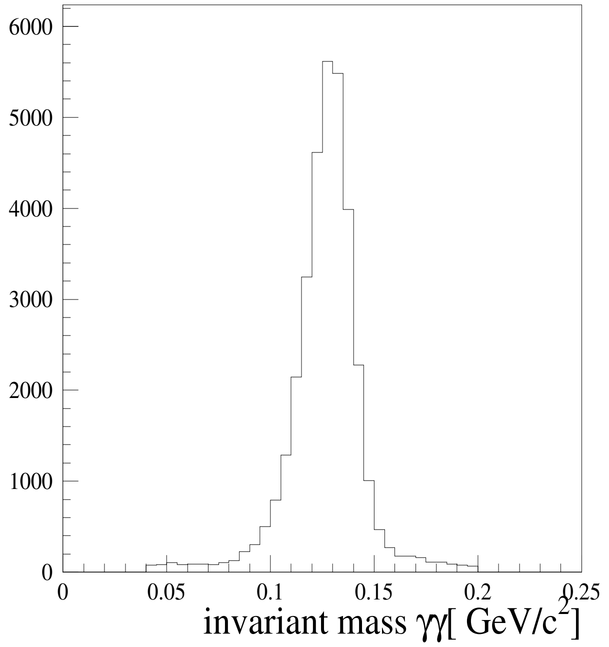

Figure 3.3: *Invariant mass of two* γ *'s of the reaction* $pd \rightarrow pd\pi^0$ *at* T_p*=320 MeV.*

The CsI crystals of the Central Detector have been used here to detect γ's from either π^o-decays or from Bremsstrahlungs reactions, but no attempt has been made to use the Central Detector to identify and reconstruct charged particles.

Therefore the CsI-crystals have been only calibrated according to a procedure described in [Kuz 93] with events of the reaction $pp \rightarrow pp\pi^o$, which had one neutral hit (lateron called CDN) in each of the two calorimeter arrays. 'Neutral' means in this case that there was no hit in the adjacent veto counters CFB. For each event then the invariant mass of the two neutral hits was calculated under the assumption that they were caused by γ's. This invariant mass was then filled into two histograms, one for each CsI element with the largest energy deposition of each array.

According to these invariant mass distributions m_i, which were then available for each crystal i, new calibration constants have been extracted with an iterative procedure. Following [Kuz 93] the new calibration constants c_i^{j+1} were calculated as

$$c_i^{j+1} = c_i^j \left(\frac{m_{i\pi^o}}{m_i} \right)^2 \left(\frac{\bar{m}}{m_{i\pi^o}} \right) \sqrt{\frac{E_2}{E_1}} \tag{3.4}$$

where c_i^j was a set of old calibration constants. The procedure gives only reliable results, if the initial values are already close to the real calibration constants. Therefore usually the calibration constants from the preceding beam time have been used as start values. In the beginning the first set of calibration constants has been determined using signals from radioactive sources or cosmic muons [Sch 95]. $\bar{m}$ is the average of all calculated invariant masses m_i and is compared to the expected invariant masses $m_{i\pi^o}$ obtained from the Monte Carlo Simulation. $m_{i\pi^o}$ was usually between 5 and 10 percent below the real π^o-mass because effects of dead material and energy leakage had to be taken into account. Finally the average energy depositions E_1 and E_2 in the two CsI arrays had to be included to force a symmetrical calibration.

The procedure to extract new constants was then iterated four or five times until it had converged.

As a result the overall invariant mass peak for π^o showed usually a width of $\sigma \approx 10\,\mathrm{MeV}$. An example of an invariant mass spectrum is shown in figure 3.3.

3.2.3 Stability of the Photomultiplier Readout

Since the signals from the scintillators were used for particle identification and energy determination, it was important to check the stability of the detectors and readout electronics during the experimental runs. For this purpose the detectors were monitored with an optical light pulser system ([Zab 94]), which flashed light into them at a frequency of several Hz.

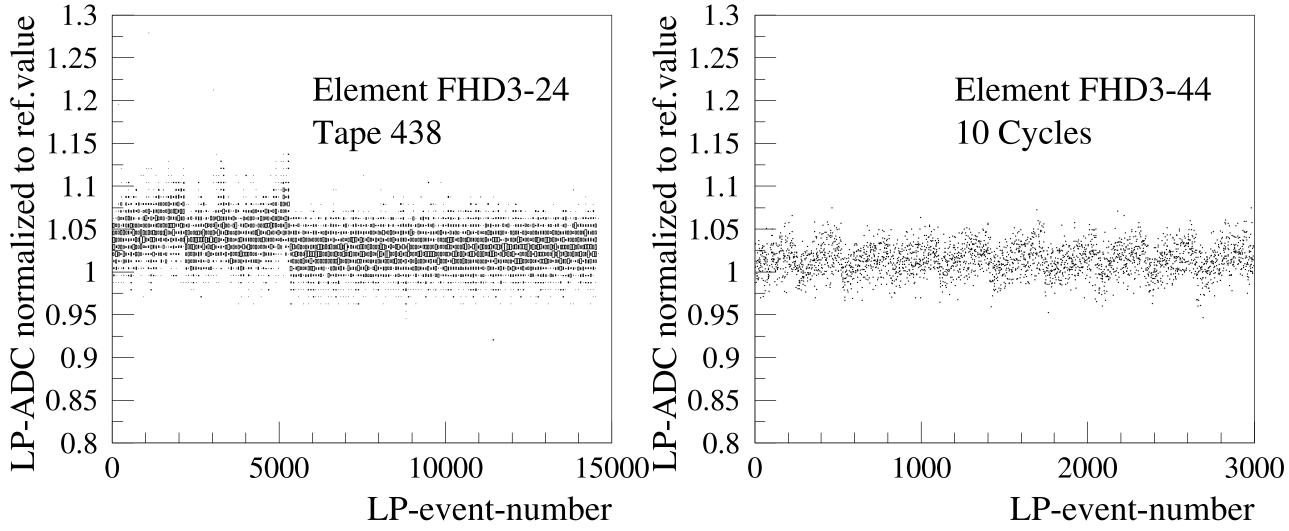

Figure 3.4: *The variation of light-pulser signals as a function of the event number for two elements of FHD 3 at a beam energy of* $T_d = 559$ *MeV taken during the September 96 run period. The scale is normalized to the reference values for these elements. The left picture shows the variations of the detector amplification during four hours, while the right picture shows fluctuations, which are related to the accelerator cycle length of 300 seconds*

Figure 3.4 shows examples of the fluctuations, which have been seen with the light pulser system. In most cases the observed long term drifts were within a 15 percent level. The reasons for these effects are not known in detail; the reconstructed energies however, have been corrected with reference to the light pulser information. Some elements also showed short term fluctuations in the order of less than 5 percent, which were connected to the accelerator cycle time. The light pulser system was only able to cope with a part of these short term fluctuations, since it always had to gather a sufficient amount of events to yield statistically significant corrections.

3.2.4 Calibration of the Luminosity Detectors (HLU)

The silicon detectors have been calibrated using the 5.5 MeV α-peak of a ^{241}Am source ([Koc 97]). The calibration had however only a limited impact because the elastically scattered dp-events have been extracted using only the coplanarity and opening angular information obtained in conjunction with the Forward Detector. In contrast to first expectations it has not been necessary to use the energy information of the silicon detectors as a further constraint to suppress background and therefore the calibration uncertainty of the silicon detectors had no effect concerning the quality of the results.

The performance and acceptance of all silicon detectors has been examined in detail in [Koc 97] and no indication for inconsistencies or inefficiencies has been found among the different, up to 18 elements of the luminosity detectors.

3.2.5 Determination of the Beam Energy and the Vertex

The mean energy of the deuterons in the beam can be calculated from the accelerator settings and is given by

$$T_d = m_d c^2 \left(\frac{1}{\sqrt{1-\beta^2}} - 1 \right), \beta = \frac{fL}{c} \tag{3.5}$$

Where f is the RF-frequency and L is the assumed closed orbit length of the deuteron beam within the ring. Usually the measured frequency is determined with a much better precision than the closed orbit length, which depends always on the settings of the magnets. In the CELSIUS ring exists no possibility to measure the beam energy directly. However, for all energies, where electron cooling has been applied, the energy was determined accurately, assuming that the high voltage of the cooler is well calibrated.

At the higher energies however, where the beam has not been cooled, a different approach has been taken to check the value of the beam energy. It was based on the assumption that the *width* of the missing mass peak of a reaction has a minimum if all parameters necessary to calculate the missing mass are set correctly. The assumption of a wrong parameter always broadens the missing mass distribution, which can be proven with Monte Carlo. The calculation of the missing mass includes however a large set of parameters, namely the beam energy the assumed vertex position and the whole set of calibration and alignment information which are necessary to reconstruct the particle momenta.

At the higher energies the analysis has therefore been performed with the beam momentum being the only free parameter and all other parameters kept fixed. The variation of the missing mass distribution for the reaction $dp \to dp\pi^0$ is shown in figure 3.5 for the highest nominal deuteron energy of $T_d = 559\,\mathrm{MeV}$, corresponding to a beam momentum of $P_d = 1552.2\,\mathrm{MeV/c}$.

It can be seen, that the width of the missing mass distribution has a minimum close to the nominal value where also the peak position is closest to the π^o-mass. The best fitting momentum value in connection with the beam frequency has lead to a value of 81.81m for the beam circumference, which is in agreement with previous experiments (e.g. [Häg 97]) and has to be compared with the design value of 81.76m.

The same method has then also been applied to determine the average vertex position. It has been found that the results fit best under the assumption of a vertex, which was shifted by -4 mm in the y-direction but did not deviate within the x- or z-directions. This is also in agreement with previous experiments ([Häg 97],[Dyr 97]), but it is nevertheless impossible to tell from the experimental data, weather the observed effects were really caused by a shift within the vertex position, as it was assumed throughout the analysis. A similar effect could also have been caused by a small inclination of the beam.

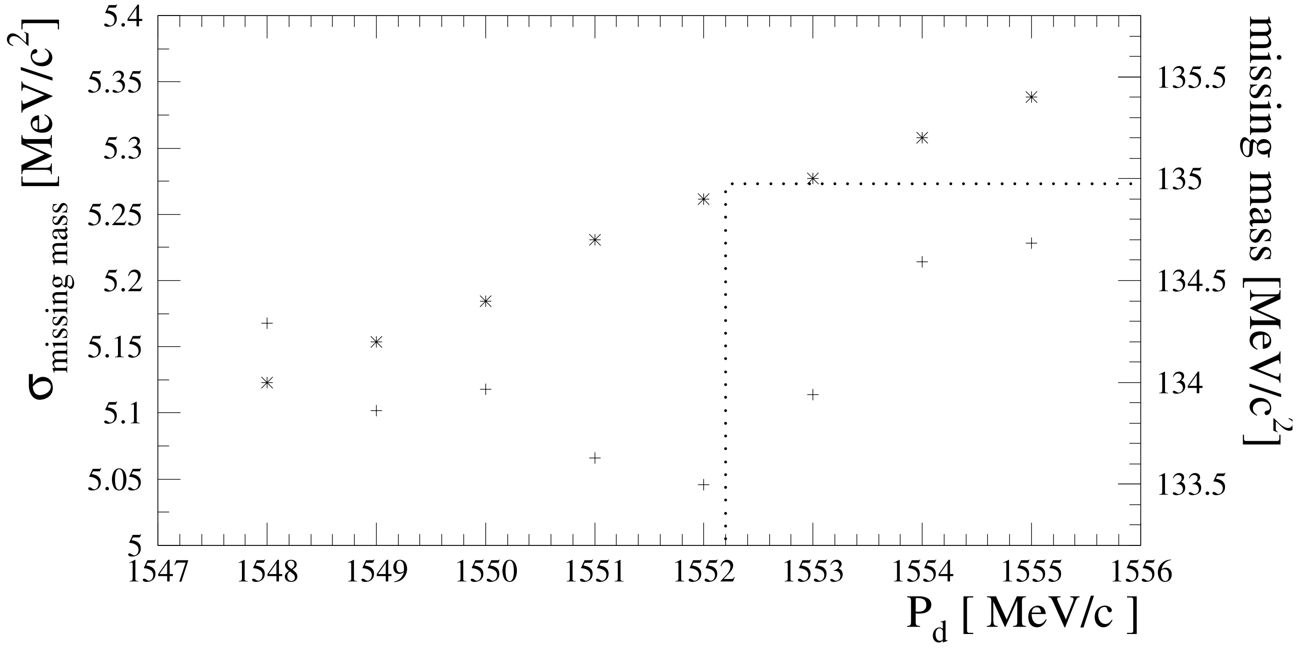

Figure 3.5: *The position (stars) and width (crosses) of the missing-mass peak for the reaction* $dp \to dp\pi^0$ *as a function of the assumed beam momentum. The width of the missing mass peak reaches its minimum close to the nominal beam momentum of* $P_d = 1552.2 MeV/c$*, which is indicated by the dotted line. At this momentum the missing mass is also close to the* π^o*-mass of* 134.98 *MeV/c*^{2} *.*

3.3 Track Reconstruction in the Forward Detector

The procedures and conditions, that had to be applied for the cluster and track reconstruction were depending on the event type and on the number of tracks, which were expected in different parts of the detector. For events with only one charged particle hitting the Forward Detector or with two particles hitting the Forward Detector under significantly different angles the identification of tracks was possible without ambiguity. This did not apply, if hits had to be expected in neighboring areas or if more than two tracks had to be reconstructed. In these cases ambiguities occurred in the cluster finding procedures, which could lead to so called *ghost tracks*. Similar effects could have also been caused by secondary interactions with the detector material.

PWREC already includes a standard procedure for cluster and track identification, which has also been used in this thesis. Tests with Monte Carlo events have shown a good performance for $dp \to dp\pi^o$ and $dp \to dp\gamma$, if the conditions were not too loose. A good **C**harged track through the **F**orward **D**etector (**FDC**) had to fulfill the condition of overlapping hits within all layers of FHD and the first layer of FRH and it was also rejected if the tracker information indicated, that the track was not coming from the target region.

For the reactions just mentioned the deuteron and proton were almost never emitted into neighboring areas of the Forward Detector . This is also true for the examined events of e.g. $dp \to dn\pi^+$ since the hardware trigger condition required two hits within different quadrants of the Forward Detector.

3.3.1 Background Considerations

The errors caused by random coincidences were expected to be small. Examinations of the efficiency of the π^+ identification with the delayed pulse technique (see section 3.4.3) did not show significant numbers of coincidences, which had to be expected in the time windows of interest.

Empty target measurements in connection with the deuteron beam (figure 3.6) have also shown very low count rates in the detector, being caused by the beam halo. For events with at least *one* charged track in the Forward Detector (T1-trigger) the count rate decreased by a factor of ten, when the target was switched off. As a result it seemed reasonable to assume, that the number of events with *two* charged tracks, that did not originate in the nominal vertex and that have not been rejected by the track reconstruction procedure can be neglected.

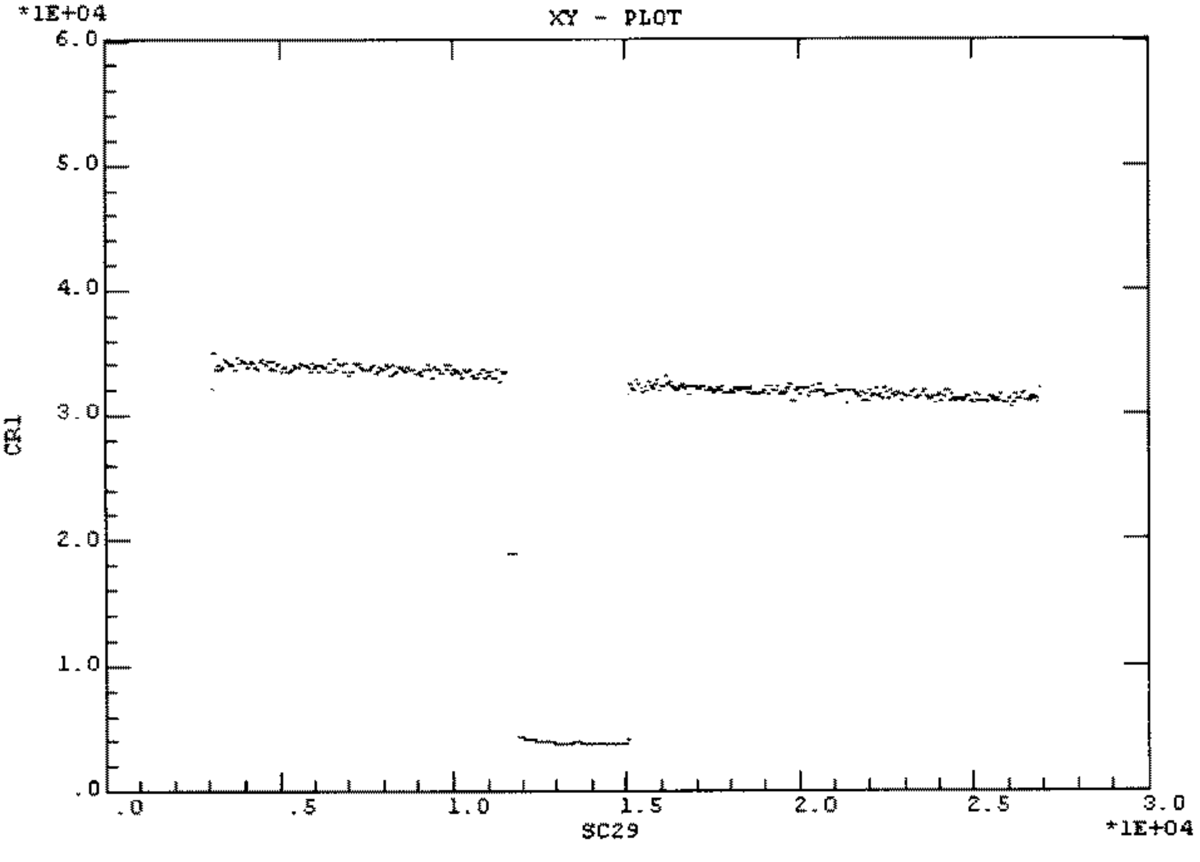

Figure 3.6: *First Level Single Charged Particle Trigger (T1) rate during one cycle (0s - 300s) at a beam energy of T_d =559 MeV. Data has been acquired during the flat top (30s - 270s). The beam intensity dropped by less than 10 percent during one cycle, which was a typical result also at other energies. For test purposes the target has been switched from its cluster-jet mode to a gas jet mode with significantly reduced intensity (120s - 150s). During this time the count rate of this simple trigger has dropped to 10 percent of its previous value, which is now probably mainly caused from beam halo reactions. According to these results it can be estimated that the fraction of misidentified second level trigger signals caused by events, which were not coming from the target region can be neglected.*

3.4 Particle Identification

The identification of most reactions within the PROMICE/WASA detector required in nearly all cases an identification of the measured particles. This was mainly due to the fact that most of the reaction channels with pion production had three or more outgoing particles with one of them had to be reconstructed from the measured four-momenta of the other particles; therefore their masses must have been known.

Only for the binary reactions $pp \to pp$, $pp \to d\pi^+$ and $dp \to dp$, which have been used in this work for detector calibration, acceptance studies and for the luminosity determination, it has not been necessary to identify the outgoing particles directly. In these cases the measurement of coplanarities, opening angles and deposited energies gave sufficient informations for the event identification.

The methods of particle identification in the PROMICE/WASA detector, which have been used, vary with the particle type and will be discussed now.

3.4.1 Protons

The proton was not only the most frequent particle detected, it was also the easiest one to identify. Here only protons, which were stopped in the Forward Detector were of interest, because the hardware-triggers used in this analysis has rejected events with hits in the FVH .

The first step towards particle identification in the Forward Detector was always the comparison of the total deposited energy (E) of a reconstructed track to the deposited energy in one of the first layers of the detector (dE). Due to the specific energy-loss dependence of the different particles, which is described by the Bethe Bloch formula [Leo 87], the particles showed up at different loci in the E/dE-plot.

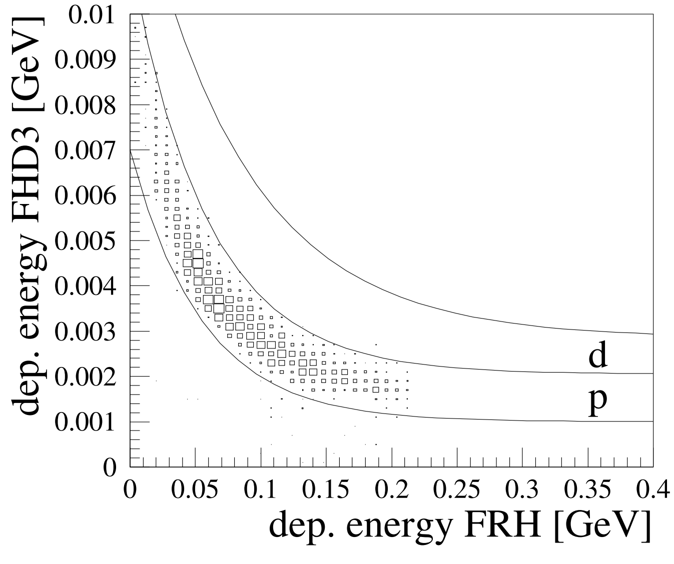

Figure 3.7: *Selected protons from the reaction $dp \to ppp\pi^-$ at T_d=559 MeV.*

Figure 3.7 shows such a plot for identified protons of the reaction $dp \to ppp\pi^-$, where the deposited energy in the third layer of the Trigger hodoscope (FHD3) is plotted versus the total energy deposition in the FRH. The choice of the layer(s), which were used to measure the dE-information has depended mainly on the particle energy. For *protons* the particle identification was only based upon the E/dE-identification using FHD3 as the dE-counter. From Monte Carlo one would expect, that the sum of all three layers of the Trigger Hodoscope would have given a better resolution, however, a good energy calibration of the thin spiral elements of the first two layers of the Trigger Hodoscope (figure 2.6) turned out to be difficult with the available elastic *pp*-data. Therefore these layers have only been used for trigger purposes and in connection with the angular track reconstruction.

In addition protons with a total deposited energy of less than 190 MeV in the Forward Detector in connection with more than 15 MeV in FRH4 were not counted, because they were assumed to be punch-throughs, which have not been vetoed by the Veto-Hodoscope FVH .

3.4.2 Deuterons

The principle of the deuteron identification in this experiment was the same E/dE method, that is also used for protons. However, in practice the deuteron identification has been difficult for two reasons.

First of all the number of protons, which were produced in the several possible reaction-channels listed in tables 1.2 was very large in comparison to the number of deuterons. Therefore the chance that an identified deuteron was in reality a misidentified proton was much larger than vice versa.

The main reason for misidentifications was, that the deuteron band lies close to and partly merges with the proton band of the E/dE-plot. Due to a limited energy resolution of the detectors, effects of dead material between the scintillator elements or secondary-reactions in the detector material one (or both) of the energy informations could have been wrong and resulted in shifts within the E/dE-plots.

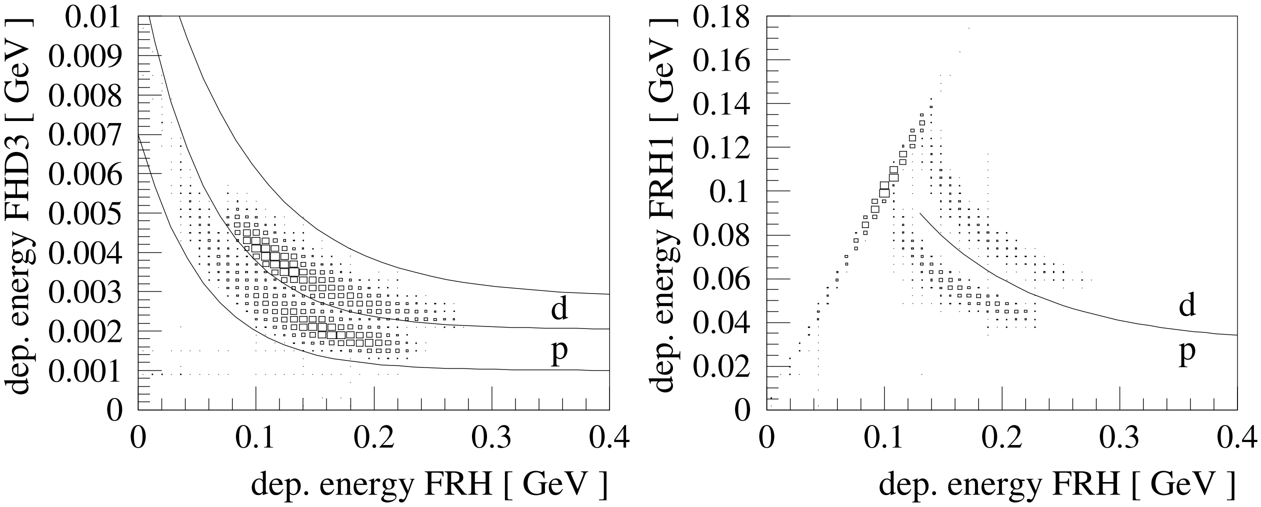

Figure 3.8: *Selected protons and deuterons from the reaction* $dp \to dp\pi^0$ *at* T_d*=559 MeV.*

Up to a certain level it was possible to tackle the problems of misidentification by improving the energy calibration of the detectors. For tracks with an energy deposition of more than 130 MeV it was also not necessary to use FHD3 as a dE-detector because deuterons of this energy penetrated also FRH2 . In these cases the E/dE-plot, which used FRH1 for dE has been used for the deuteron identification, because of the better energy resolution of the Range-Hodoscope. Figure 3.8 shows the E/dE-plots for identified events from $dp \to dp\pi^0$ at $T_d = 559$ MeV.

Deuteron Secondary Reactions

The effects of dead-material and secondary reactions, however, could have only been taken into account by the GEANT [CERN 93a] based detector simulation WMC. While WMC has been successfully used to describe protons hitting the Forward Detector in many experiments before (e.g. [Bet 97], [Bro 95], [Dyr 97], [Häg 97], [Joh 99], [Kur 95], [Mör 95], [Sch 95]), the description of deuterons had to be checked, in particular concerning the accuracy of the energy reconstruction and of the detection efficiency .

Deuterons with energies of up to 300 MeV, as they were expected here, undergo breakup-reactions in the scintillator to an extent, which could *not* have been neglected. The procedure that has been used to simulate the deuteron secondary reactions was based upon the following assumptions (see also [Kup 95]) and used the GEANT/GHEISHA interface ([CERN 93a], [Fes 85]).

It was assumed that the cross-section for interactions between deuterons and the nuclei of the detector (A) is

$$\sigma_{dA} = \sigma_{pA} + \sigma_{nA} - \Delta \tag{3.6}$$

The Glauber-correction Δ was expected to be small and therefore neglected (impulse approximation). In our simulation the interactions of deuterons with the plastic scintillator material was of particular interest. The plastic scintillator material has the approximate formula $(CH_2)_n$, but since the σ_{dH} is assumed to be much smaller than σ_{dC} the interactions between deuterons and C will be dominant. The additional assumption $\sigma_{pC} = \sigma_{nC}$, due to the isoscalar composition of ^{12}C, leads to:

$$\sigma_{dA} \approx 2\sigma_{pA} \tag{3.7}$$

and gives the probabilities for the secondary interactions of deuterons in the Forward Detector, which has then been used by GEANT.

In the case of an interaction it was furthermore assumed, that it has been either elastic dA-scattering or a quasi-free NA-reaction, where N is either the proton or the neutron with equal probability. The NA-reaction has then been simulated by GEANT while the other nucleon proceeded unaffected with the initial deuteron velocity. (An example for such a secondary interaction is shown in figure 2.11.)

The relation between elastic dA-scattering and inelastic dA-reactions is however not well known. Within the simulation it was simply assumed that elastic scattering accounts for 20% of the total cross section σ_{dA} and 80% are caused by quasi-free NA-reactions.

Cross Checks of the Monte Carlo Description

The description above is certainly only an approximation and therefore it has been necessary to check the agreement between Monte Carlo and experimental data. The only possible cross-check in this case has been the reaction $pp \to d\pi^+$ at $T_p = 400$ MeV. This data sample has been taken one week before our first experimental run in September 1996 with the same experimental setup. The elastic pp-scattering from this data sample has also been used for the energy calibration of the Forward Detector .

The reaction $pp \to d\pi^+$ had the benefit that it was possible to be identified using *only* the coplanarity and opening angles of two outgoing particles. The background was small and came mainly from $pp \to pn\pi^+$ (see also [Bet 97]). It was furthermore possible to examine two cases where either the deuteron and the π^+ have hit the Forward Detector or the deuteron has hit the Forward Detector and the pion has hit the Central Detector. The second one has been chosen, because it gave a wider energy and angular spectrum for the deuterons.

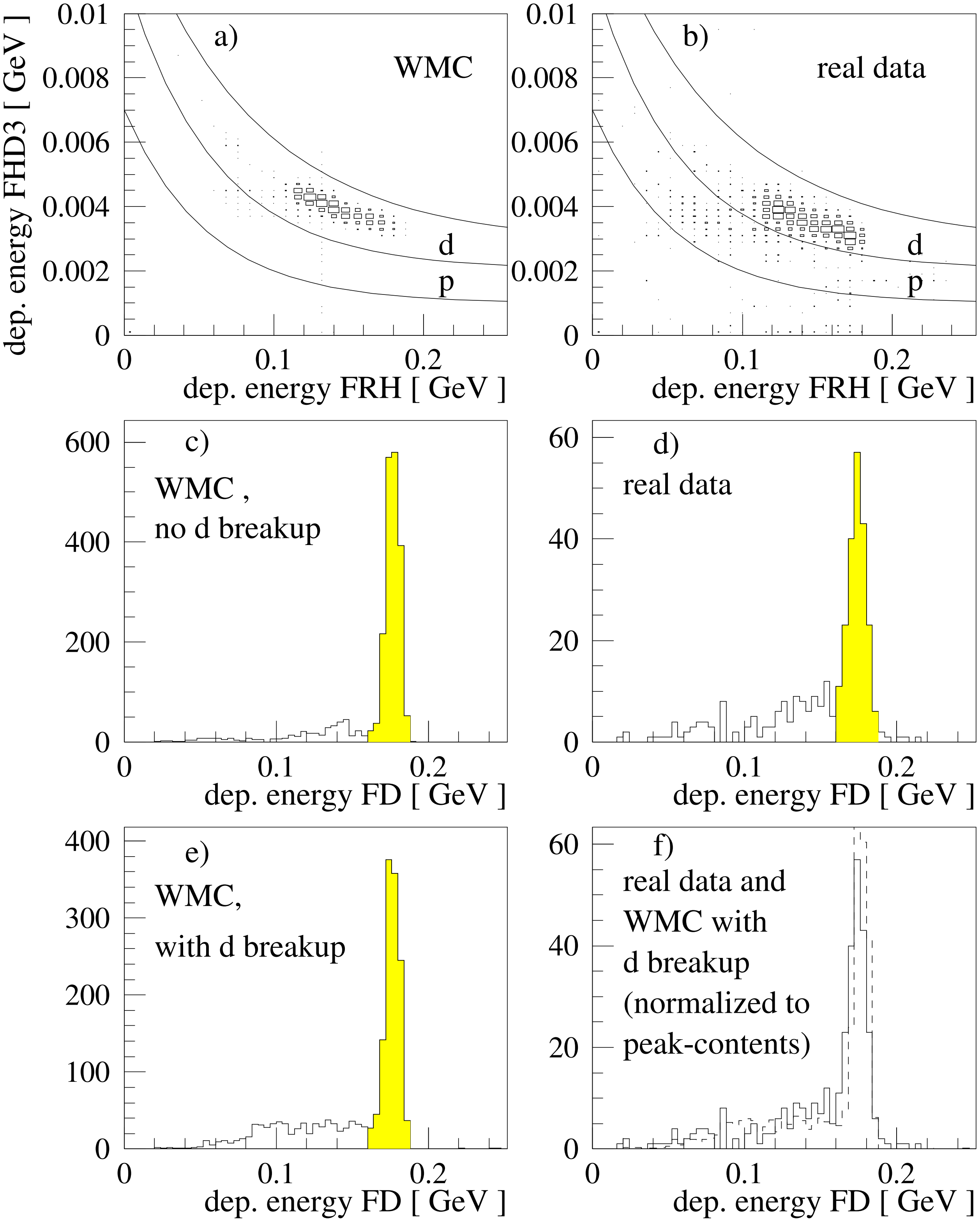

Figure 3.9: *Selected deuterons from the reaction* $pp \to d\pi^+$ *at* T_d*=400 MeV. c)-f) show subsamples of a) and b) with the condition of* $6.5^o < \Theta_d < 7.5^o$

The results in figure 3.9 a) and b) show E/dE plots for the Forward Detector where the deuteron band is clearly visible. It is also visible, that there are several hits, which had an energy deposition within FHD3 that is expected for deuterons, while the total deposited energy of the deuteron band is smeared out to smaller values. This is the expected effect when a deuteron has hit the Forward Detector, has passed the 15 mm thin FHD and has interacted within FRH before it was stopped. A similar effect appears of course also, if the deuteron has deposited some of its energy in the dead material between different FRH elements.

This can be seen more clearly, if one looks for example at a subsample of mono-energetic deuterons, which have been selected with a cut on the deuteron angle of $6.5^o < \Theta_d < 7.5^o$ (figure 3.9 c)-f)). The deposited energy spectrum shows a peak (grey) at the energy of 170 MeV and a tail (white) at smaller energies (Fig. 3.9d), that is underestimated by a factor of 2.8 in Monte Carlo without any d-breakup (Fig. 3.9c). Introducing the d-breakup into WMC reduced the peak-content (Fig. 3.9e). The relation peak/tail is now 1.8 in comparison with 1.7 for real data and 4.8 for WMC-data without d-breakup. Similar results were achieved looking at other deuteron energies.

In total the examination of $pp \rightarrow d\pi^+$ showed, that WMC succeeds to describe the deuteron nuclear losses within a 15 percent level.

A more detailed examination was however limited by the available statistics and by the fact, that the real $pp \rightarrow d\pi^+$ data sample always included small background from $pp \rightarrow pn\pi^+$.

It is later on assumed, that the systematical error for the deuteron identification due to uncertainties in the WMC description and limited precision of the detector calibration is 15 percent.

3.4.3 π^+

The π^+ identification was of particular interest for the $dp \rightarrow dn\pi^+$ event reconstruction.

One approach to identify π^+ in the Forward Detector was to use the same E/dE method as for protons. This was however not sufficient, because the background from e.g. electrons or high energetic protons was not negligible within this region of the E/dE plot. In addition was the resolution of the energy reconstruction for the π^+ limited due to its decay into a μ^+ (plus ν_μ) with a mean life time of 26ns [PDG 94]. The μ^+ itself could then have added up to 4.2 MeV to the measured energy in the scintillator, if the decay occurred within the ADC-time window of 200 ns. The subsequent decay of the μ^+ into $e^+ + \nu_e + \bar{\nu_\mu}$ might have contributed with an even larger energy of up to 50 MeV [Kur 95]. This was however not very probable due to its long mean life time of 2.2 μs [PDG 94].

The shortcomings of the pion-decay concerning the energy reconstruction converted however into a benefit for the particle identification itself with a long-range-multi-hit-TDC, that has been installed [Kur 95] and looked for delayed pulses in all elements of the Range Hodoscope and the third layer of the Trigger Hodoscope. The time window of this TDC was set to 0.16-6 μs with respect to the start of the dataacquisition. Within this time window 87.5% of the delayed signals from the μ^+-decay into e^+ have occurred [Kur 95].

The requirement of an additional delayed pulse in connection with the E/dE-information was a clean signature of the π^+-events with almost no background.

However, there were different ways to look for delayed pulses. The basic principle was to reconstruct the track of every charged particle, which has hit the Forward Detector and to look for a delayed pulse within the element where the particle was stopped. It has of course been possible, that the μ^+-decay occurred in one of the neighboring elements, because of the kinetic

μ^+-energy of roughly 4 MeV originating from the π^+ decay or simply because of scattering or threshold effects. Therefore it was possible to include these neighboring elements into the search for the delayed pulse. In addition one had to consider the possibility of a random coincidence with a different event, which occurred within the $6\mu s$-time-window of the TDC. Therefore some elements in front of the element where the track stopped have been used as a veto within the 0.16-6 μs time window. In this case it may have happened, that also good π^+-tracks have been rejected if a veto-element was hit by the e^+.

In view of these alternatives an analysis code has been developed ([Joh 99]), which offers five different options for the π^+-identification.

1. No delayed pulse is required, the π^+ is identified only with the E/dE method.
2. At least one delayed pulse is required in the last element hit by the track. The corresponding elements in FHD3 are used as a veto.
3. At least one delayed pulse is required in the last element hit by the track. The corresponding elements in the adjacent layer in front are used as a veto.
4. At least one delayed pulse in the last element hit by the track or in a neighboring element. The corresponding elements in the adjacent layer in front are used as a veto.
5. At least one delayed pulse in the last element hit by the track or in a neighboring element. The corresponding elements in FHD3 are used as a veto.

It has been of interest for this experiment to determine the efficiency of the different options and to see if the results were well described by the WMC-code.

Again the reaction $pp \rightarrow d\pi^+$ at $T_p = 400$ MeV has been chosen to compare real data and Monte Carlo. This time, however, events have been selected where the deuteron and the π^+ both hit the Forward Detector, again only by using opening angles and coplanarities. This data set had the disadvantage, that only π^+ with angles $\Theta_{\pi^+} > 11^o$ have been detected, which stopped in FRH3. It contained also a small amount of background from $pp \rightarrow pn\pi^+$. The selected data samples have then been analysed using the different options for the π^+-identification

	WMC $pp \rightarrow d\pi^+$		real $pp \rightarrow d\pi^+$	
Option	events	percentage	events	percentage
1	3397	:=100%	55134	:=100%
2	2355	69%	30749	56%
3	2014	59%	27992	51%
4	2572	76%	37874	68%
5	2619	77%	38528	70%

Table 3.1: *Number of identified events for* $pp \rightarrow d\pi^+$ *at* $T_p = 400$ *MeV . The efficiencies are calculated with respect to the results for option 1.*

Tabular 3.1 gives an overview about the efficiencies of the different options. The tabulated values for WMC vary slightly with the thresholds, which were assumed for the long-range-TDC. According to [Bet 97] a 5 MeV threshold for FRH1 and 3 MeV for FRH2 to FRH4 have been used in the experiment.

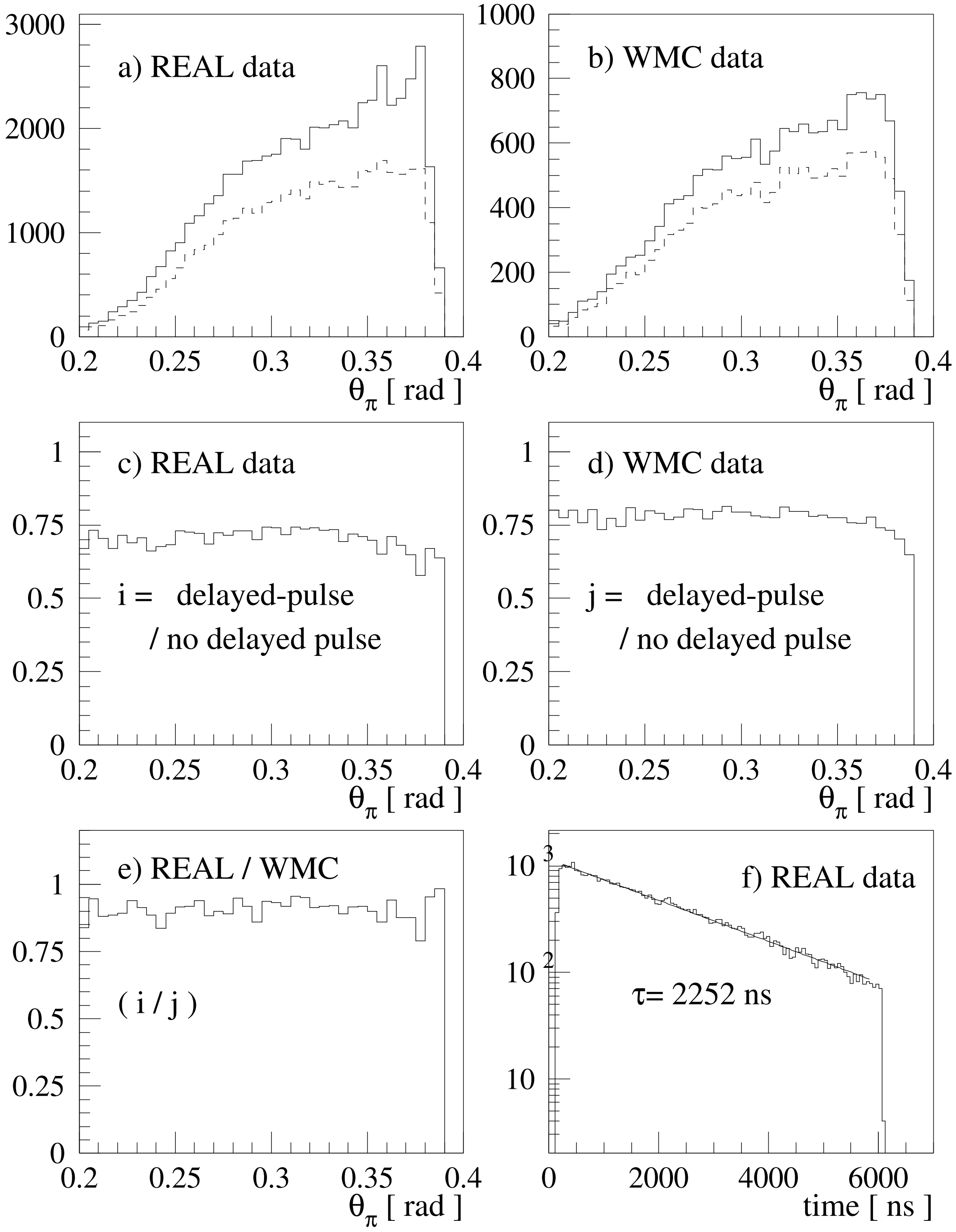

Figure 3.10: *a) and b) are angular distributions of* π^+*-hits from* $pp \rightarrow d\pi^+$ *at* $T_p = 400\,MeV$ *. The dashed histograms are subsamples, which were obtained if a delayed pulse was requested with option 5.*
c) and d) show the efficiencies (obtained from a) and b)),
e) compares these efficiencies for real data and Monte Carlo,
f) is the delayed pulse time distribution. The time constant is $2.252\mu s$ *for real data in comparison with* $2.225\mu s$ *for Monte Carlo.*

As expected option 5 gave the best efficiency, because it has included a larger number of elements into the search for delayed pulses than options 2 and 3 and has not set such a strict veto condition as option 4. However WMC seemed to overestimate the efficiency by a factor of 1.1, which is not understood in detail. One reason was certainly, that the number of π^+ in real data, which have been selected with the E/dE technique (option 1), still contained a small amount of background, which did not generate a delayed pulse. This would result in an underestimation of their delayed pulse efficiency. Other explanations could have been threshold effects for the long-range-TDCs or small shifts for their time-windows.

The small uncertainty for the efficiency of the π^+-identification with the delayed pulse technique was however acceptable, since it was comparable to the one for the deuteron-identification and its systematic error was smaller than the one for the simple E/dE method. Nevertheless it was also important to check that the delayed pulse technique did not introduce an angular dependence of the acceptance, which was not described by WMC. Therefore the π^+-angular distributions have been compared for results obtained with option 1 and 5 both for real data and WMC.

The results are shown in figure 3.10, where the angular distributions of the π^+ are compared for the two cases where option 1 (solid line) and 5 (dashed line) have been used for the analysis of real data (a) and WMC (b). As shown in c) and d) the efficiency does not depend on the pion angle except for the outer rim of the detector, where it drops slightly. This is however also well described by WMC, which can be seen in e) where the efficiencies for real data are divided by those obtained from WMC. Within the statistical limits WMC and real data differed only by a constant factor of 1.1, which is later on applied to correct the absolute cross sections for $dp \rightarrow dn\pi^+$. In total a systematic error of 15 percent is assumed for the efficiency of the π^+-identification.

The advantage of the delayed pulse technique can be clearly seen, if one looks at the E/dE plots and missing mass distributions for the reaction of interest, $dp \rightarrow dn\pi^+$ in figure 3.11. The background from e.g. punch through protons within the E/dE plot has been eliminated and the data sample is nearly free from background.

This can be also seen in figure 3.10 f) where the time distribution of the delayed pulses is shown. The measured time constant of $2.252\mu s$ reflects mainly the $2.197\mu s$ life time of the μ^+ (plus the $26ns$ for the π^+)[PDG 94] and compares favorably with a result of $2.225\mu s$ obtained from WMC. If one assumes a correct time calibration of the TDC, it is possible to estimate, that the background for π^+ from e.g. random coincidences or other particles is not more than one percent.

3.4.4 Photons

The ability of the PROMICE/WASA setup to detect γ's with the Central Detector was one of its main features. The direct measurement of the angles and energies of the decay-γ's from π^o or η allowed both the identification and momentum reconstruction of the neutral mesons. In addition γ's originating from Bremsstrahlungs reactions like $dp \rightarrow dp\gamma$ have been observed.

The energy resolution of the Central Detector has been found to be in the order of $\approx 10-15\%$ (FWHM) [Häg 97][Sch 95]. The angular resolution was mainly given by the granularity of the detector, but for events with multiple hits due to the spread of the electromagnetic showers a weighted average has been calculated with a resolution in the order of 5% FWHM [Häg 97].

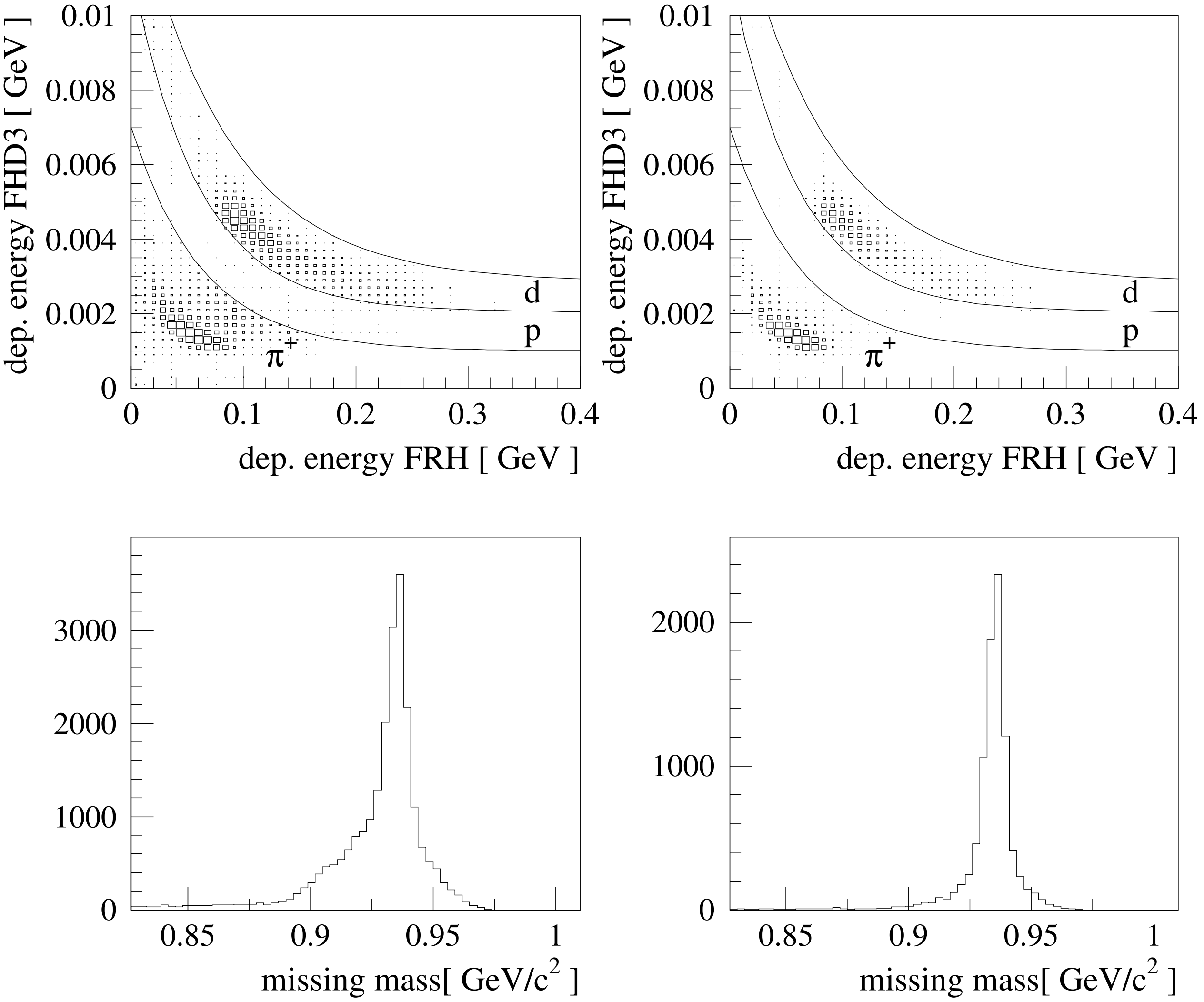

Figure 3.11: *E/dE-plots and missing mass distribution for selected events from the reaction* $dp \rightarrow dn\pi^+$ *at* T_d*=559 MeV. The left column shows events, where only the E/dE information (option 1) has been used to identify the* π^+ *while the right column also requests a delayed pulse with option 5.*

3.4.5 π^o

A π^o decays instantaneously ($\tau = 8.5 \cdot 10^{-17} s$) with a branching ratio of 98.8 percent into two γ's ([PDG 94]). Some of the γ's have then been detected with the two CsI modules of the Central Detector and the π^o has been identified by the $\gamma\gamma$ invariant mass as shown in figure 3.3. The width of the invariant mass peak was usually in the order of $\sigma = 10$ MeV and all $\gamma\gamma$ coincidences with an invariant mass between 70 and 170 MeV/c^2 were accepted as valid π^os. The background below the invariant mass peak has been estimated to be less than 5 percent at all energies and has been neglected throughout the analysis.

The reconstruction of π^os via $\gamma\gamma$ invariant masses was mainly performed for events with the hardware trigger T10. This trigger had an unknown efficiency in the order of 50 percent. Therefore no total cross sections will be calculated, based upon the direct identification of π^os.

3.4.6 Not Identified Particles

In principle it was possible to look for signals caused by the secondary interaction of **neutrons** from e.g. $dp \rightarrow dn\pi^+$ in the detector material. The signature of a neutron hit in the Forward Detector would have been a signal from at least one layer of the FRH with no signal from the corresponding elements of FHD. Nevertheless the information one could have got would have only been a rough estimation of the neutron azimuthal angle, which was limited by the granularity of the FRH. Since these signals were also not included in the hardware-triggers, no gain in acceptance could have been achieved.

Due to the reaction kinematics neutrons hitting the Central Detector have only been expected for the reaction $dp \rightarrow ppn$ (or $dp \rightarrow ppn\gamma$). Such neutron hits have not been examined since the hardware trigger conditions were selected to discriminate most of these events.

Therefore no attempt has been made to use the PROMICE/WASA experiment for direct neutron detection.

The only reaction expected to produce a $\boldsymbol{\pi^-}$ was $dp \rightarrow ppp\pi^-$. It would have been nice if one had detected the π^- the same way as the π^+, but unfortunately this was not possible due to its negative charge. The different sign of the charge had the consequence that the π^- formed pionic atoms with the nuclei of the detector and had therefore a much higher probability for a hadronic interaction within the detector material than the π^+. Therefore it has not been possible to use the delayed pulse technique for the π^- identification. An attempt has however been made to look also for delayed pulses within the events of $dp \rightarrow ppp\pi^-$ shown in figure 3.15. In total four π^- candidates have been found (in agreement with WMC).

As a consequence no further attempts have been made to look for π^-.

In principle it was also possible to identify $\mathbf{^3H}$ and $\mathbf{^3He}$ in the Forward Detector using E/dE techniques, but the kinematics of the reactions $dp \rightarrow {}^3\mathrm{He}\pi^o$ and $dp \rightarrow {}^3\mathrm{H}\pi^+$ forced most of the heavy nuclei into the forward cone of the beam-pipe, which reduced the acceptance of the Forward Detector to a minimum. An attempt to identify events from $dp \rightarrow {}^3\mathrm{He}\pi^o$ using the $\gamma\gamma$ trigger of the Central Detector did not show any positive results. $dp \rightarrow {}^3\mathrm{H}\pi^+$ has not been covered by one of the hardware triggers and could therefore not be examined.

Electrons and **positrons** originating from e.g. pion decays or conversion of high energetic photons were only considered as background for other particles. No attempt has been made to identify them directly, for example to reconstruct the Dalitz decay of the neutral pion.

3.5 Energy Reconstruction

The energy calibration of the PROMICE/WASA detector has been performed for protons. However, the scintillation efficiency, defined as the fraction of ionization energy converted to fluorescent light energy, depends on the type of the charged particle producing the ionization [Cra 70]. Electrons generate more light than do heavy particles (e.g. protons or deuterons) of equal energy when stopped in the scintillator. The response to electrons is linear except for very small particle energies of less then 100 keV . For heavier particles it is nonlinear up to much higher energies. The effect of this non-linearity is often called *quenching* and has been examined for several particles and scintillator types in general (e.g. [Goo 60], [Bir 64], [Cra 70], [Bec 76]) and for the PROMICE/WASA setup in particular (e.g. [Wat 93b], [Zlo 93]). For protons the response functions are well described even up to high energies. However, for deuterons and in particular for pions available data is scarce and the necessary corrections applied had to be checked with known reactions like $pp \rightarrow d\pi^+$.

The results applied in this thesis are based upon the parameterization obtained in [Zlo 93]. The parameterization relates the light output L (in arbitrary units) with the deposited energy ΔE (in units of MeV) via

$$L = A_1 \Delta E - A_2 \left(1 - e^{-A_3 \Delta E^{A_4}}\right) \tag{3.8}$$

and

$$\Delta E = B_1 L + B_2 \left(1 - e^{-B_3 L^{B_4}}\right) \tag{3.9}$$

with the parameters ([Zlo 96]):

Parameter	Protons	Deuterons	π^+
A_1	0.95842	0.94861	0.97720
A_2	9.7621	17.913	2.0387
A_3	0.092224	0.058884	0.29650
A_4	0.77388	0.78967	0.65941
B_1	1.0295	1.0213	1.0201
B_2	12.792	29.820	2.3560
B_3	0.16465	0.10641	0.37157
B_4	0.55597	0.52635	0.51469

For all particles the kinetic energies obtained with the PWREC procedure were in a first approximation calculated based upon calibration constants and quenching parameters for protons. As a consequence for deuterons and π^+ the energies had to be corrected by calculating the light output for protons with equation 3.8 and inserting the result into equation 3.9 with the appropriate parameters.

3.6 Event Identification

This section describes the final step of the event reconstruction process, the identification of the event type. While the procedures for the track reconstruction, particle identification and energy reconstruction of the tracks have been identical for all events, the conditions for the final identification of an event depended on the event type and are discussed now.

3.6.1 $dp \to dp\pi^o$

The identification of the $dp \to dp\pi^o$-reactions has been based upon three different approaches:

- by requiring two charged tracks in the Forward Detector (FDCFDC), which were identified as a deuteron and a proton, and by identification of the π^o via missing mass;
- by requiring two charged tracks in the Forward Detector (FDCFDC), which were identified as a deuteron and a proton, and by reconstruction of the π^o via missing mass and by requiring at least one γ-hit in the Central Detector (CDN);
- by requiring one charged track in the Forward Detector (FDC), which was identified as a deuteron, and by identification of the π^o from the invariant mass of two γ's hitting the inner crystals of the Central Detector (CDNCDN).

All three cases required the identification of the deuteron to clearly distinguish the reaction from $dp \to ppn\pi^o$.

For all three cases a set of energy dependent selection criteria (*cuts*) has been applied, which were given by the kinematics of the reaction. They have included maximum angles and energies of the forward going deuterons and protons and are listed in table 3.2.

$dp \to dp\pi^0$

T_d [MeV]	$\Theta_{d,max.}$ [^{o}]	$E_{d,max.}$ [MeV]	$\Theta_{p,max.}$ [^{o}]	$E_{p,max.}$ [MeV]	additional conditions
558	16	370	-	290	
514	15	350	-	250	
491	14	350	-	230	
454	11.5	290	-	180	No hits in FRH4
436	10.5	280	16	120	No hits in FRH3 or 4

Table 3.2: *The energy dependent selection criteria for* $dp \to dp\pi^0$.

During the data acquisition the hardware-trigger, which required two charged particles in the Forward Detector has been modified at the two lowest energies. In addition to the FVH the last ($T_d = 455 MeV$) or the last two ($T_d = 437 MeV$) layers of the Range Hodoscope (FRH 3 and FRH 4) have been used as a veto to suppress background. These trigger-conditions did not affect the detector acceptance for the pion production reactions but they reduced the acceptance for the proton of the Bremsstrahlungs reaction $dp \to dp\gamma$, which has not been considered during the planning period of the experiment.

FDCFDC and FDCFDCCDN

The identification of those events where the proton and the deuteron have hit the Forward Detector (FDCFDC) was based upon the two charged particle trigger **PTWJ12V** and gave the best statistics for this reaction. It covered most of the phase space but excluded events with the (assumed) spectator proton being emitted into the beam pipe.

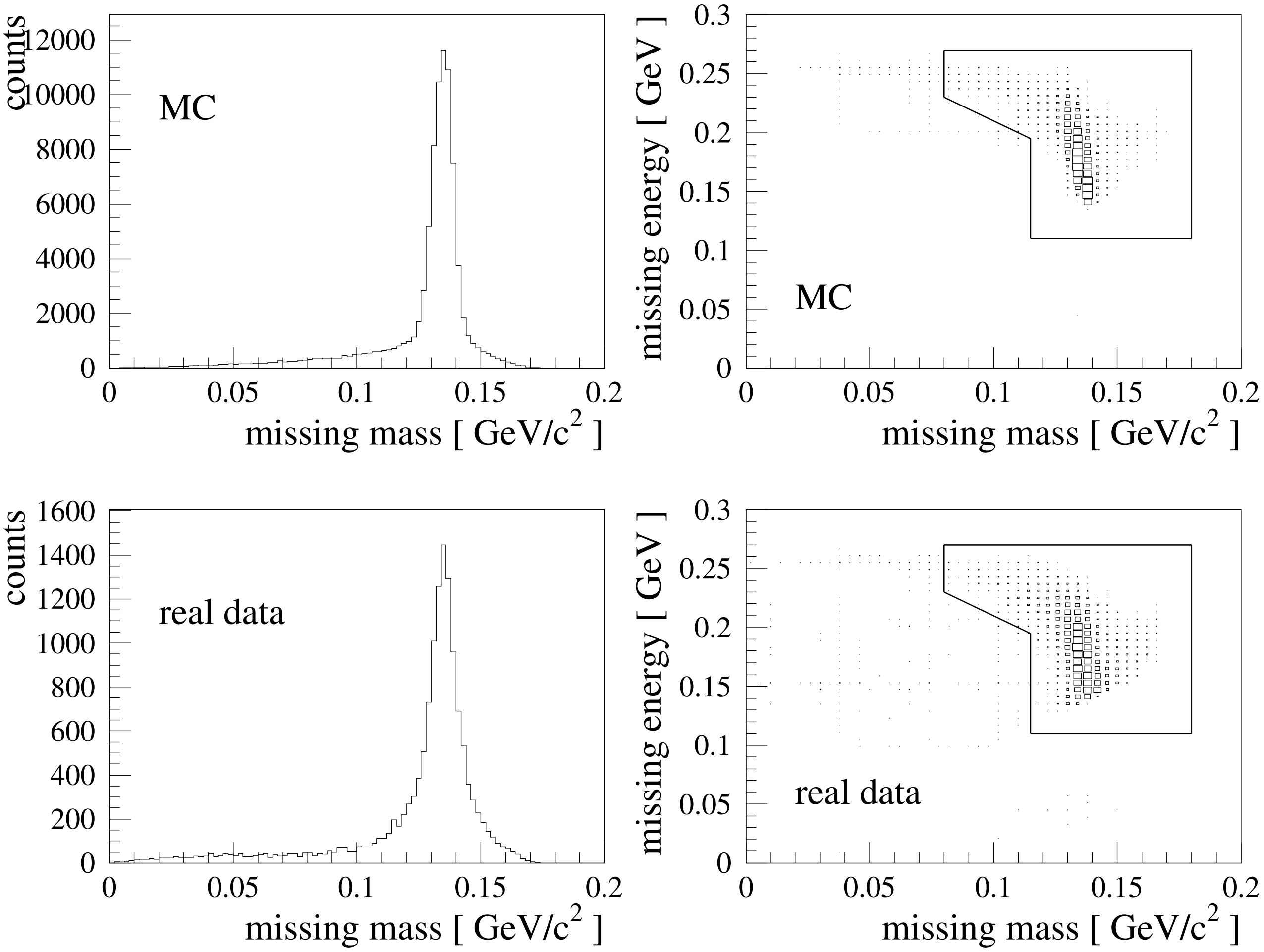

Figure 3.12: *Missing Mass distributions for* $dp \rightarrow dp\pi^o$ *at* $T_d = 559\,MeV$ *for Monte Carlo and experimental data. The right column shows the missing mass distribution plotted against the* π^o *energy and the applied missing mass cut.*

A missing mass distribution obtained at the highest beam energy of $T_d = 559MeV$ is shown in figure 3.12 in comparison to a result from WMC. The distribution in the left column shows a tail to lower masses, which is only partly due to underlying background reactions like $dp \rightarrow dp\gamma$ and $dp \rightarrow ppn$, but it also includes good events from $dp \rightarrow dp\pi^o$. This interpretation can be deduced from the two dimensional plot in the right column, where the missing mass distribution is plotted against the missing energy of the proton and deuteron, which is equivalent to the π^o energy in the lab system. For events with large π^o energies the deuteron and proton had small relative momenta and were therefore more likely emitted into neighboring areas of the Forward

Detector closer to the beam pipe. For these events the accuracy of the energy reconstruction decreased and resulted in smaller missing masses, which was however well reproduced by Monte Carlo simulations. As a consequence the final event samples have been selected with the two dimensional cuts within the missing-mass versus missing-energy plot. The limits varied with the beam energy and have been taken from Monte Carlo simulations.

The quality of the data concerning background suppression has been improved significantly, if the detection of a γ-hit in any of the CsI-crystals of the Central Detector was required (CDN). This reduced the event-statistics by about a factor of three but did not significantly affect the detector acceptance within phase space, since the γ-angular distributions did not depend much upon the momentum distribution of the π^o.

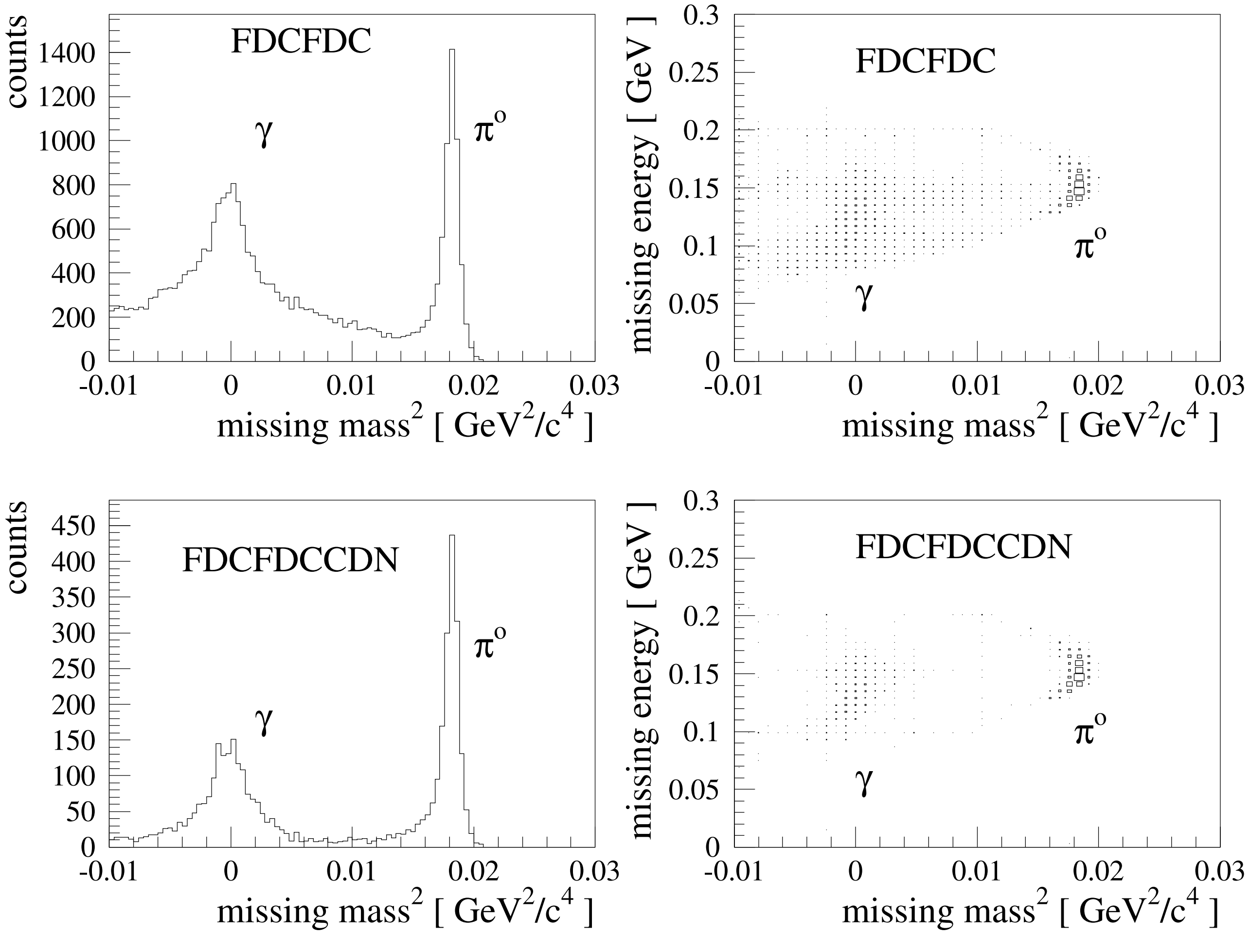

Figure 3.13: *The squared missing mass distributions for events with one deuteron and one proton identified within the Forward Detector at a beam energy of $T_d = 455\,MeV$. The energy dependent selection criteria from table 3.2 have been applied here. The upper two plots show the whole set of data while the lower plot shows the subsample, which was obtained if an additional γ-hit was requested within the Central Detector .*

The result of the additional γ-hit-condition is shown in figure 3.13 for the beam energy of $T_d = 455 MeV$, where the underlying background seemed to be strongest without the condition. Using this additional constraint the background for the π^o production was reduced to a negligible minimum.

The analysis has lateron been performed both with and without the requirement of the γ hit and both procedures have produced similar cross sections, which are later shown in figure 4.19. The results concerning the contributions of different production mechanisms, which are explained later on, are however mainly based upon those events where a γ had been detected to reduce the effects of background contributions to a minimum. Only at the lowest energy of 437 MeV the requirement of a γ-hit has not been used, due to the limited available statistics.

As shown in figure 3.13 the analysis of the $dp \to dp\pi^o$ reaction revealed also a data sample of dp events with a single γ in the outgoing channel. This will be later on referred to as 'Bremsstrahlung'. The procedures to extract these events will be discussed in section 3.6.5.

FDCCDNCDN

The identification of $dp \to dp\pi^o$ events using the Central Detector for the π^o identification was also possible. I had the advantage, that it did not require a proton-hit in the Forward Detector. However, the deuteron had to be identified to separate the reaction from $dp \to ppn\pi^o$.

The requirement of the two decay-γ's (CDNCDN) in coincidence with the identified deuteron in the Forward Detector (FDC) gave already a clean missing-mass distribution around the proton mass (figure 3.14). In addition the energy dependent selection criteria in tabular 3.2 have been applied accordingly.

However, this approach had to be based upon the hardware-trigger **T10**, set for two neutral hits in the Central Detector . The efficiency of this hardware-trigger has proved to include a possible systematical uncertainty of up to 50 percent. As a result no absolute cross sections are later on calculated, using this approach of event identification. The analysis of $dp \to dp\pi^o$ concerning the contributions of different reaction mechanisms has also not been based upon this approach, if not explicitly stated otherwise.

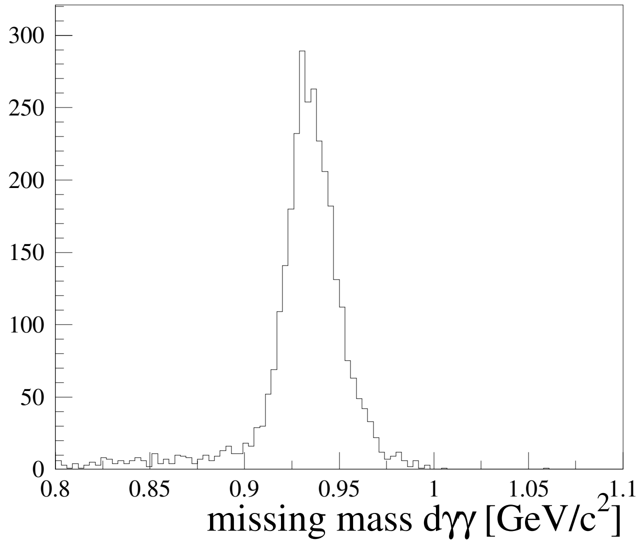

Figure 3.14: *Missing mass of a deuteron and two γ's of the reaction $dp \to dp\pi^o$ at T_d=559 MeV.*

3.6.2 $dp \to dn\pi^+$

The $dp \to dn\pi^+$ data samples have been selected under the condition of a deuteron identified with E/dE methods and a π^+ identified with option 5 for the delayed pulse technique. Similar to $dp \to dp\pi^o$ a set of energy dependent cuts has been applied, which is given in table 3.3.

As explained in section 3.4 the requirement of the delayed pulse gave a very clean π^+ data sample (figure 3.11) and in the following analysis possible contributions from background

$dp \to dn\pi^+$

T_d [MeV]	$\Theta_{d,max.}$ [^{o}]	$E_{d,max.}$ [MeV]	$\Theta_{\pi^+,max.}$ [^{o}]	$E_{\pi^+,max.}$ [MeV]	other conditions
559	15.5	370	-	170	
515	14	340	-	160	
492	11.5	320	-	150	

Table 3.3: *The energy dependent selection criteria for* $dp \to dn\pi^+$.

reactions have therefore been neglected.

The analysis of $dp \to dn\pi^+$ has only been possible at the beam-energies of T_d =492, 515 and 559 MeV. At the lower energies of T_d =437 and 454 MeV the detector acceptance for the deuteron became too small. Here the deuterons were emitted into the beam pipe due to the higher threshold of T_d =433 MeV for this reaction.

3.6.3 $dp \to ppp\pi^-$

$dp \to ppp\pi^-$ was the only reaction discussed here with more than two charged particles in the outgoing channel. The signature of this reaction was therefore quite different from those of the $dp \to dNx$ reactions.

On the one hand it has been easier to identify, since there were no implications concerning the effects of deuteron secondary interactions. On the other hand the reliable identification of a π^- has in practice not been possible with the Forward Detector due to its large probability for hadronic interactions within the detector. As a result the identification of the $dp \to ppp\pi^-$-reaction was only based upon the reconstruction of three protons.

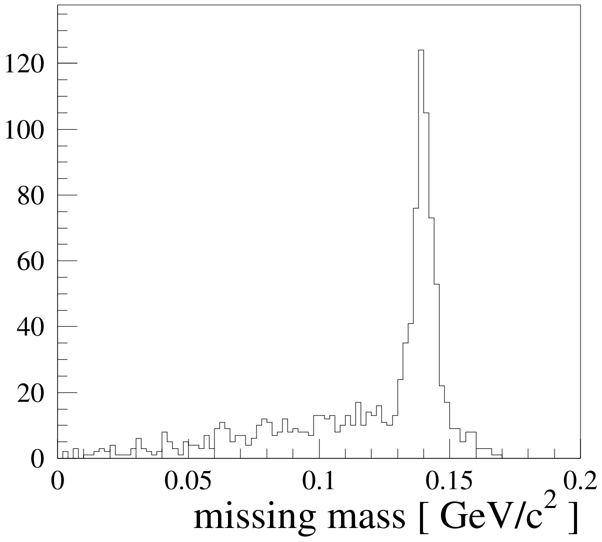

Figure 3.15: *missing mass distribution for the reaction* $dp \to ppp\pi^-$ *at* T_d*=559 MeV.*

It has to be noted that for this reaction the standard track finding procedures did not give the best results. The analysis of $dp \to ppp\pi^-$ can in fact be well compared to the problems, which occurred in the analysis of $pp \to pp\pi^+\pi^-$, that has also been measured with the PROMICE/WASA setup [Joh 99],[Bro 99]. The fact that up to four charged particles have hit the Forward Detector increased the number of ambiguities during the track reconstruction procedure and more sophisticated methods could have been applied to increase the efficiency of the track reconstruction.

Since the analysis of this thesis focussed on the $dN\pi$-reactions the reconstruction of $dp \to ppp\pi^-$ has been performed only using the standard track finding procedures in connection with

E/dE particle identification (figure 3.7).

The requirement of three coincident protons gave a significant peak at the missing mass of the π^- but it still contained background (figure 3.15). In contrast to the $dp \to dp\pi^o$ or $dp \to dn\pi^+$ the statistics were quite limited for this reaction and there was also no extra condition, that could have been applied as an additional constraint to distinguish the $dp \to ppp\pi^-$-events from the underlying background. Therefore the quality of the $dp \to ppp\pi^-$ sample has to be considered with some caution and it is later on only used for an *estimation* of the total cross sections, which are about two orders of magnitude smaller than the comparable cross sections for $dp \to dN\pi$.

3.6.4 $dp \to ppn\pi^o$

The second four body channel with single pion production is $dp \to ppn\pi^o$ for which an attempt has been made to extract events too. These events have been identified by detection of two protons with the Forward Detector and the π^o via $\gamma\gamma$ coincidence in the Central Detector .

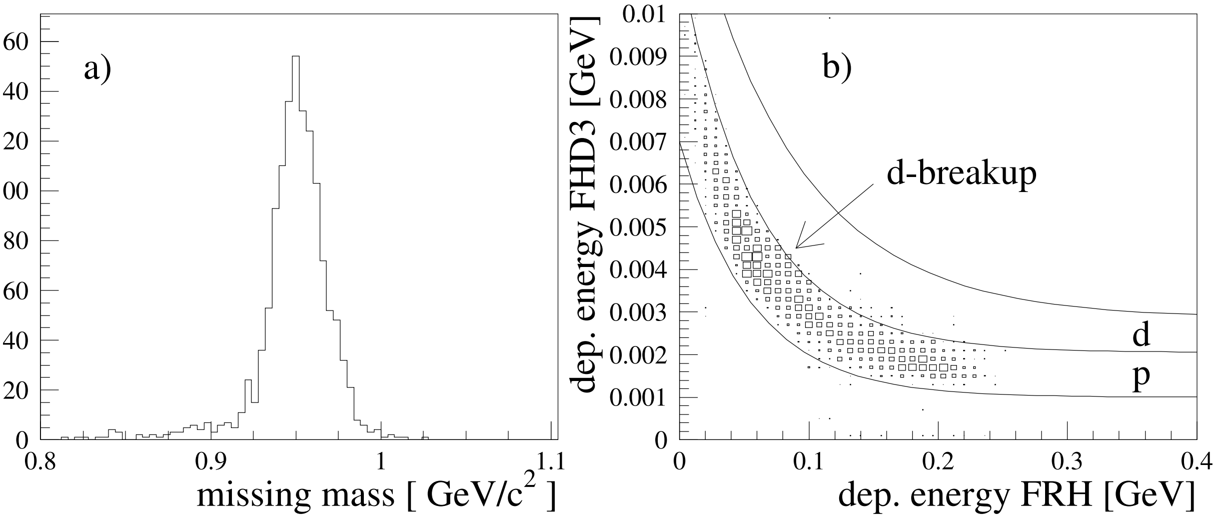

Figure 3.16: *missing mass distribution (a) and EdE-plot (b) for the reaction* $dp \to ppn\pi^o$ *at* T_d*=559 MeV.*

The missing mass distribution of the three detected particles shows a pronounced peak approximately around the neutron mass with up to 1300 events at $T_d = 559\,\mathrm{MeV}$ (figure 3.16a). Its width of $\sigma \approx 15 MeV/c^2$ and the fact that it is shifted to more than $950 MeV/c^2$ can however not only be attributed to uncertainties of the detector calibration. The explanation has been extracted from the E/dE plot of the 'identified' protons (figure 3.16b). In contrast to other reactions like e.g. $dp \to ppp\pi^-$ (figure 3.7) the proton band for $dp \to ppn\pi^o$ is smeared out towards the deuteron band. This effect can only have been caused by the deuteron breakup of the reaction $dp \to dp\pi^o$, which has already been discussed in section 3.4.2. Events from $dp \to dp\pi^o$ are then misidentified as $dp \to ppn\pi^o$.

It was extremely difficult to separate the $dp \to dp\pi^o$-background on an 'event by event' basis and therefore it was not possible to give reliable absolute cross sections for $dp \to ppn\pi^o$. Data has rather been used to fit the experimental spectra with different model calculations, which have included assumed production mechanisms for $dp \to ppn\pi^o$ as well as contributions from $dp \to dp\pi^o$ background.

The analysis of $dp \to ppn\pi^o$ has then always yielded upper limits for their total cross sections, which were at least one order of magnitude below the corresponding ones for $dp \to dp\pi^o$, so that the $dp \to ppn\pi^o$ contribution as background for $dp \to dp\pi^o$ could be easily neglected, but not vice versa.

3.6.5 $dp \to dp\gamma$

As shown in section 3.6.1 the triggers set for the pion production $dp \to dp\pi^o$ yielded automatically several thousand events of the 'Bremsstrahlungs'-reaction $dp \to dp\gamma$ at all beam energies. The observation of these large number of events was surprising and interesting in itself. To estimate their contribution as possible background for $dp \to dp\pi^o$, to check the detector performance and to satisfy curiosity an attempt has been made to extract these events.

The applied procedure was very similar to the one that has been used for $dp \to dp\pi^o$, namely identification of deuteron and proton in the Forward Detector.

However, in contrast to the π^o-production mechanism the Bremsstrahlungs reaction did not allow strict cuts on the deuteron or proton distributions within the Forward Detector. The opening angles between the proton and the deuteron and therefore also their maximum relative momenta were limited only by the outer rim of the Forward Detector. As a result a cut has only been applied on the maximum deuteron energy. This energy dependent cut is listed in table 3.4.

While the cut on the deuteron energy did not affect the detector acceptance for this reaction, the hardware trigger conditions, which have been set to reduce the background for the pion production reactions, resulted in a limited acceptance for the protons of the Bremsstrahlungs reaction. The use of the last or last two layers of the FRH as a veto at the two lower energies limited the maximum kinetic energy of the protons. This effect can be observed in the proton energy spectrum in figure 4.27 at $T_p \approx 250$ MeV, but can of course be reproduced with the Monte Carlo simulation.

$dp \to dp\gamma$

T_d [MeV]	$\Theta_{d,max.}$ [^{o}]	$E_{d,max.}$ [MeV]	$\Theta_{p,max.}$ [^{o}]	$E_{p,max.}$ [MeV]	other conditions
559	-	370	-	-	
515	-	350	-	-	
492	-	350	-	-	
455	-	340	-	-	No hits in FRH4
437	-	330	-	-	No hits in FRH3 or 4

Table 3.4: *The energy dependent selection criteria for* $dp \to dp\gamma$.

As it has already been observed in figure 3.13 the data samples, which were only based upon the identification of two charged tracks as a deuteron and a proton, still contained some background. While this background usually accounted for less than ten percent of the π^o-events it contributed to more than fifty percent of the possible γ-events. As a result it has been crucial for the examination of $dp\gamma$ to require the γ-hit in one of the crystals of the Central Detector,

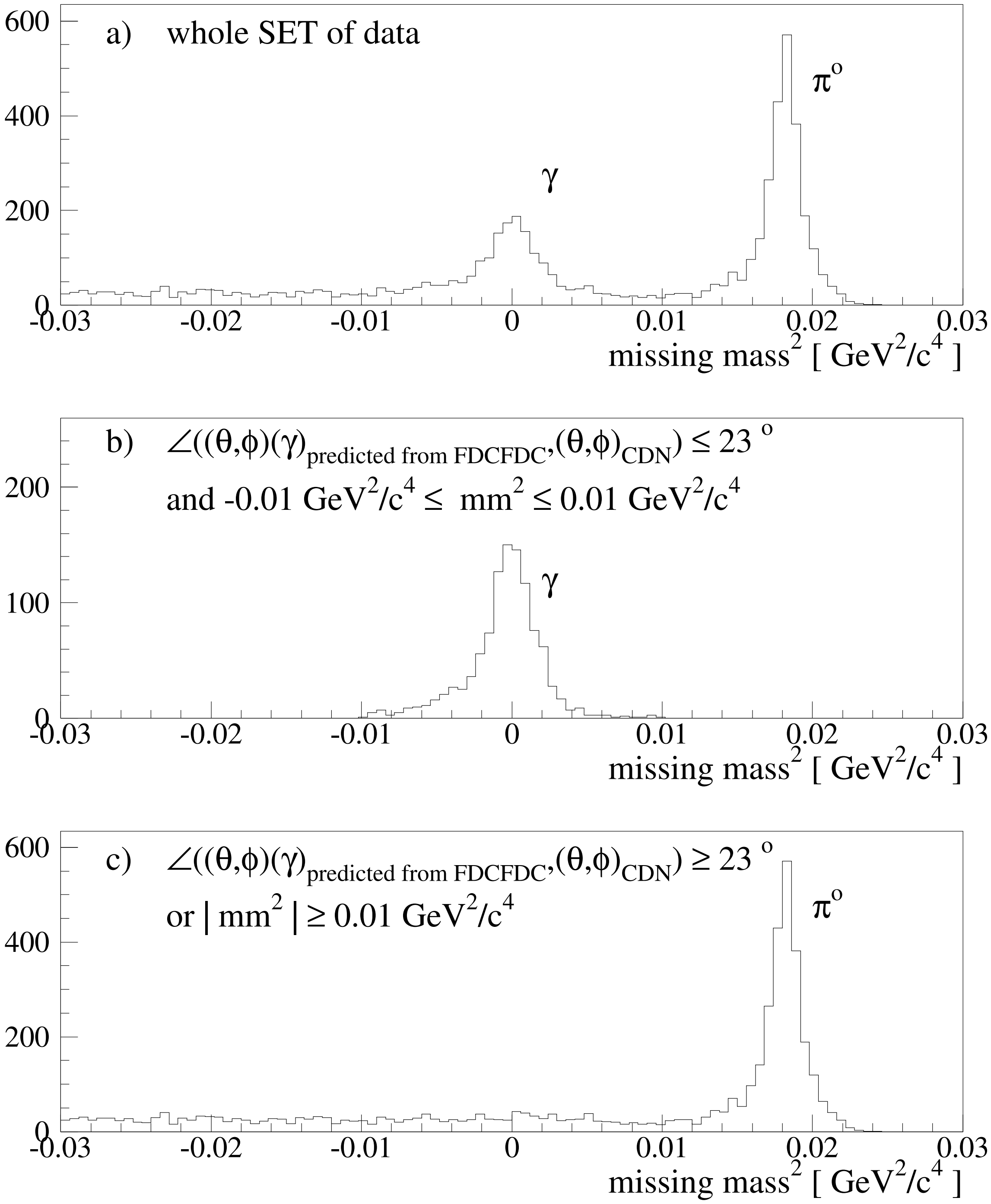

Figure 3.17: *The squared missing mass distributions of possible* $dp\gamma$ *events at a beam energy of* $T_d = 492$ *MeV. a) shows the event sample, which has been obtained under the condition of an identified deuteron and an identified proton plus one neutral hit in the Central Detector (CDN). b) shows the remaining event sample under the additional constraint on the* γ*-angle and after a cut on the squared missing mass. c) is the complement to b) and contains the background.*

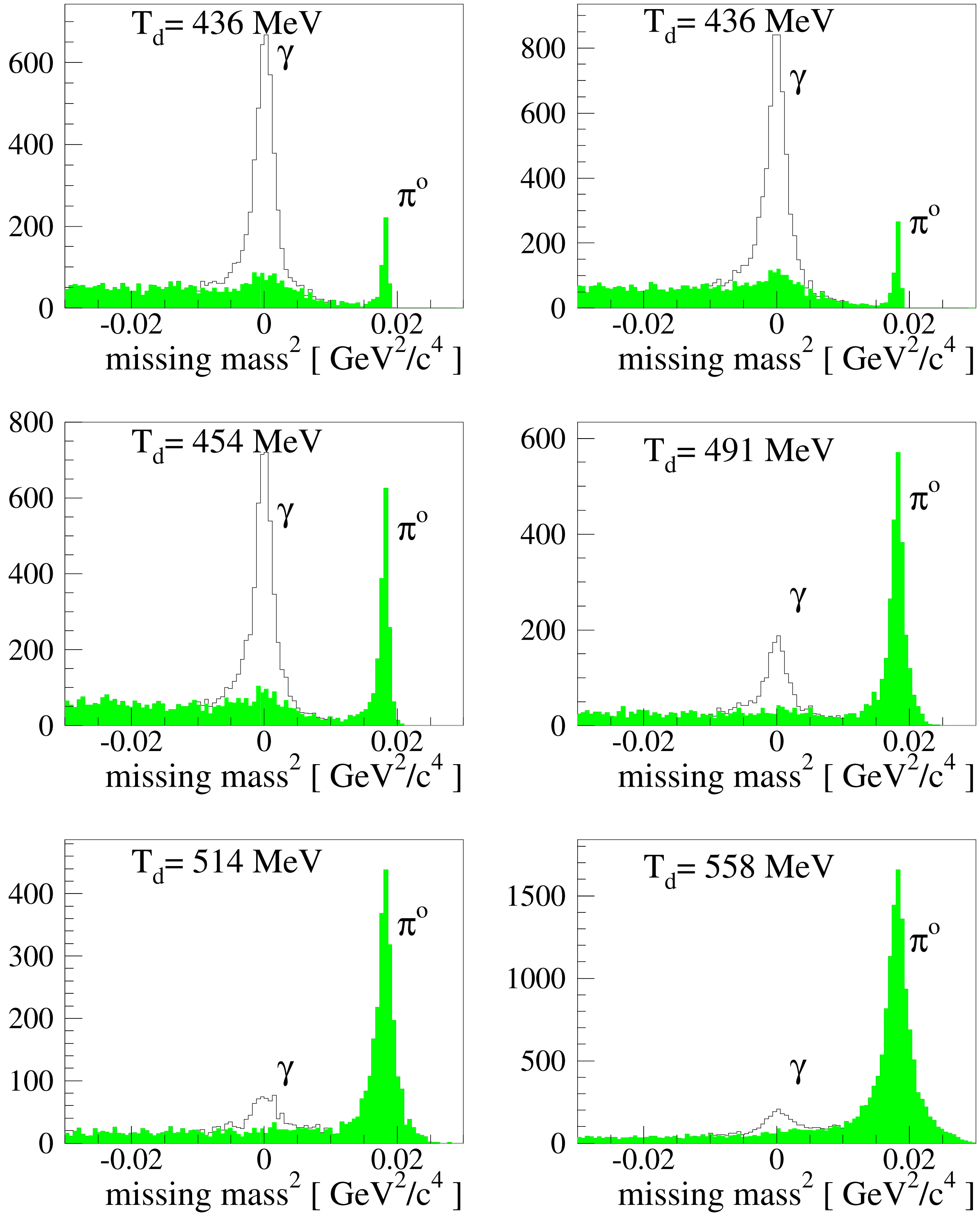

Figure 3.18: *Squared missing-mass distribution for preselected events for all projectile energies under study. The dpγ-events (white) are separated from the background (grey). The decreasing statistics for the γ-events at higher energies reflects only the different integrated luminosities.*

even if this reduced the acceptance. With this detection of the third ejectile the resulting event sample was overdetermined, and this has then been used to separate the remaining background.

Both, direction and energy of the γ could be predicted from the measured momenta of the proton and the deuteron and have then been compared with the measured results. The energy information of the Central Detector was however only reliable, if the γ did not hit the outer crystals because otherwise energy leakage effects of the electromagnetic showers came into play. To exclude theses effects one would have had to limit the analysis to those events with a maximum energy deposition within the *inner* crystals, which would then have reduced the detector acceptance by another factor of two. Therefore only the angular information, given by the granularity of the Central Detector, has been used as a further constraint to separate good events from background.

The final condition to accept a $dp\gamma$ event was, that the predicted γ-angle did not deviate by more than 23^o in the laboratory system from the measured angular information obtained with the Central Detector. In addition a generous cut on the squared missing mass has been applied ($|mm^2_{dp}| \leq 0.01 GeV^2/c^4$) to exclude possible random coincidences mainly from the π^o-decays. The quality of these cuts is shown in figure 3.17 for the energy of $T_d = 492\,\mathrm{MeV}$. With these cuts it was possible to extract clean $dp \to dp\gamma$ data samples at all energies. Figure 3.18 shows them together with the separated background. The discussion of these event-samples continues in section 4.5.

3.6.6 Other Reaction Channels

Other possible reaction channels have not been examined in detail for the following reasons:

- $\boldsymbol{dp \to {}^3\mathrm{H}\pi^+}$, $\boldsymbol{dp \to {}^3\mathrm{He}\pi^o}$ and $\boldsymbol{dp \to {}^3\mathrm{He}\gamma}$

  All these reactions had a particle with the mass number A=3 in the final state. The use of inverse kinematics forced them into a narrow forward cone and in most cases the particles escaped undetected into the beam pipe. None of these reactions has been covered by the main hardware-trigger PTWJ12V.

- $\boldsymbol{dp \to pnn\pi^+}$

  The identification of this reaction would have required to use the PROMICE/WASA experiment for neutron detection. Since the efficiencies were not well known, this has not been tried.

- $\boldsymbol{dp \to ppn}$ and $\boldsymbol{dp \to ppn\gamma}$

  As described in section 2.4 the use of the downstream veto FVH as a hardware-trigger condition has been applied to suppress the background from these reactions. As a result no attempt has been made to identify them during the offline analysis.

Chapter 4

Results and Discussion

Overview

In the previous chapters it has been shown, that the analysis yielded data sets of up to 6 observables for several reactions at different energies. These data sets will be discussed now in comparison with different reaction models, that have been implemented in the Monte Carlo event generation process for the GEANT detector simulation WMC.

Both, experimental and Monte Carlo data sets, consist of histograms like e.g. energy- and angular-distributions in the lab-system, which are both *not* corrected for the acceptance of the detector. In order to find the best description of the experimental data in terms of these models a general fitting procedure has been applied and the results of this procedure have then been used to discuss the contributions of possible reaction mechanisms and to calculate the total cross sections for four of these reactions.

In the subsequent sections 4.1 and 4.2, the determination of the detector acceptance and the fitting procedure for a decomposition of the experimental distributions into fractions associated with different reaction mechanisms are described in general terms. These tools are then applied to the four reactions $dp \rightarrow dp\pi^o$, $dp \rightarrow dn\pi^+$, $dp \rightarrow ppp\pi^-$ and $dp \rightarrow dp\gamma$ and the results are discussed in greater detail, in particular for the first two reactions.

4.1 Acceptance

The extraction procedures for the different experimental distributions with N_{exp} extracted events and for the luminosities have been described in chapter 2 and 3. According to

$$\sigma_{tot} = \frac{N_{exp}}{L\epsilon_{PW}} \tag{4.1}$$

the last ingredient necessary to extract the total cross sections is the acceptance ϵ_{PW} of the detector. Since the PROMICE/WASA experiment was not able to detect all events, the acceptance was always below one. It has been reduced by :

- the geometrical limits of the detector, e.g. the beam pipe, the outer rim of the Forward Detector, the limited angular range covered by the Central Detector etc.
- the detection efficiency for different particles, e.g. the limited efficiency for deuteron detection due to secondary interaction losses, the efficiency of the delayed pulse technique for π^+, etc.

- the efficiency of the hardware trigger. For example the requirement of hits in *two* elements of the first two layers of FHD (Trigger PTWJ12V) reduced the acceptance, whenever these two particles have randomly hit the same element in the spiral planes of the hodoscope (compare figure 2.6).
- the efficiency of the analysis code.

This means, that for a reaction with two detected particles the acceptance is a function depending on at least six different parameters namely the particle energies and angles:

$$\epsilon_{PW} = \epsilon(\Theta_1, \Theta_2, \Phi_1, \Phi_2, E_1, E_2) \tag{4.2}$$

In practice it has not been possible to determine such a function in a parameterized or tabulated way. Instead the Monte Carlo Simulation WMC has been used to extract the acceptance by comparing the number of simulated events with the subset of reconstructed events. The acceptance is then given as

$$\epsilon_{MC} = \frac{N_{rec}}{N_{gen}} \tag{4.3}$$

with

N_{gen} : Number of generated events, used as input for WMC
N_{rec} : Number of WMC-events, reconstructed by PWREC

Following this approach the acceptance is correctly defined under the assumption that (*i*) WMC gave a realistic description of the detector and (*ii*) the right population of the events in phase space has been given as input for WMC.

The detector description of WMC has been cross checked as a part of this thesis (compare e.g. chapter 3.4) and also in several other works (e.g. [Bet 97], [Bro 95], [Dyr 97], [Häg 97], [Joh 99], [Kur 95], [Mör 95], [Sch 95]). The errors caused by the Monte Carlo description of the detector are therefore expected to be small.

The population of phase space, however, depends on the reaction mechanism thus with the reaction model adopted. The output of these models had to *fit* the experimentally observed spectra, like e.g. energy or angular distributions. This requirement is obviously restricted to the regions of nonvanishing detector acceptance. Regions of phase space not covered by the detector had to be filled in Monte Carlo mode according to the models, which were describing the experimentally observed data best. This approach is justifiable, if the detector covers a large fraction of phase space. Nevertheless it can introduce significant systematical errors, if only small areas of phase space are within the detector acceptance and the models fail to describe the invisible parts.

Since the acceptance of the detector was very different for the reactions of interest the acceptance will be later discussed in more detail for each reaction channel individually.

A general fitting procedure has been applied in all cases to extract the weight of the production mechanisms contributing to the experimentally observed spectra. It will we described now.

4.2 Fitting Procedure

Although the input for the fitting procedure from the experiment and from Monte Carlo varied with the type of reaction, the general structure of the procedure was in all cases the same.

The analysis of the experimental data sets using PWREC yielded a set of observables r consisting of e.g. energy and angular distributions. They have been stored in the format of histograms using HBOOK [CERN 95b]:

$r(i,j)$: number of experimentally observed events

with

$i = 1,\ldots,I$: histogram-id
$j = 1,\ldots,J(i)$: bin of histogram i;
(only bins with contents $r(i,j) > 0$ were included in the fitting procedure)

For each of the reaction models N_0 Monte Carlo events have been generated and processed with WMC. Similar to the experimental data set $r(i,j)$ these events have then been analysed with PWREC and yielded the corresponding histograms

$m_K(i,j)$: number of reconstructed WMC events

with the index

$K = A,\ldots,N$: physical models

The aim of the fitting procedure was now to find a set of weighting factors $(a,b,\ldots,n)$, describing the experimental data $r(i,j)$ in a reasonable way.

$$r(i,j) \approx f(i,j) = a \cdot m_A(i,j) + b \cdot m_B(i,j) + \ldots + n \cdot m_N(i,j) \tag{4.4}$$

The function $f(i,j)$, containing the *incoherently* added spectra of the models A to N, is usually called a *fit* and it was requested, that all parameters $a,b,\ldots,n$ were not negative. To judge on the quality of the fit a $\chi^2(a,b,\ldots,n)$ has been defined:

$$\chi^2(a,b,\ldots,n) = \frac{1}{I}\sum_{i=1}^{I}\frac{1}{J(i)}\sum_{j=1}^{J(i)}\frac{\left(r(i,j)-f(i,j)\right)^2}{r(i,j)} \tag{4.5}$$

Per definition the *best fit* of the experimental data was achieved at the minimum of $\chi^2(a,b,\ldots,n)$ and the tool, that has been used to minimize χ^2 was the MIGRAD routine implemented in MINUIT [CERN 94a],[Gre98]. The values $a,b,\ldots,n$ at the minimum of χ^2 represent the relative contributions of the different reaction mechanisms to the total cross section of the reaction under study.

The number of events N_{gen}, which had to be generated to get the best fit with the smallest $\chi^2(a,b,\ldots,n)$ was then

$$N_{gen} = N_0 \cdot \sum_{k=a}^{n} k \tag{4.6}$$

and using equations 4.1 and 4.3 with $N_{rec} \approx N_{exp}$ and $\epsilon_{PW} \approx \epsilon_{MC}$ one can calculate the total cross sections

$$\sigma_{tot} = \frac{N_{gen}}{L} \tag{4.7}$$

For data sets with a prescaled hardware-trigger the prescaling factor P had to be multiplied to the total cross section.

This approach required, that the number of events N_0 processed with the Monte Carlo simulations was large in comparison with the experimental data, because otherwise the statistical error of the Monte Carlo data had to be considered. To minimize the statistical error caused by the Monte Carlo simulation, $N_0 = 10^6$ events have been generated and processed for each model. Since later on between two and ten models have been applied, in total up to 10^7 Monte Carlo events have been used to describe experimental data samples, which itself did not contain more than 10^5 events. As a result the *statistical* errors caused by the Monte Carlo data have been neglected.

4.3 Discussion of $dp \to dp\pi^o$ and $dp \to dn\pi^+$

For the main reaction of interest, $dp \to dp\pi^o$, the applied physical models will be described in more detail now and are discussed in comparison with the experimental results. $dp \to dn\pi^+$ is expected to be isospin related to $dp \to dp\pi^o$, if a pure quasifree reaction mechanism is assumed. The models for $dp \to dp\pi^o$ were therefore also applied for $dp \to dn\pi^+$ and the results will also be shown although the detector acceptances differed significantly.

4.3.1 Reaction Mechanisms for $dp \to dN\pi$

As it has been outlined in the introduction in section 1.2 there exist several microscopical models under discussion for pion production mechanisms in the two nucleon systems $NN \to NN\pi$ and $Np \to d\pi$.

Pion production in the $3N$ system, however, can be even more complicated since in principle all three nucleons can be involved. A first step of simplification is to assume, that the pion production process itself is described by a pure nucleon nucleon interaction. For this mechanism one can then use the known $NN \to NN\pi$ cross sections without worrying about the real nature of this process in the NN system in terms of a matrix element. The third nucleon has then to be taken into account by some kind of initial and/or final state interaction, but it does not participate in the production mechanism.

Even then there are several different mechanisms available, shown in figure 4.1. The simplest one is given in figure 4.1a . It assumes, that the pion production proceeds through a simple $Np \to d\pi$ mechanism described by the known $Np \to d\pi$ cross section. The third nucleon is only involved due to the fact, that it takes away its initial momentum given by the deuteron momentum distribution, but no additional momentum transfer is included. It is therefore called a *spectator* nucleon. [MN 93] have performed the only detailed calculations for this mechanism without and with a deuteron-nucleon final state interaction (figure 4.1b). This will be referred to as the *spectator model.*

However, one can also think about more complicated reaction mechanisms including for example quasi-free pion production via $NN \to NN\pi$ (figure 4.1c), inclusion of NN rescattering (figure 4.1e) and/or resonant pion production (figure 4.1d+f).

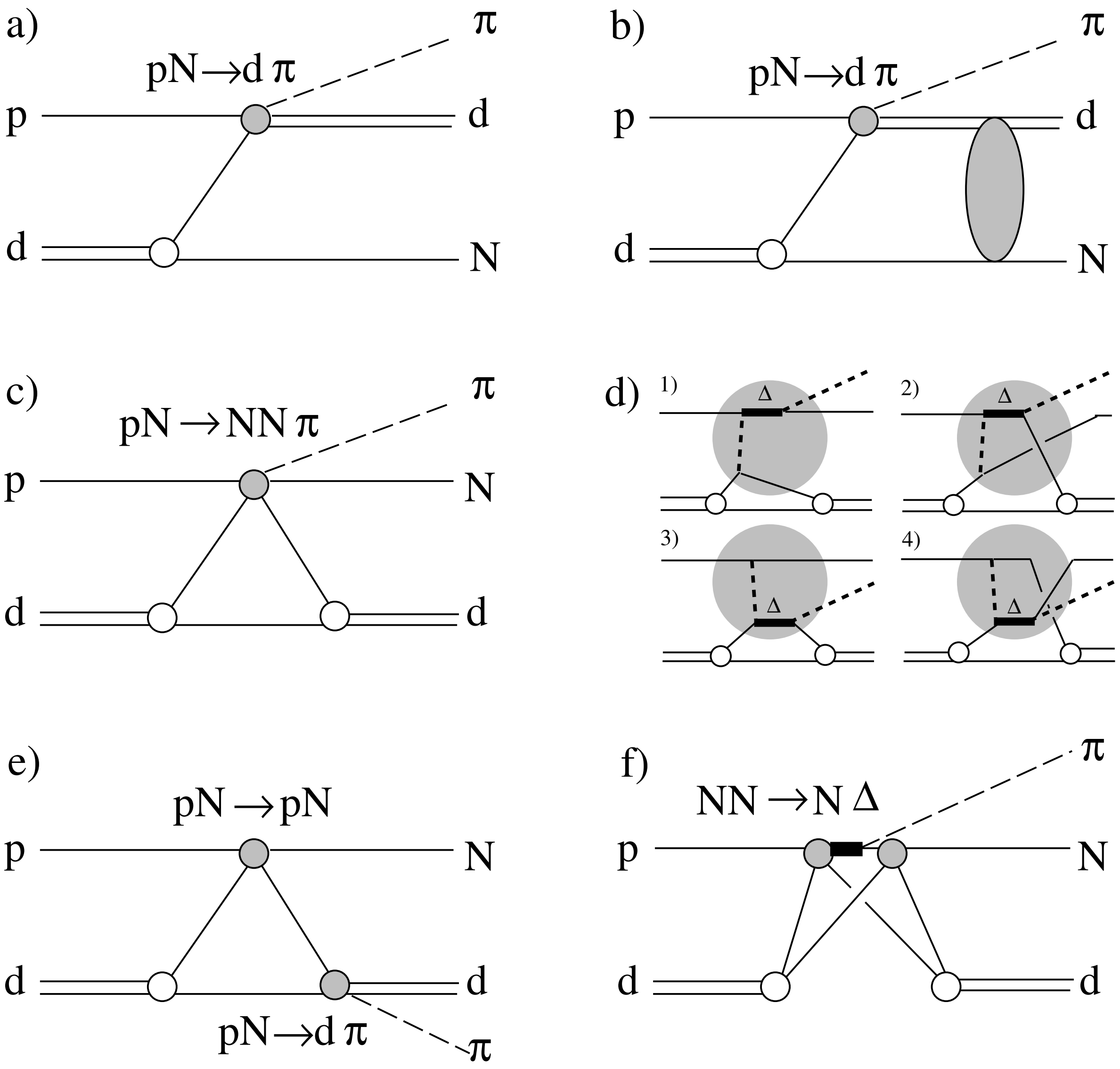

Figure 4.1: *Diagrams for some possible $dp \to dN\pi$ production mechanisms: (a+b) quasi-free production mechanism via $pn \to d\pi$ (in (b) with FSI), also called spectator model. (c-f) so called coherent mechanisms; (c+d) include quasi-free production via $pN \to NN\pi$ without (c) and with (d) π production via Δ resonance; (e) single scattering and (f) double scattering graphs. [Roh 94]*

Throughout this analysis two different approaches have been used to describe the experimental data. First of all the spectator model from [MN 93] has been included in the Monte Carlo simulation WMC. In addition a phenomenological partial wave parameterization similar to [Roh 94] has been applied to describe those reaction mechanisms, where all nucleons participate. The second approach somehow treats the deuteron as a fundamental particle, because it does not explicitly take into account its composition of the loosely bound proton and neutron. This will be later on called *coherent* pion production. It makes no statement about the detailed production mechanisms proposed in figure 4.1c-f. The two models are described now in more detail.

4.3.2 The Spectator Model of [MN 93]

For $pd \to pd\pi^o$ [MN 93] have argued, that it seems justified to assume, that mainly quasifree production via $pn \to d\pi^o$ as plotted in figure 4.1a+b contributes to the total cross section. The quasifree pion production via $pn \to pn\pi^o$ or $pp \to pp\pi^o$, as shown in figure 4.1c, was expected to be small, since the deuteron form factor enters twice and most of the flux should go into the competing four-body-state $dp \to ppn\pi^o$. In addition the free $pp \to pp\pi^o$ cross sections in the near threshold regions are much smaller than those for $pn \to d\pi^o$.

[MN 93] have therefore not included rescattering terms in their calculations and also additional resonant pion production processes via an intermediate $N\Delta$ state as shown in figure 4.1d have not been considered.

As a consequence their spectator model is based upon two main ingredients:

- the nucleon momentum (κ) probability density of the deuteron $|\Phi_d(\kappa)|^2$, obtained from the Bonn potential [Mac 87], where the S and D-state probabilities of the deuteron were added incoherently. It is shown in figure 1.6;
- the total cross section for $Np \to d\pi$.

For the total cross section a fit to the $np \to d\pi^o$ data from [Hut 91] (also shown in figure 1.4) yielded the parameterization

$$\sigma_{tot} = \frac{1}{2}[(184\mu b)\eta + (781\mu b)\eta^3] \tag{4.8}$$

valid for values of $\eta < 1$ in the $pn \to d\pi^o$ center of mass system. For larger center of mass energies a Lorentzian form was fitted to the world's supply of $pp \to d\pi^+$ cross sections. The result was then scaled according to

$$\sigma(pp \to d\pi^+)/\sigma(pn \to d\pi^o) = 2, \tag{4.9}$$

a factor arising from isospin invariance (compare table 1.1).

The derivations in their model are not repeated here and the interested reader should refer directly to [MN 93]. The main result of their calculations was the prediction of the *total* cross section for $pd \to Nd\pi$ reactions. Following their notation it is given as:

$$\begin{aligned}\sigma_I(\eta_I) \quad = \quad & \frac{(2\pi)^{-2}}{s^2 + m_p^4 + m_d^4 - 2sm_p^2 - 2sm_d^2 - 2m_p^2 m_d^2} \\ & \times \int ds_2 dt p_p^* \sqrt{s_2} \frac{E_T' E_B' E_s'}{E_n^* E_p^*} |\Phi_d(\kappa)|^2 \sigma_{II}(\eta_{II})\end{aligned} \tag{4.10}$$

where

$\sigma_I(\eta_I)$: the total cross section in the $pd \to Nd\pi$ system (I).

$\sigma_{II}(\eta_{II})$: the total cross section in the $pN \to d\pi$ system (II).

s: the square of the total invariant mass in the $pd \to Nd\pi$ system.

s_2: the square of the total invariant mass in the $pN \to d\pi$ system.

t: $(P_B - P_s)^2$ the four momentum transfer from the beam proton to the spectator.

p_p^*, E_n^*, E_p^*: the initial proton and neutron momenta and energies in the $pN \rightarrow d\pi$ system.

E_T', E_B', E_s': the initial deuteron *T*arget, proton *B*eam and final *s*pectator energies in the $pd \rightarrow Nd\pi$ frame, where the $d\pi$ system is at rest.

$|\Phi_d(\kappa)|^2$: the deuteron wave function in momentum space with

κ: the neutron (or proton) momentum in the deuteron.

The angular and energy distributions of the outgoing particles have not been predicted as a part of their model. However, the judgment of the quality of the spectator model and the quantification of its contribution to the total cross sections in comparison with other models required also the predictions of these observables as an indispensable input for the fitting procedure. As a consequence [Roh 94] has extended the calculations from [MN 93] by introducing a parameterization of the *differential* cross section for $Np \rightarrow d\pi$:

$$\frac{d\sigma_{II}}{d\Omega_{p_\pi^*}} = a_0 \left(1 + \frac{a_2}{a_0} P_2(\cos\Theta_\pi^*) + \ldots\right) \tag{4.11}$$

with the Legendre polynomial P_2, and the two parameters $a_0 = \sigma_{II}/4\pi$ and $a_2 = (47.2\mu b)\eta_{II}^3$, obtained from a fit to the experimental $Np \rightarrow d\pi$ data. This resulted in a Lorentz invariant matrix element:

$$|M_{spec}|^2 = \frac{E_T'\,E_B'\,E_s'}{4\,E_d^+\,E_s^+\,E_\pi^+\,E_N^*\,E_B^*}\;|\Phi_d(\kappa)|^2\;16\,(2\pi)^2\;\frac{s_2\,p_B^*}{p_\pi^*}\frac{d\sigma_{II}}{d\Omega_\pi^*}(\cos\theta_\pi^*) \tag{4.12}$$

where

E_d^+, E_s^+, E_π^+: the final deuteron, spectator and pion energies in the $pd \rightarrow Nd\pi$ center of mass system.

Using the matrix element $|M_{spec}|^2$ it was possible to generate events with the correct four-momenta in the $pd \rightarrow Nd\pi$ center of mass system. They have then been transformed into the $p_B d_T$ system in [Roh 94] and into the inverse $d_B p_T$ system in this work.

4.3.3 Coherent Mechanisms

The spectator model does not take into account contributions from reaction mechanisms with all three nucleons participating in the momentum transfer. Although no detailed calculations for these mechanisms exist, it is possible to follow a purely phenomenological approach and to make a partial wave expansion for $dp \rightarrow Nd\pi$ [Roh 94].

The matrix element was defined via

$$|M|^2 = |<\Psi_f(\vec{p}_N, \vec{p}_d, \vec{p}_\pi)|T|\Psi_i>|^2 \tag{4.13}$$

with the initial and final state wave functions Ψ_i and Ψ_f and the transition operator T.

For a three body final state $dp \rightarrow Nd\pi$ the wave function can be factorized into two parts

$$\Psi_f(\vec{p}_N, \vec{p}_d, \vec{p}_\pi) = \Psi_{Nd}(\vec{p}_{Nd})\Psi_\pi(\vec{q}), \tag{4.14}$$

where $\vec{p}_{Nd}$ is the momentum of the nucleon relative to the deuteron in the Nd center of mass system and $\vec{q}$ the momentum of the pion with respect to this Nd subsystem.

In the derivations in [Roh 94] the matrix element has then been assumed to follow a dependency of the angular momentum states Ll:

$$|M|^2_{Ll} \propto |\vec{p}_{Nd}|^{2L} |\vec{p}_\pi|^{2l} \tag{4.15}$$

, where L is the angular momentum in the Nd-subsystem and l that of the pion with respect to it. For P-waves the possible angular dependency has been included in the parameterization by expanding the Matrix element according to [Wat 51]:

$$|M|^2_{Pl} \propto |\vec{p}_{Nd}|^2 (1 + a\cos^2\Theta_N) |\vec{p}_\pi|^{2l} \tag{4.16}$$

The parameter a is unknown and has therefore been left free. This model does not include any microscopic assumptions on the nature of the production mechanism. It is also a simplification, since each partial wave consists also of different eigenstates if all spin degrees of freedom are considered and e.g. interference terms are also not considered. A more detailed parameterization of the matrix element seems however useless, since the large number of possible free parameters cannot be fixed due to the lacking experimental data.

For practical reasons (computing time) the simulation of the coherent contributions had to be restricted to the lowest partial wave parameterizations.

Therefore the following 8 partial wave contributions have been included in the Monte Carlo simulation and fitting procedures in addition to the spectator-model:

$\lvert M\rvert^2 \propto$ constant	Ss wave (L=0, l=0)
$\lvert M\rvert^2 \propto \lvert\vec{p}_\pi\rvert^2$	Sp wave (L=0, l=1)
$\lvert M\rvert^2 \propto \lvert\vec{p}_{Nd}\rvert^2$	Ps wave (L=1, l=0) isotropic
$\lvert M\rvert^2 \propto \lvert\vec{p}_{Nd}\rvert^2 \lvert\vec{p}_\pi\rvert^2$	Pp wave (L=1, l=1) isotropic
$\lvert M\rvert^2 \propto \lvert\vec{p}_{Nd}\rvert^2 \lvert\vec{p}_\pi\rvert^4$	Pd wave (L=1, l=2) isotropic
$\lvert M\rvert^2 \propto (\lvert\vec{p}_{Nd}\rvert \cos\Theta_N)^2$	Ps wave (L=1, l=0) anisotropic
$\lvert M\rvert^2 \propto (\lvert\vec{p}_{Nd}\rvert \cos\Theta_N)^2 \lvert\vec{p}_\pi\rvert^2$	Pp wave (L=1, l=1) anisotropic
$\lvert M\rvert^2 \propto (\lvert\vec{p}_{Nd}\rvert \cos\Theta_N)^2 \lvert\vec{p}_\pi\rvert^4$	Pd wave (L=1, l=2) anisotropic

Table 4.1: *The applied parameterizations for coherent production mechanisms*

The incoherent sum of the partial wave contributions (table 4.1) will lateron be called the *coherent contributions*. It does not make a statement concerning the detailed production mechanism for $dp \to dN\pi$. Nevertheless it is based upon the assumption, that all nucleons participate in the reaction mechanism, which is inherent in the ansatz in equation 4.14.

4.3.4 Final State Interaction

[MN 93] have also used a Watson approximation [Wat 52] to predict the influence of the *pd* final state interaction for $pd \to pd\pi^o$, which was expected to be strong especially in the near threshold region, where the outgoing particles have small relative momenta and S-waves dominate. The πd and πN final state interactions were expected to be weak and have therefore been neglected. [MN 93] obtained a final-state weight factor ξ_{fsi}, which depends on the relative momentum k_f between the outgoing deuteron and proton in their center of mass system:

$$\xi_{fsi}(k_f) = \frac{1}{C_0^2 k_f^2}\left[\frac{2}{1+\cot^2\delta_Q} + \frac{1}{1+\cot^2\delta_Q}\right], \tag{4.17}$$

where the two terms correspond to channel-spin quadruplet(Q) or doublet(D) scattering and have been parameterized by

$$C_0^2 k_f \cot\delta_{Q/D} = -\frac{H(\gamma)}{R} - \frac{1}{a_{Q/D}} + \frac{1}{2} r_{0Q/D} k_f^2 + P_{Q/D} r_{0Q/D}^3 k_f^4 + \ldots, \tag{4.18}$$

with

$a_{Q/D}$	scattering length.
$r_{0Q/D}$	effective range.
$P_{Q/D}$	shape parameter.
μ	reduced mass of the *pd* system.
γ	$\gamma = \mu c\alpha/(\hbar k)$; $\alpha = 1/137$.
C_0	Coulomb penetration factor ${C_0}^2 = 2\pi\gamma/(exp(2\pi\gamma) - 1)$.
R	characteristic Coulomb length $R = 2\hbar/(\mu c\alpha)$.
$H(\gamma)$	$H(\gamma) = \gamma^2 \sum_{n=1}^{\infty} \frac{1}{n(n+\gamma^2)} - ln\gamma - .57722$.

The expansion coefficients $a_{Q/D}$, $r_{0Q/D}$ and $P_{Q/D}$ have been obtained from a fit to *pd* elastic-scattering phase shifts [Arv 74] and are

	a [fm]	r_0 [fm]	P [fm^3]
Doublet	2.73	2.27	0.08
Quartet	11.88	2.63	-0.54

Table 4.2: *Effective range parameters for pd-FSI [Arv 74].*

When the integrand in the phase space integral, equation 4.10, is multiplied by the resulting final state factor ξ_{fsi}, taken at the appropriate momentum k_f, a cross section $\sigma_{I,fsi}$ results, that is of arbitrary normalization but should reflect the modification of the energy dependence by the final state interaction.

[Roh 94] has also given the final state factor for *nd* final state interaction. In contrast to *pd* the Coulomb repulsion does not contribute, i.e. $C_0 = 1$ and $R \to \infty$. For the *nd* doublet state there exists a bound state of the triton in the exit channel and therefore the parametrization of equation 4.18 had to be replaced by

$$k_f \cot \delta_D = -\frac{0.095}{a_D} + \frac{1}{2} r_{0D} k_f^2 - \frac{0.905}{a(1+k/k_0)^2)}, \tag{4.19}$$

with

	a [fm]	r_0 [fm]	k_0^{-1} [fm]
Doublet	0.29	1.70	21.0
Quartet	6.14	1.89	-

Table 4.3: *Effective range parameters for nd-FSI [Oer 67].*

The resulting weight factor for the final state interaction is shown in figure 4.2 both for *dp* and *dn* FSI. The influence of the Coulomb repulsion term reduces the probability for $dp \to dp\pi^o$ events with small relative *dp* momenta. In contrast for $dp \to dn\pi^+$, where no Coulomb interaction occurs, events with small *nd* momenta are favored. This effect and the different elastic *pd* and *nd* cross sections used as input for the calculation of final state interaction have therefore an isospin invariance breaking effect.

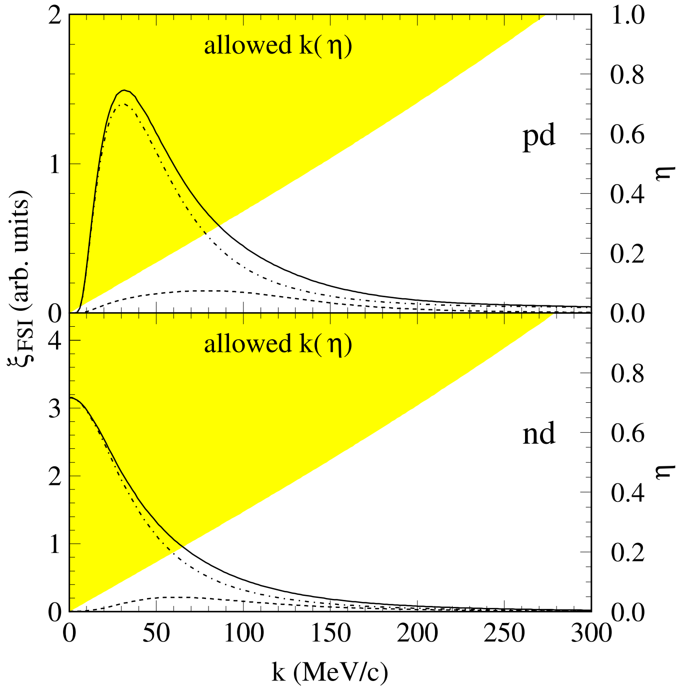

Figure 4.2: *The weight function (solid line) for pd and nd FSI with the contributions from the doublet (dashed line) and quartet state (dot-dashed line) [Roh 94]. The grey area shows the range of relative momenta k accessible as a function of η.*

For me it is however questionable, that Nd final state interaction should be applied for the spectator model. Indeed in nucleon nucleon interactions $NN \to NN\pi$ nucleon nucleon final state interaction according to [Wat 52] has been applied in several model calculations. The main reason was the assumption, that the nucleons participating in the pion production process are interacting at a small distance due to the short range nature of the strong interaction. Therefore they are assumed to have an increased probability for a final state interaction before they can get out of the range of their mutual forces [Wat 52].

However, the two following ingredients of the spectator model, are in conflict with the situation favoring dp final state interactions:

- First of all in the spectator model it follows from momentum conservation in the initial deuteron, that the spectator nucleon has a momentum *opposite* to that of one of the nucleons participating in the pion production process (figure 4.1a).
- The second assumption was, that in the pion production process the spectator nucleon is *too far away* to participate in the pion production mechanism.

As a consequence it seems natural to assume, that a pure spectator nucleon with a momentum pointing in a direction away from the pion production vertex, should only have a *small* probability to get again into a short range with the final state deuteron necessary for a final state interaction.

Throughout the following description the final state interaction has therefore *not* been applied for the spectator model in the first step of simulations. Another reason was, that the spectator model including FSI also looses its predictive power for the total cross sections.

4.3.5 Description of the Experimental $dp \to dN\pi$-data

The discussion of the main reaction of interest, $dp \to dp\pi^o$, and the supposedly isospin-related channel $dp \to dn\pi^+$ will be given on the following pages starting at the highest beam energy of T_d=559 MeV close to the two nucleon threshold and then proceed to lower values of η.

For $dp \to dp\pi^0$ results will be shown at all beam energies, which were based upon the FDC-FDCCDN analysis procedure (compare section 3.6.1). Only at the lowest energy of 437 MeV the available statistics did not allow the requirement of a neutral γ hit and therefore the results were based upon the FDCFDC procedure only.

For a consistency check the results will also be compared with the $dp \to dp\pi^0$ data sample based upon the FDCCDNCDN procedure at two energies, but no cross sections have been calculated based upon this data sample, due to unknown trigger efficiencies for this procedure.

The description of the data is mainly based upon the results obtained from the previously described fitting procedure. The observables used as input for the fitting procedure were depending on the applied analysis procedures and will be listed explicitly for each case.

Discussion of $dp \to dp\pi^0$ at $\eta = 0.86$ (FDCFDCCDN)

For the $dp \to dp\pi^o$ one data set has been obtained with the analysis procedure FDCFDCCDN, requiring the deuteron and proton being detected in the Forward Detector (FDCFDC) and one γ hit in the Central Detector (CDN) as described in section 3.6.1.

The fitting procedure has then included the following six observables in the laboratory system:

$\boldsymbol{\theta_d}, \boldsymbol{\theta_p}$: the deuteron and proton polar angles.

$\mathbf{E_d}, \mathbf{E_p}$: the deuteron and proton kinetic energies.

$\angle_{\mathbf{dp}}$: the opening angle between the two tracks.

$\boldsymbol{\Delta\phi_{dp}}$: the difference in azimuth of the two tracks, also called their 'coplanarity'.

The fact that four of the six spectra include angular information and only two refer to the energy information reflects also, that the measured angles have smaller systematical errors than the reconstructed energies.

Figure 4.3 shows the experimentally observed spectra at the deuteron beam energy of $T_d = 559\,\mathrm{MeV}(\eta = 0.86)$. At this beam energy close to the so called quasi-free threshold π^o-production with a zero spectator proton momentum in the initial deuteron rest frame became possible. The experimental spectra are given in comparison with the selected best fit and its contributions from the spectator model and the sum of the coherent partial waves.

The first row shows the deuteron energy and angular spectra. Both, experimental and Monte Carlo data show a significant peak in the deuteron energy spectrum at approximately 190 MeV. This peak is an experimental artifact; it originates in the layer structure of the FRH (compare figure 2.7). Deuterons being stopped at the end of the first layer of the FRH gave the same deposited energy information as deuterons being stopped with a small energy deposition in the second layer. Here energy losses in the dead material between the layers and also the energy thresholds of the ADCs of the second layer (FRH2) prevented a better energy resolution. For the protons, shown in the second row the same effect is smeared out, because they have hit the Forward Detector in a larger angular range and therefore the effective thickness of the FRH differed stronger than for the deuterons.

The angular distribution of the outgoing protons shows a significant rise of hits at small polar angles. This is expected, if the pion production proceeds according to the spectator model, which is shown as the dashed line. Pure spectator protons favored momenta close to half the initial deuteron beam momentum. Therefore in this experiment with an initial deuteron beam they were expected to be emitted at small laboratory angles close to the beam pipe with approximately half of the initial deuteron energy.

Although the experimental data at this energy show significant contributions from the quasi-free pion production the spectator model *alone* fails to describe the spectra. A significant fraction of events shows proton momenta, which differ significantly from the spectator assumption. This can be best observed at proton laboratory angles of more than 10^o. These protons must have participated in the momentum transfer necessary for the pion production. According to the best fit the spectator model contributes with 59 percent to the total cross section for $dp \to dp\pi^o$ at this beam energy.

The applied event reconstruction procedure (FDCFDCCDN) required the reconstruction of the proton with laboratory angles of more than 4^o. As a consequence a significant number of events with spectator protons emitted under smaller angles into the beam pipe were

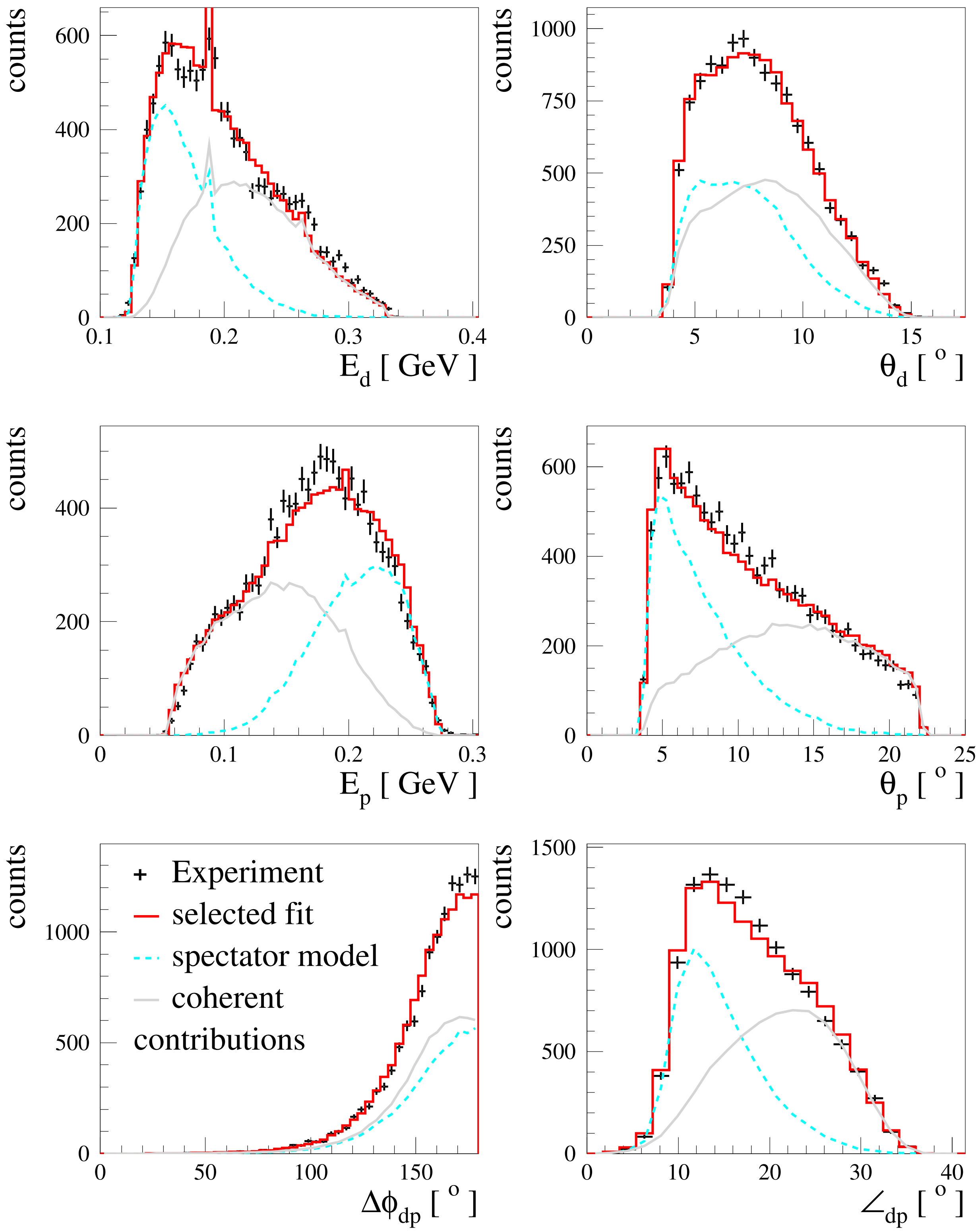

Figure 4.3: *Comparison of the experimental angular and energy distributions for* $dp \to dp\pi^0$ *at* $T_d = 559\,MeV$ *(*$\eta = 0.86$*). (FDCFDCCDN)*

escaping detection. Therefore the region of phase space with zero spectator momentum in the initial deuteron rest frame was not experimentally accessible with this reconstruction procedure. However, this region is also of particular interest to quantify the spectator model contribution.

Discussion of $dp \to dp\pi^0$ at $\eta = 0.86$ (FDCCDNCDN)

The event sample obtained with the requirement of the deuteron hit in the Forward Detector (FDC) in connection with a $\gamma\gamma$ coincidence in the Central Detector (CDNCDN) gives better access to this region of phase space because it allowed the protons to escape undetected under small angles.

For the data samples obtained with the FDCCDNCDN analysis the proton distributions have therefore not been used in the fitting procedure, since the proton detection was not required for the event identification. Instead the π^o angular information, reconstructed from the two neutral tracks in the Central Detector , has been included in the fit. Due to the fact, that the π^o angle could not be reconstructed with the same accuracy as the angles of the charged particles hitting the Forward Detector, it seemed reasonable not to include more observables like e.g. the coplanarity or opening angle between the deuteron and pion in the fitting procedure. This would have increased the sensitivity of the results to systematical errors in the π^o reconstruction. The fitting procedure was therefore based upon the three observables:

$\boldsymbol{\theta}_{\mathbf{d}}$: the deuteron polar angle.

$\mathbf{E}_{\mathbf{d}}$: the deuteron kinetic energy.

$\boldsymbol{\theta}_{\pi^o}$: the π^o polar angle.

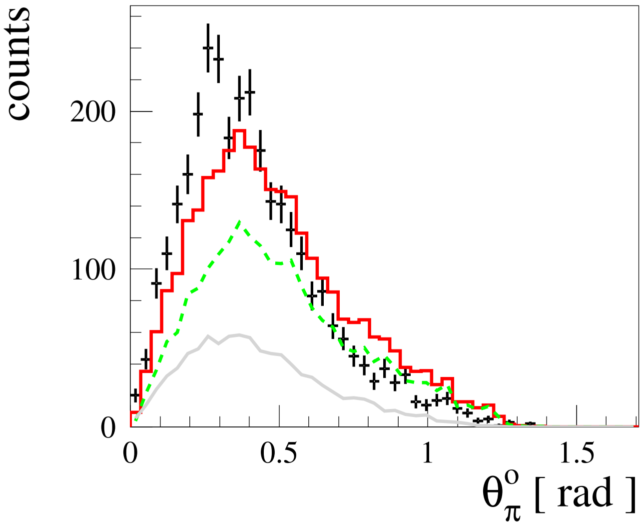

Figure 4.4: *π^o polar angle for $dp \to dp\pi^o$ at T_d=559 MeV.*

The obtained data sample is shown in figures 4.4 and 4.5. For those events with the proton detected in the Forward Detector the proton distributions and the opening angles and coplanarities between the deuteron and proton are also given, although not included in the fit. For events without a detected proton the opening angle and coplanarity are set to zero in the spectra, showing that the number of undetected protons also follows the model expectations from Monte Carlo. 40 percent of the observed events have no proton-hit in the Forward Detector.

In the best fit the spectator model has been found to contribute with approximately 74 percent, but again also a coherent contribution had to be added to describe the experimental data. This is in particular visible in the deuteron energy spectrum. According to the spectator model close to the quasifree threshold the spectator proton kinetic energy should be distributed around half the beam energy and therefore also the excess energy of the $d\pi^o$ system would be limited, which should prevent the observation of deuterons with more than 200 MeV kinetic energy in the lab

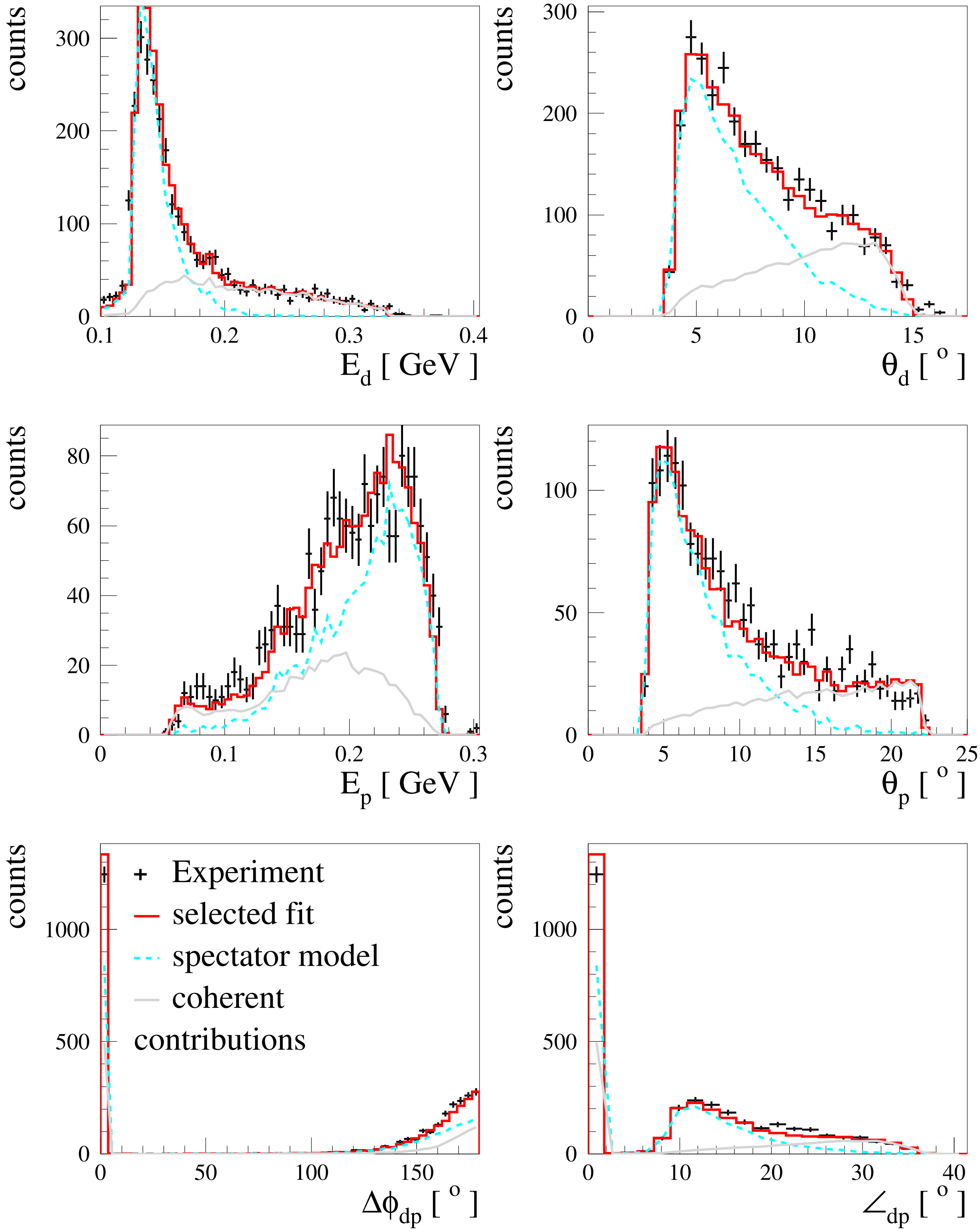

Figure 4.5: *Comparison of the experimental angular and energy distributions for* $dp \to dp\pi^0$ *at* $T_d = 559\,MeV$ *(*$\eta = 0.86$*). (FDCCDNCDN)*

system. The presence of high energetic deuterons is again a strong indication for the presence of coherent mechanisms.

It can be assumed that the 15 percent discrepancy between the spectator model contributions in the two $dp \to dp\pi^0$ data samples is mainly due to the limited accuracy of the π^o angular reconstruction in the FDCCDNCDN procedure. This is indicated by the fact, that in figure 4.5 the number of low energy deuterons, typical for the spectator model, and also the number of undetected protons are slightly overestimated by the Monte Carlo description.

Discussion of $dp \to dn\pi^+$ at $\eta = 0.78$ (FDCFDC)

Assuming that the isospin invariance of

$$\sigma(pp \to d\pi^+)/\sigma(pn \to d\pi^o) = 2, \tag{4.20}$$

(compare table 1.1) is also valid for the corresponding dp reactions according to

$$\sigma(dp \to dn\pi^+)/\sigma(dp \to dp\pi^o) = 2, \tag{4.21}$$

the examination of the channel $dp \to dn\pi^+$ should give results comparable to $dp \to dp\pi^o$. However, the assumption of isospin invariance seems only justified for the spectator model of [MN 93] as shown in figure 4.1a). As soon as other mechanisms come into play isospin invariance may not easily be transferred from the $pN \to d\pi$ to the $dp \to dN\pi$ reactions. For final state interaction this has already been discussed. Another example may be a process including a single scattering term $pN \to pN$ as shown in figure 4.1e). For $dp \to dp\pi^0$ this process may include elastic $pp \to pp$ as well as $pn \to pn$ scattering, but for $dp \to dn\pi^+$ only $pn \to pn$ is possible.

The $dp \to dn\pi^+$ events have only been identified via detection of the deuteron and the pion in the Forward Detector (FDCFDC). The experiment covered therefore a region of phase space comparable with the previously shown FDCCDNCDN-data sample for $dp \to dp\pi^o$, because the spectator nucleon was allowed to escape undetected and only forward going pions were identified.

For the $dp \to dn\pi^+$ reaction the π^+-energy has not been included in the fitting procedure, since the kinetic energy of the π^+ could not be reconstructed with the same accuracy as the proton energy due to the poorly known quenching effects for pions. The fit for $dp \to dn\pi^+$ has therefore only been based upon

$\boldsymbol{\theta_d, \theta_{\pi^+}}$: the deuteron and π^+ polar angles.

$\mathbf{E_d}$: the deuteron kinetic energy.

$\angle_{\mathbf{dp}}$: the opening angle between the two tracks.

$\boldsymbol{\Delta\phi_{dp}}$: the azimuthal difference of the two tracks.

Figure 4.6 shows the results. The deuteron distributions are comparable with the previous results for $dp \to dp\pi^o$. Again a significant rise of the deuteron kinetic energy below 200 MeV is observed, indicating the contribution from the spectator model. However, the number of events with deuterons of higher energies is increased compared to the $dp \to dp\pi^o$ data and the result from the best fit yields a spectator model contribution of only 52 percent. This is not surprising since all spectra shown have been obtained at the same deuteron beam energy, but due to the

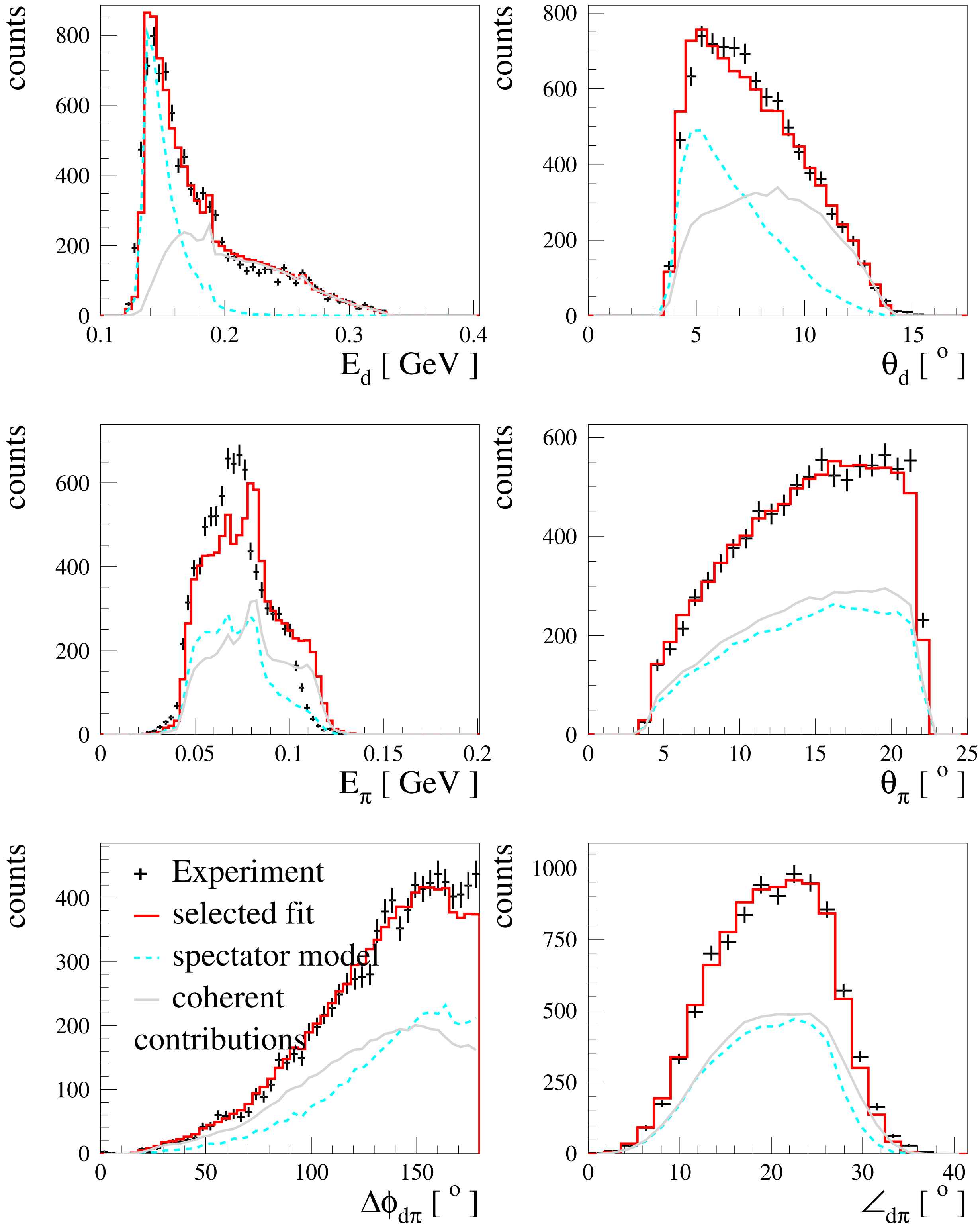

Figure 4.6: *Comparison of the experimental angular and energy distributions for* $dp \to dn\pi^+$ *at* $T_d = 559\,MeV$ *(*$\eta = 0.78$*).*

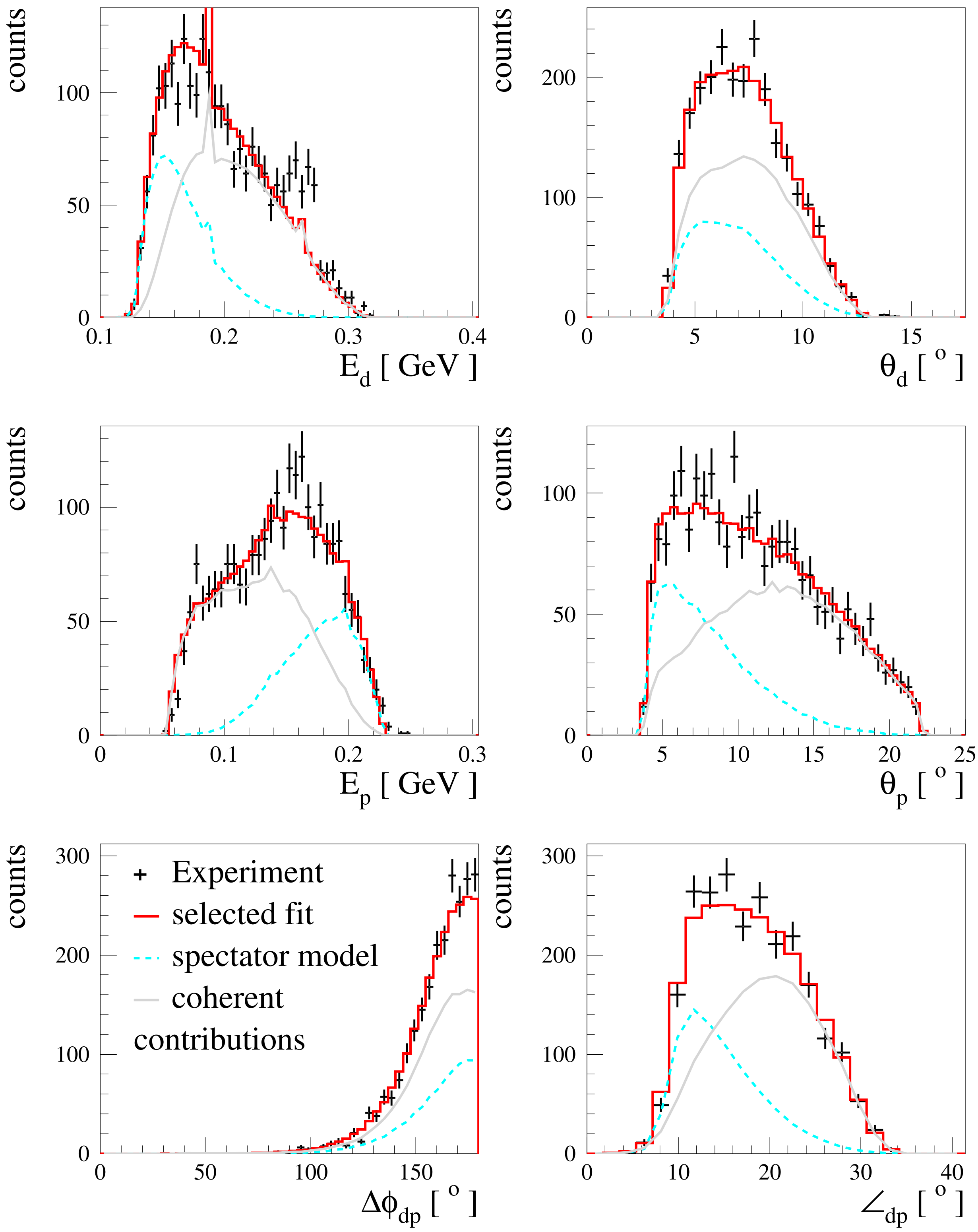

Figure 4.7: *Comparison of the experimental angular and energy distributions for* $dp \to dp\pi^0$ *at* $T_d = 515\,MeV$ *(*$\eta = 0.70$*). (FDCFDCCDN)*

mass differences of the outgoing particles the maximum pion momenta η differ. For $dp \to dn\pi^+$ at T_d=559 MeV it is only $\eta = 0.78$ compared to $\eta = 0.86$ for $dp \to dp\pi^o$ and therefore small differences should be expected.

Discussion of $dp \to dp\pi^0$ at $\eta = 0.70$ (FDCFDCCDN)

The preceding results for $dp \to dn\pi^+$ indicate already a trend, namely: **The relative contribution of the spectator model reduces with approach of the threshold**.

This trend seems to continue further with decreasing η: At the deuteron kinetic energy of $T_d = 515$ MeV, corresponding to $\eta = 0.70$, the signature of the quasifree process, small (spectator-) proton angles and small deuteron energies, has lost its dominance as shown in figure 4.7. At this energy a 44 percent contribution of the spectator model is extracted with the fitting procedure.

Discussion of $dp \to dp\pi^0$ and $dp \to dn\pi^+$ at $\eta = 0.61$

In order to avoid one potential ambiguity for lower values of η, the deuteron beam energies have been chosen to allow a direct comparison of the $dp \to dp\pi^o$ data at $T_d = 492$ MeV ($\eta = 0.61$) with the results from $dp \to dn\pi^+$ at $T_d = 515$ MeV ($\eta = 0.62$).

The spectra are given on the following three pages, again for $dp \to dp\pi^0$ applying the two analysis procedures FDCFDCCDN and FDCCDNCDN and for $dp \to dn\pi^+$ the FDCFDC procedure with the previously defined observables used as input for the fit routines.

All experimental results contradict again a pure quasi-free assumption. The bulk of the protons were emitted at larger angles and a large fraction of deuterons was hitting the Forward Detector with energies above 200 MeV. For $dp \to dp\pi^0$ the fitting procedure yielded spectator model contributions of 40 percent for FDCFDCCDN, 38 percent for FDCCDNCDN and 26 percent for $dp \to dn\pi^+$. The lower value for $dp \to dn\pi^+$ should not be taken as an evidence for the failure of the assumption of isospin invariance. It is more likely caused by the limited acceptance in phase-space for $dp \to dn\pi^+$. This will be demonstrated later on.

Discussion of $dp \to dp\pi^0$ (FDCFDCCDN) at $0.3 < \eta \leq 0.5$

At even lower energies ($\eta < 0.5$) the available phase space continues to shrink, which is also visible in the observed spectra. The use of inverse kinematics forced the deuterons in a narrow cone around the beam pipe, which became the limiting factor in acceptance and prevented measurements closer to thresholds.

At $T_d = 455$ MeV ($\eta = 0.43$ for $dp \to dp\pi^0$) the differences in shape between the spectator model and the coherent contributions is still visible but much less pronounced than for higher values η (figure 4.11). At the lowest beam energy of $T_d = 437$ MeV , however, the differences in shape have lost most of their significance and also the statistical errors within the spectra are larger.

Nevertheless the fitting procedure can be applied and converges; it results in a spectator model contribution of 25 percent for $dp \to dp\pi^0$ at $\eta = 0.43$. At the lowest energy of $T_d = 437$ MeV ($\eta = 0.32$) one data sample exists for each beam time shown in figure 4.12 and 4.13. Following the expectation from the previous data samples they yielded only very small spectator model contributions of 13 percent for the September 1996 data and 15 percent for the April 1997 data. Due to the similarity of the competing distributions, these numbers have a higher inherent uncertainty than the percentages for higher η.

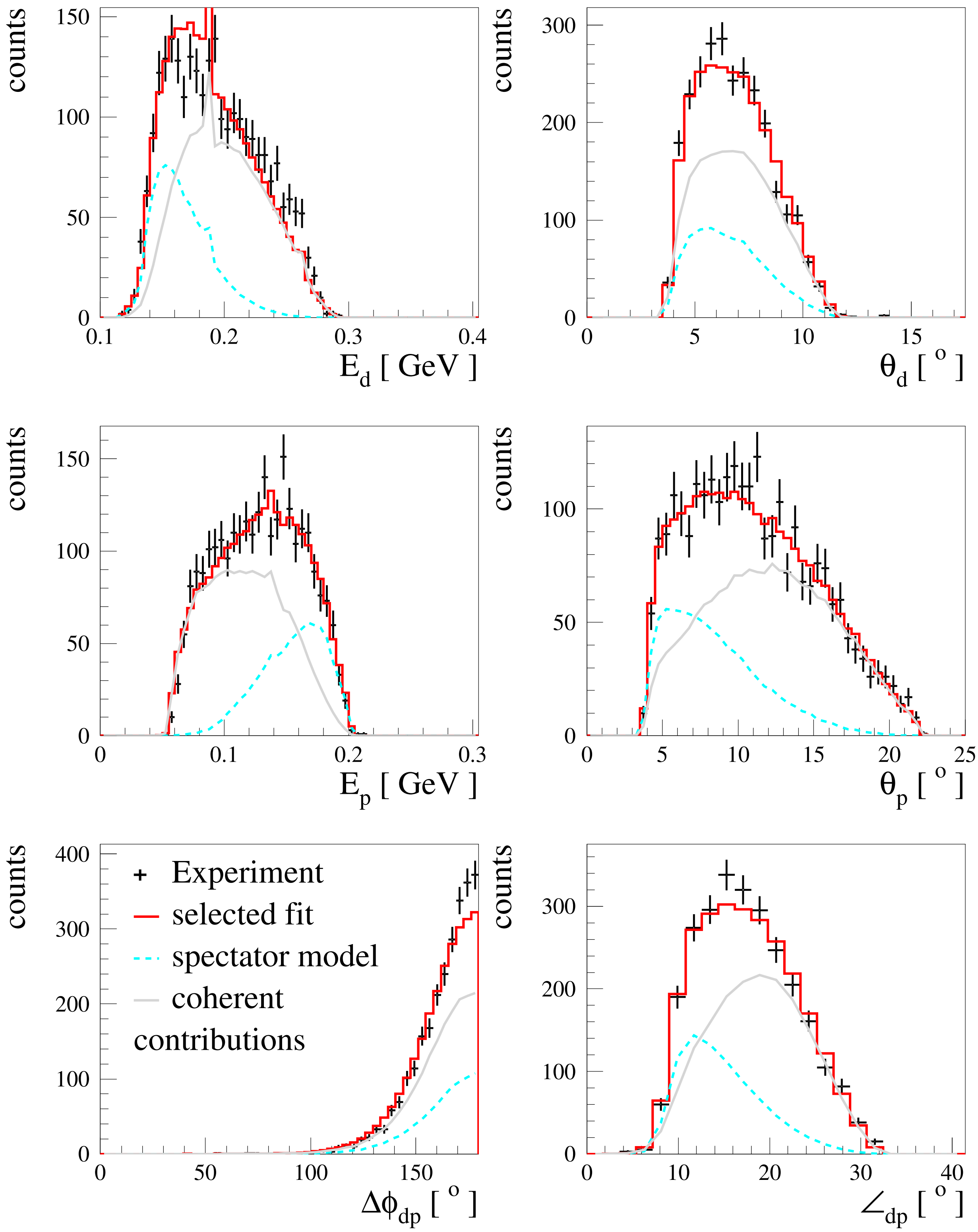

Figure 4.8: *Comparison of the experimental angular and energy distributions for* $dp \to dp\pi^0$ *at* $T_d = 492\,MeV$ *(*$\eta = 0.61$*). (FDCFDCCDN)*

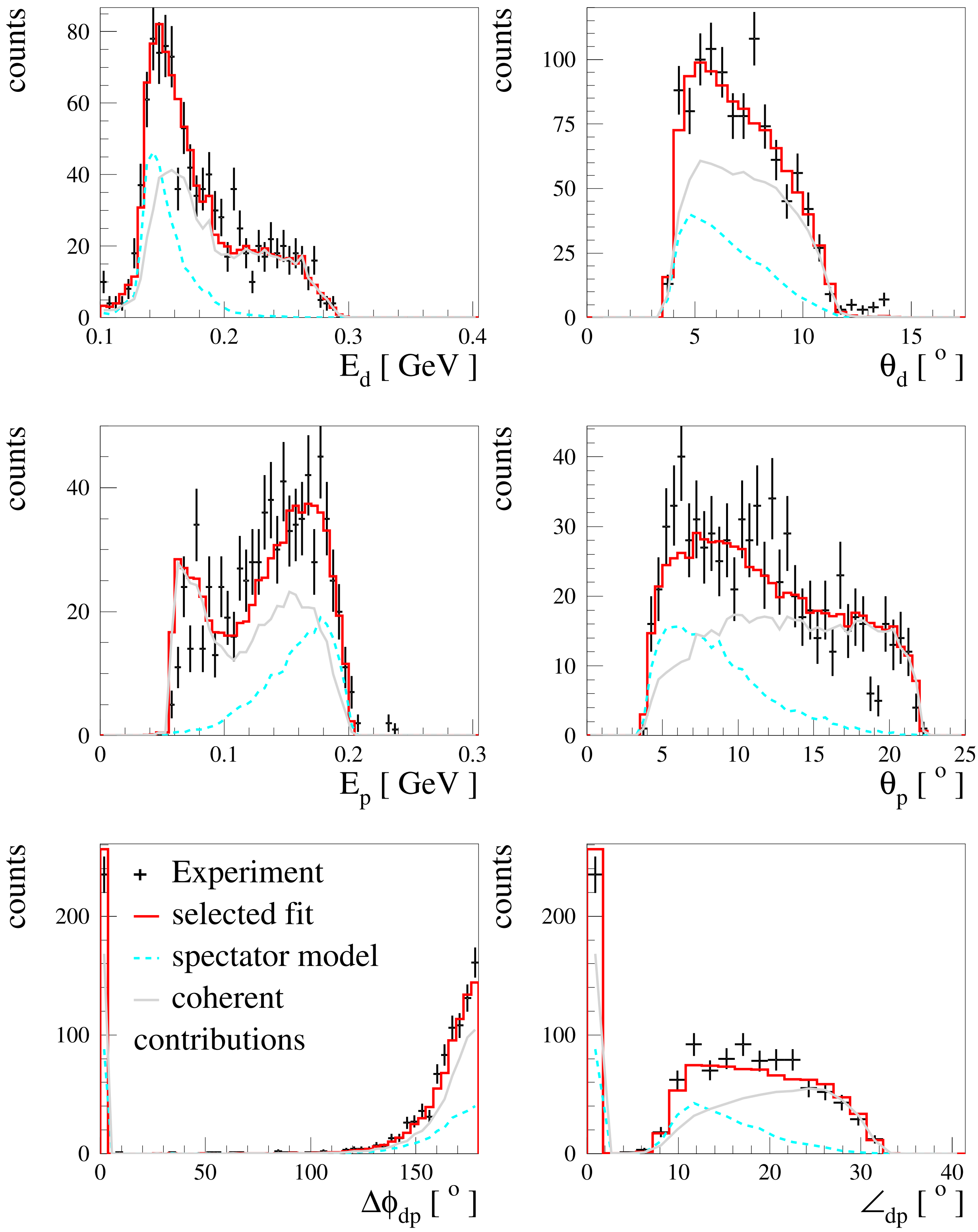

Figure 4.9: *Comparison of the experimental angular and energy distributions for* $dp \to dp\pi^0$ *at* $T_d = 492\,MeV$ *(*$\eta = 0.61$*). (FDCCDNCDN)*

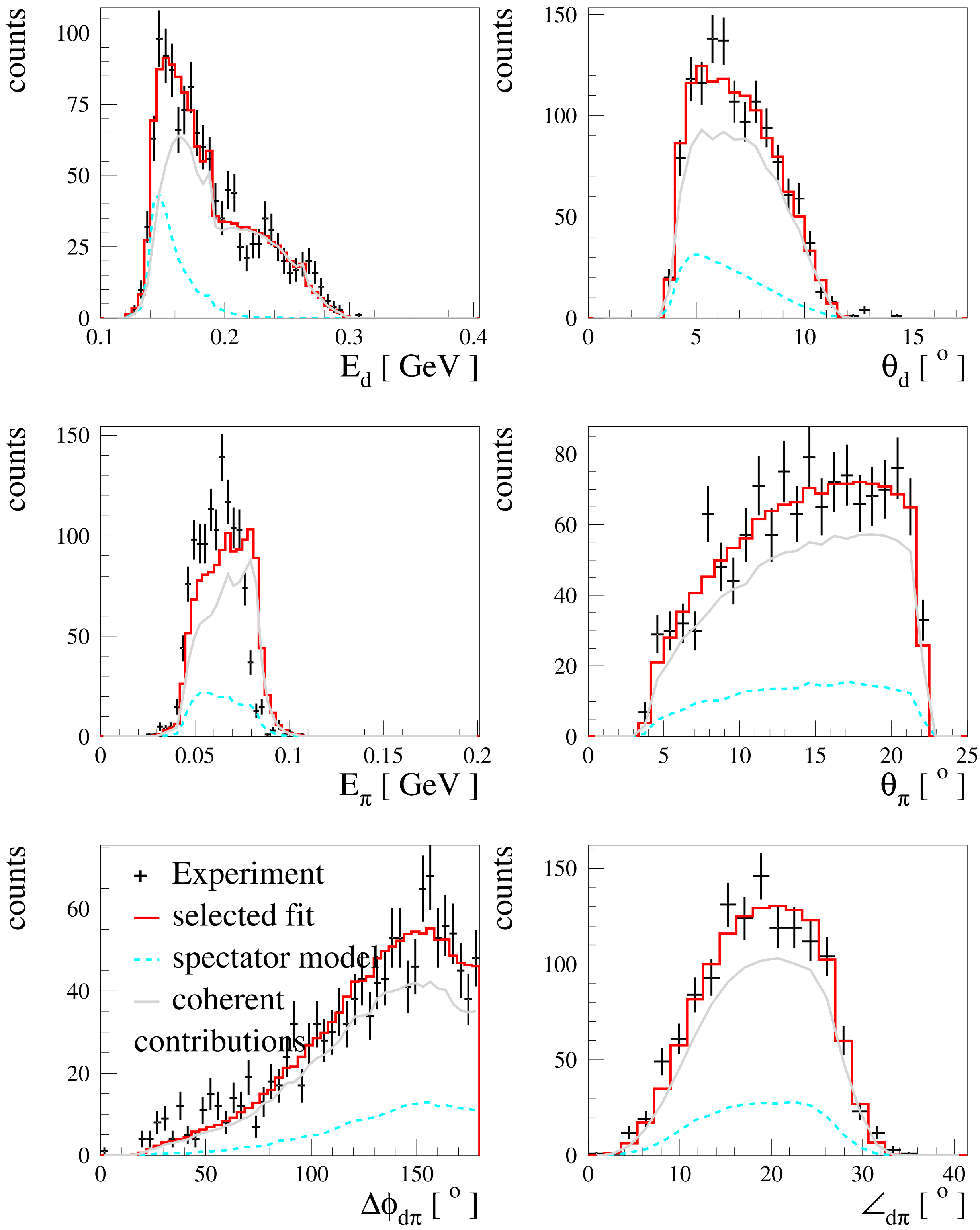

Figure 4.10: *Comparison of the experimental angular and energy distributions for* $dp \rightarrow dn\pi^+$ *at* $T_d = 515$ *MeV* ($\eta = 0.62$)*.*

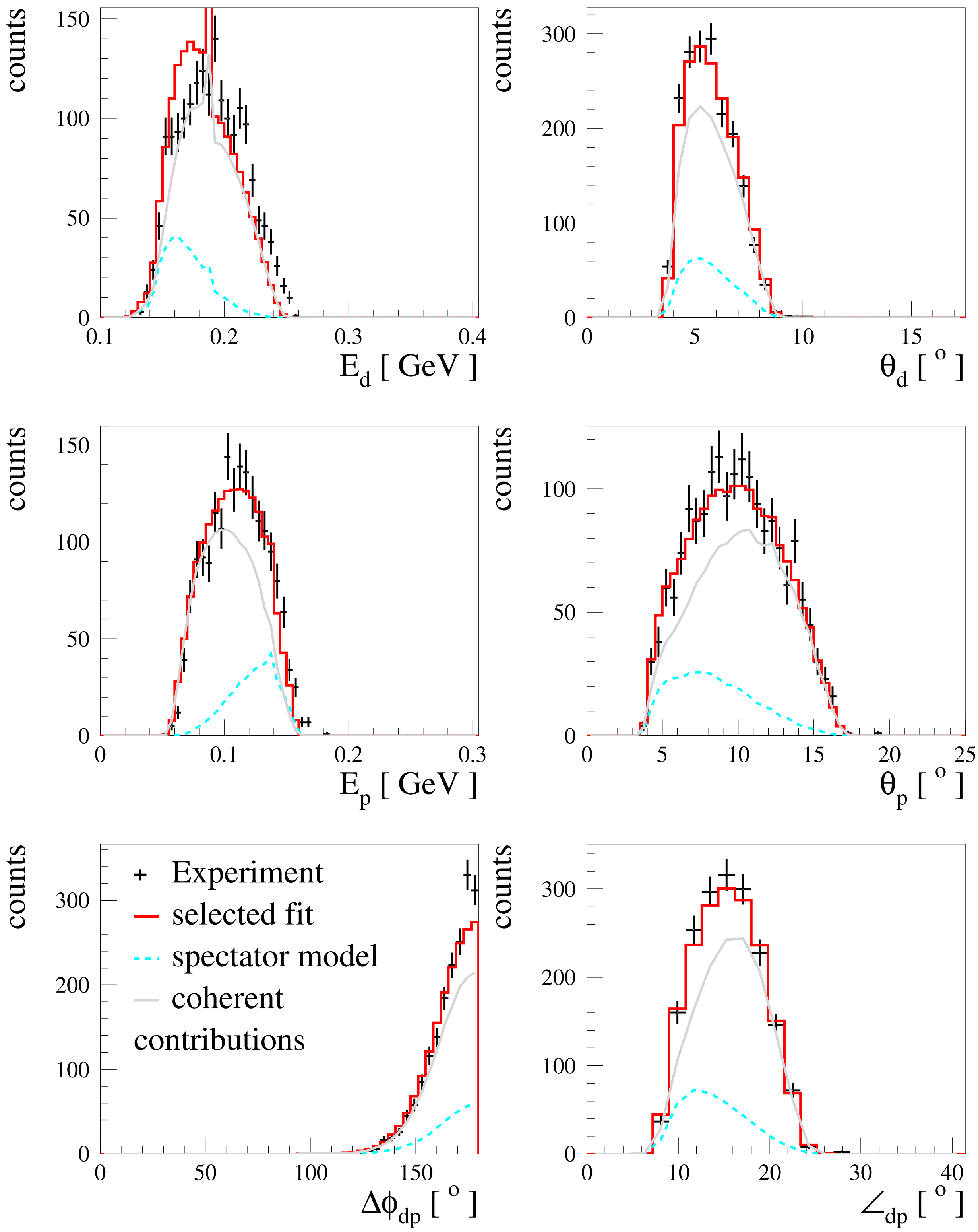

Figure 4.11: *Comparison of the experimental angular and energy distributions for* $dp \to dp\pi^0$ *at* $T_d = 455$ *MeV* ($\eta = 0.43$)*. (FDCFDCCDN)*

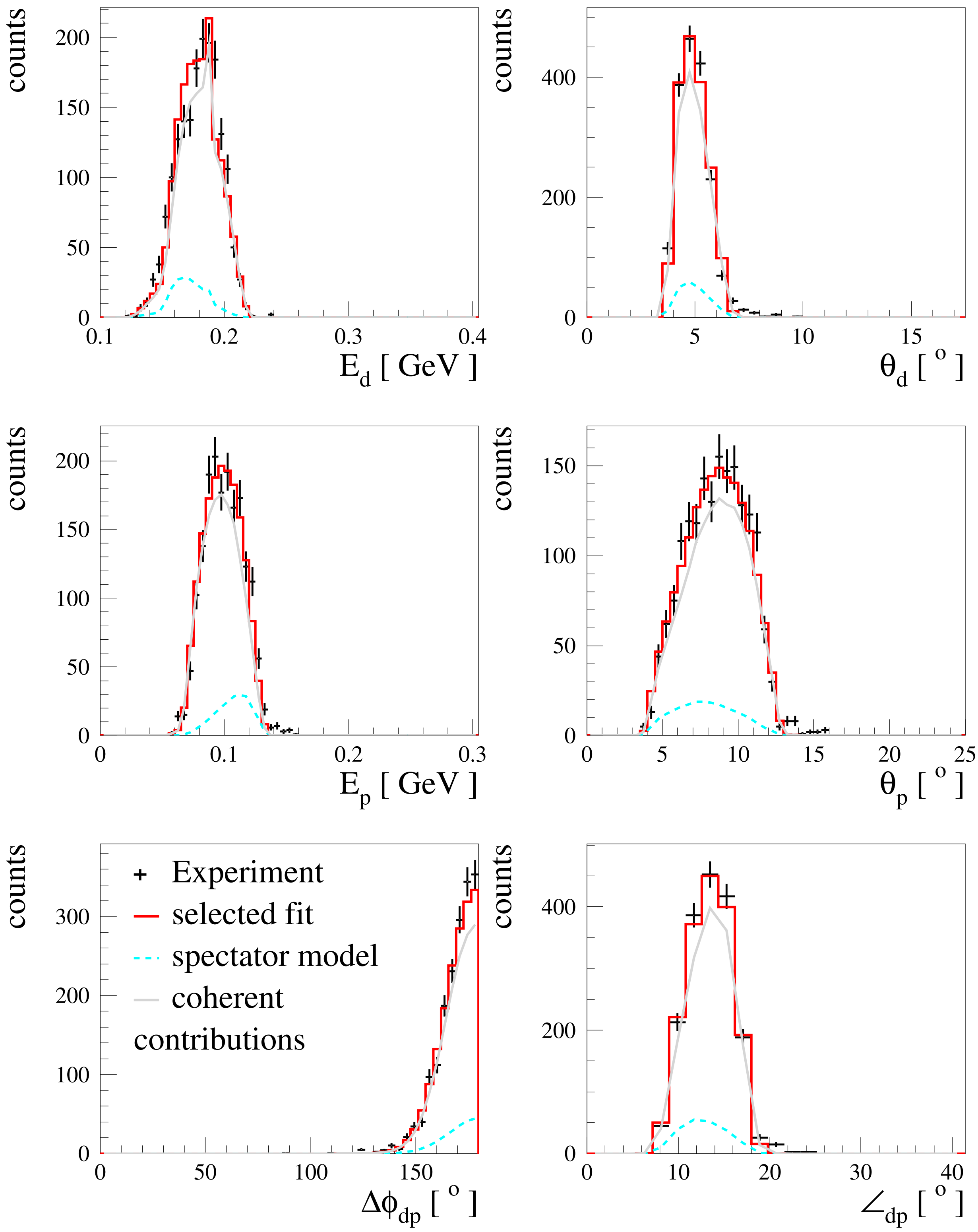

Figure 4.12: *Comparison of the experimental angular and energy distributions for* $dp \to dp\pi^0$ *at* $T_d = 437\,MeV$ *(*$\eta = 0.32$*). The data sample was taken during the September 1996 run. (FDCFDC)*

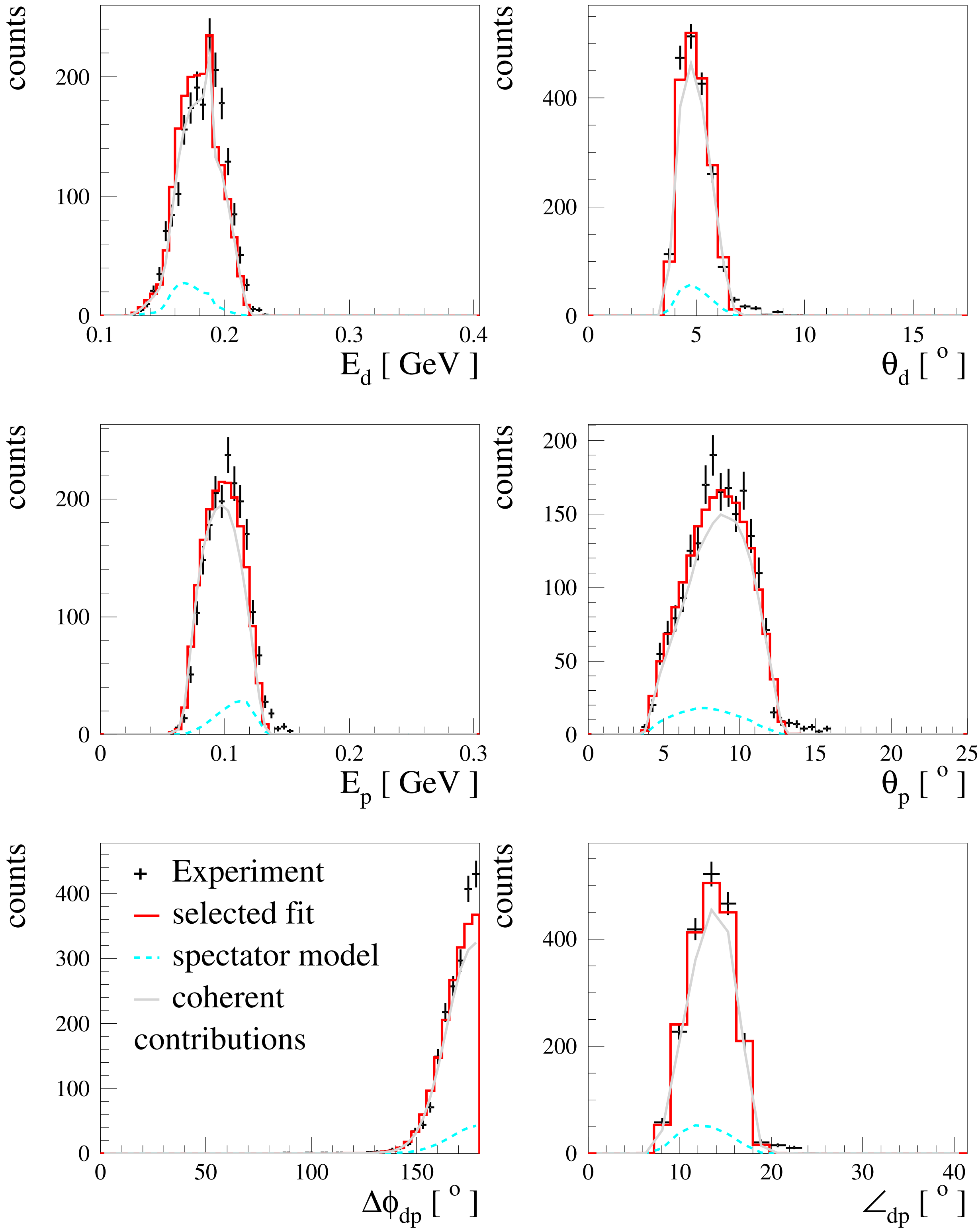

Figure 4.13: *Comparison of the experimental angular and energy distributions for* $dp \to dp\pi^0$ *at* $T_d = 437$ *MeV* ($\eta = 0.32$)*. The data sample was taken during the April 1997 run. (FDCFDC)*

The Dependence of Model Contributions on Projectile Energy

The results obtained for the relative contributions are summarized in figures 4.14 and 4.15. Figure 4.14 shows the spectator model contribution for $dp \rightarrow dp\pi^0$ (FDCFDCCDN) over the whole measured energy range. According to the results obtained with the fitting procedure it rises almost linearly with η from 13 percent at $\eta = 0.32$ to 59 percent at $\eta = 0.86$. For $dp \rightarrow dn\pi^+$ (FDCFDC) a similar trend is observed, however with a 15 percent discrepancy at $\eta = 0.62$.

Uncertainties in the Model Description

As described before the Monte Carlo description of the reaction mechanisms was based upon a combination of the spectator model and the coherent partial wave parameterizations given in table 4.1. Throughout the analysis attempts have also been made to study, to what extent a variation of the boundary conditions for the fit procedure might affect the results. For this purpose the different minimization procedures available in MINUIT [CERN 94a] (e.g. SIMPLEX and MIGRAD) have been applied with different start values and step sizes, yielding however practically always the same model contributions.

It has also been checked, if the exclusion of individual coherent partial waves in the fitting procedure affects the results of the fit. It turned out, that the fractional contributions from the spectator model and the sum of the coherent mechanisms never changed significantly for $dp \rightarrow dp\pi^0$ (FDCFDCCDN), if single partial waves were omitted from the analysis. However, the relative weight of the individual partial wave contributions in the sum of the coherent model was observed to vary considerably. Under these circumstances it seemed not justifiable to perform a more detailed investigation of single coherent partial wave contributions.

For $dp \rightarrow dn\pi^+$ and $dp \rightarrow dp\pi^0$ (FDCCDNCDN) the results of the fit were particularly sensitive to the inclusion of partial wave contributions, which favored regions of phase space not covered by the detector acceptance. This did not only affect the relative weight of the partial waves with respect to each other, but also their total weight in comparison to the spectator model contribution.

It is obvious, that the fit procedure could not give reliable results for the partial wave contributions favoring the regions of phase space not covered by the detector, because a significant change of their contributions only resulted in a small variation of χ^2. It can therefore be suspected, that the deviations in the model contributions between $dp \rightarrow dp\pi^0$ (FDCFDCCDN) on the one hand and $dp \rightarrow dp\pi^0$ (FDCCDNCDN) or $dp \rightarrow dn\pi^+$ on the other hand are very likely caused by limited and partly incongruent detection acceptances.

The applied fitting procedure was therefore only able to give reliable results, if a large fraction of the available phase space was covered by the detector. This phase space coverage will be demonstrated now for $dp \rightarrow dp\pi^0$ and $dp \rightarrow dn\pi^+$ for three representative energies.

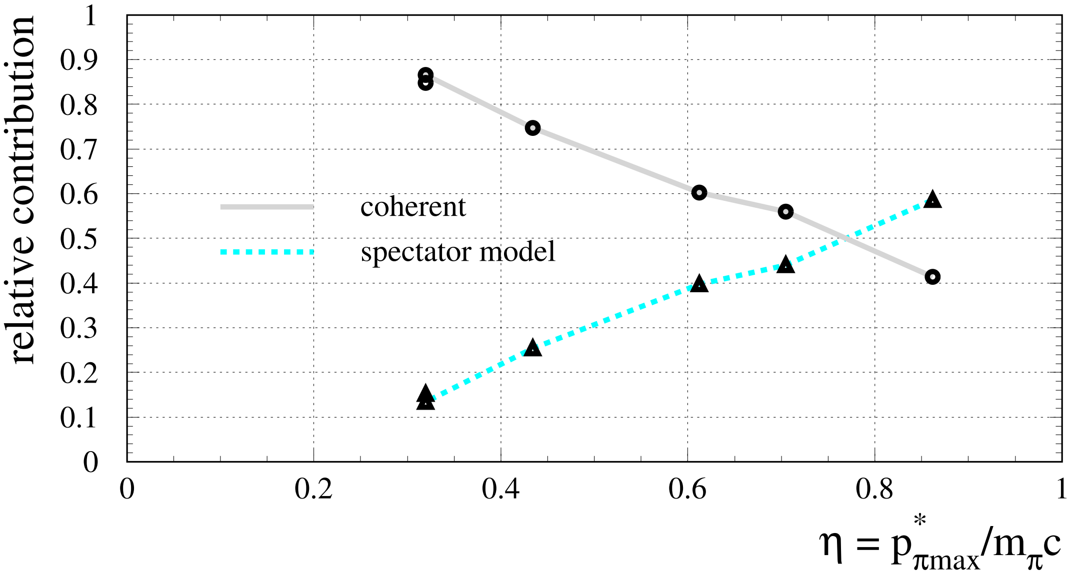

Figure 4.14: *Contributions of the quasifree and the coherent production mechanisms to the total* $dp \to dp\pi^o$ *distributions for different energies.*

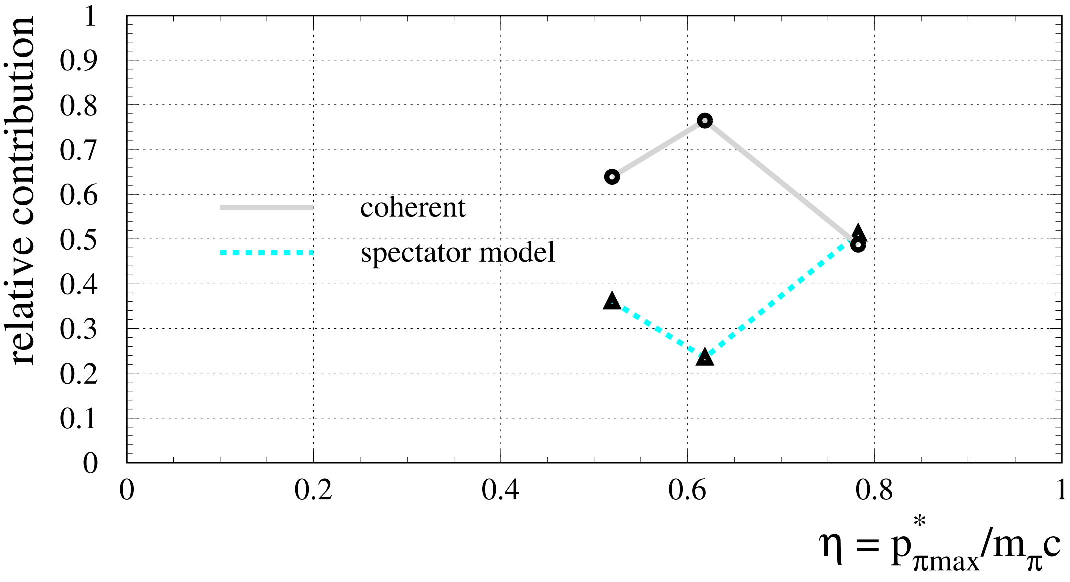

Figure 4.15: *Contributions of the quasifree and the coherent production mechanisms to the total* $dp \to dn\pi^+$ *distributions for different energies.*

4.3.6 Phase Space Coverage for $dp \to dp\pi^0$ and $dp \to dn\pi^+$

For demonstration of the acceptance in phase space for the PROMICE/WASA detector it is suitable to compare the Dalitz Plot for accepted Monte Carlo events of the different reactions. In a Dalitz plot the density of the points is proportional to the squared matrix element [Byk 73]. A pure phase space distribution with a constant matrix element therefore leads to a uniformly filled plot.

For comparison I follow again [Roh 94] and define the variables x and y from the linear transformations

$$x = 100 \frac{\{s_{N\pi} - s_{d\pi}\} - \{(m_N + m_\pi)^2 - (m_d + m_\pi)^2\}}{s - (m_N + m_d + m_\pi)^2} \tag{4.22}$$

$$y = 100 \frac{s_{Nd} - (m_N + m_d)^2}{s - (m_N + m_d + m_\pi)^2} \tag{4.23}$$

with

s_{Nd} : Invariant mass of the Nd system
$s_{d\pi}$: Invariant mass of the $d\pi$ system
$s_{N\pi}$: Invariant mass of the $N\pi$ system
m_i : Masses of the particles i,

which ensure that the contour of kinematically allowed $dp \to dN\pi$ events in the xy plane is independent of the beam energy. Beyond that the differences in particle masses between $dp \to dp\pi^0$ and $dp \to dn\pi^+$ cancel.

Dalitz Plots at $\eta \approx 0.8$

In figure 4.16 the Dalitz plots are given for the highest energies of $T_d = 559$ MeV. The results in the first two lines contain the Monte Carlo distributions for a pure phase space distribution and for the spectator model. In the first column the complete event samples generated as input for WMC are shown. The center and right columns show the fraction of events remaining after the detector simulation WMC and the event reconstruction in PWREC have been applied. In the bottom line the experimental results are given. For $dp \to dn\pi^+$ the reconstructed Dalitz plot is always shifted to smaller values in x due to uncertainties in the π^+ energy determination caused by badly known quenching corrections and contributions from its decay into μ^+.

Looking at $dp \to dp\pi^0$ the detector acceptance at this energy was mainly limited by the lower angular limit of the beam pipe and for protons also by the outer rim of the Forward Detector. For $dp \to dn\pi^+$ the acceptance in phase space was significantly reduced due to the small angular range covered for the π^+ detection.

Other constraints in the analysis, like e.g. the requirement of the single γ hit in the Central Detector, inefficiencies in the particle detection due to e.g. secondary interaction losses for deuterons or due to the application of the delayed pulse technique for the π^+, did of course reduce the efficiency of the event reconstruction procedure. Nevertheless they had only a limited influence on the acceptance in phase space, because they did not favor specific regions of phase space.

Figure 4.16 reveals that the two reactions have probed different regions of phase space, but with some overlap. For $dp \to dn\pi^+$ the PROMICE/WASA experiment was in particular

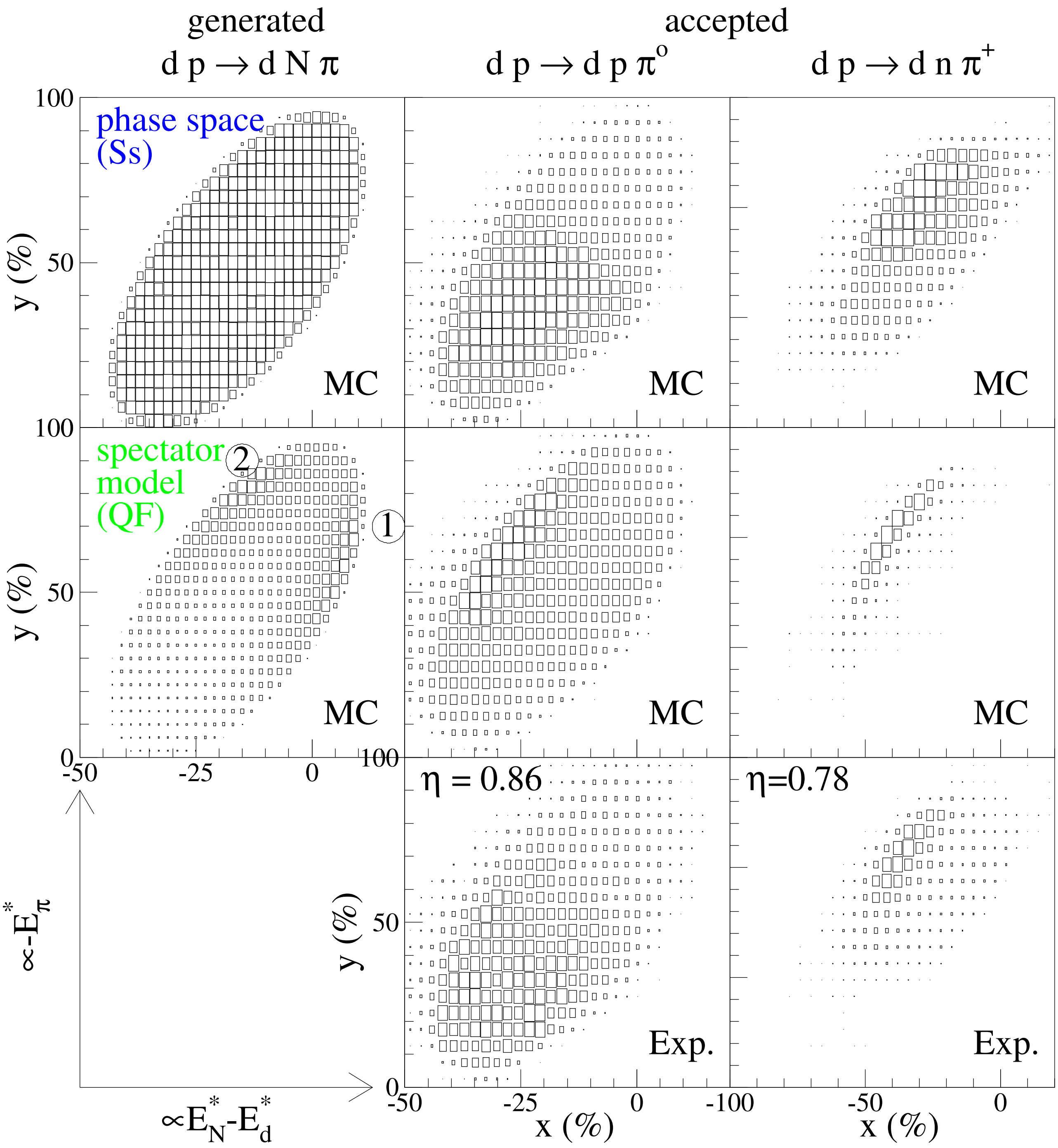

Figure 4.16: *The Dalitz Plots for* $dp \rightarrow dN\pi$ *at* $T_d = 559$ *MeV. The top two lines show the Dalitz plots obtained from Monte Carlo for a pure phase space distribution and for the spectator model without final state interaction. The left column shows all generated events and the center and right columns give the subsamples of accepted events for* $dp \rightarrow dp\pi^0$ *(FDCFDCCDN) and* $dp \rightarrow dn\pi^+$ *(FDCFDC). The line at the bottom shows the experimental events.*

sensitive to the quasifree process, where the pion was, with respect to the beam direction, emitted at forward angles (② in figure 4.16) in the $pp \to d\pi^+$ subsystem and the (spectator-) nucleon could escape undetected, but it had no acceptance for π^+ being emitted into other directions.

For $dp \to dp\pi^0$ on the other hand the detector showed a wide acceptance for coherent mechanisms, but due to losses in the beam pipe it was partly limited for the spectator model.

It is instructive to compare the acceptance with the previous Indiana experiment shown in figure 1.8 for a similar center of mass energy. For $pd \to nd\pi^+$ the Indiana experiment covered a comparable phase space volume, but for π^+ emitted under opposite directions in the $pp \to d\pi^+$ subsystem (①). For $pd \to pd\pi^0$ on the other hand the detector was limited to a very small region of phase space and therefore extremely sensitive to the applied models. At this energy it had practically no acceptance for quasifree $pd \to pd\pi^0$ events.

Dalitz Plots at $\eta \approx 0.6$

At lower energies ($\eta \approx 0.6$) shown in figure 4.17 the outgoing (spectator) nucleon could not be emitted with zero momentum in the initial beam-deuteron rest frame and had therefore a smaller probability to escape undetected into the beam pipe. In addition no protons could be emitted at large angles outside of the Forward Detector acceptance.

For $dp \to dp\pi^0$ the fraction of phase space covered by the detector had therefore a maximum at these energies. For $dp \to dn\pi^+$ the acceptance did not change significantly compared to the previous case. However, going to lower beam energies for $dp \to dn\pi^+$ the deuterons were emitted into narrower forward cones than for $dp \to dp\pi^0$ due to the pion mass differences and below $\eta = 0.5$ the acceptance of the PROMICE/WASA detector for $dp \to dn\pi^+$ dropped rapidly.

Dalitz Plots at $\eta \approx 0.3$

At the lowest beam energy of $T_d = 437$ MeV ($\eta = 0.32$ for $dp \to dp\pi^0$, $\eta = 0.13$ for $dp \to dn\pi^+$) no $dp \to dn\pi^+$ events could be observed, because the deuterons were always emitted into the beam pipe. For $dp \to dp\pi^0$ at this energy the beam pipe also became the limiting factor and has cut out a larger fraction of phase space as shown in figure 4.18. This angular limitation prevented also measurements closer to threshold, where already excellent data from [Roh 93] exist.

Comparing the generated event samples in figure 4.18 it becomes also clear that for all applied models the available phase space is very narrow and the events are more or less evenly distributed. On the one hand this is disadvantageous for a good separation of the applied models used as input for the fitting procedures; on the other hand the uncertainties from extrapolation of the results to uncovered regions of phase space are reduced. The most significant information obtained from the low energy data was therefore the total cross section and not the specification of reaction mechanism obtained from the partial wave analysis.

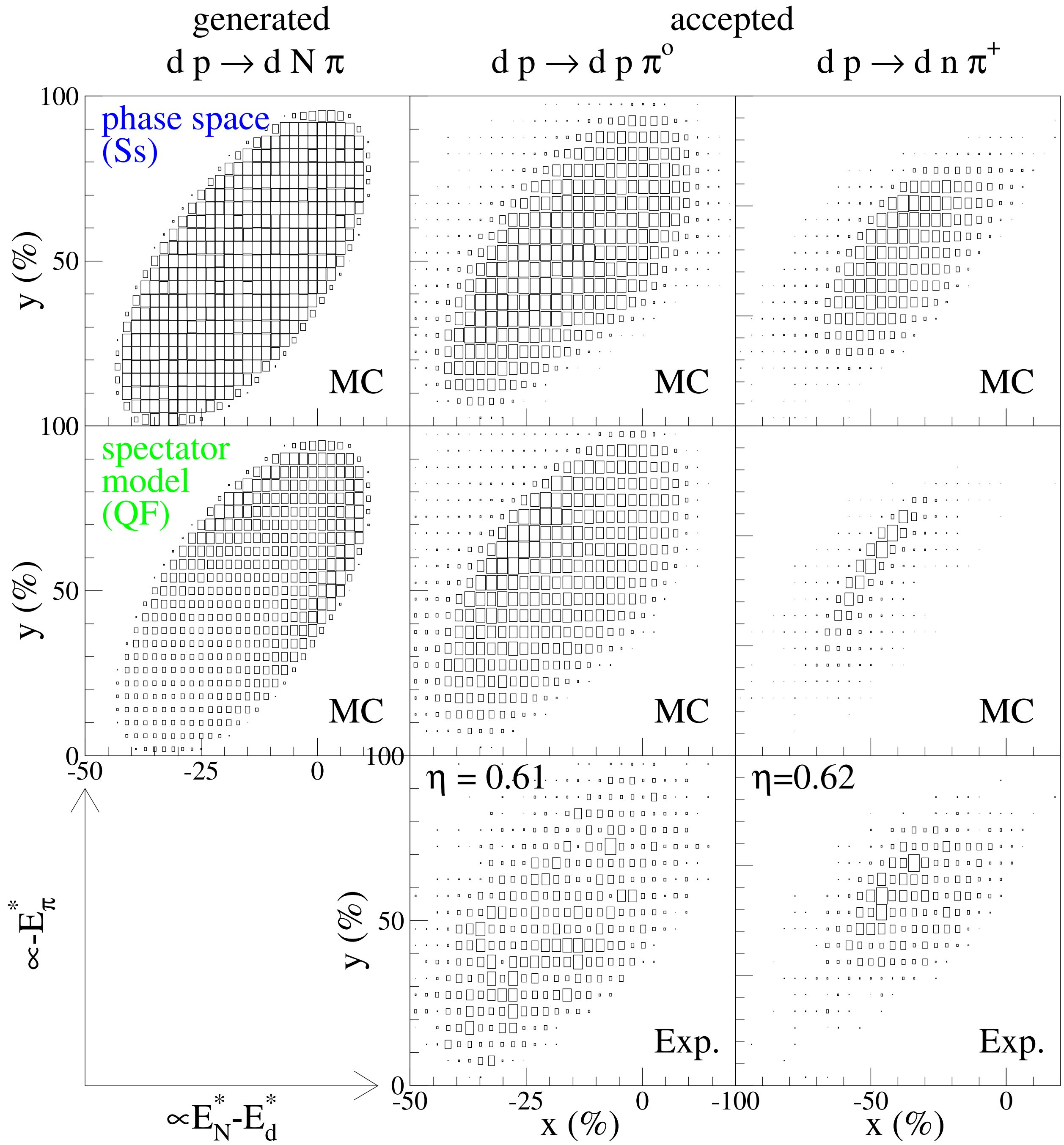

Figure 4.17: *The Dalitz plots at* $\eta \approx 0.6$*. This* η*-value corresponds to a deuteron beam energy of* T_d*=492 MeV for* $dp \to dp\pi^0$ *and* T_d*=515 MeV for* $dp \to dn\pi^+$ *.*

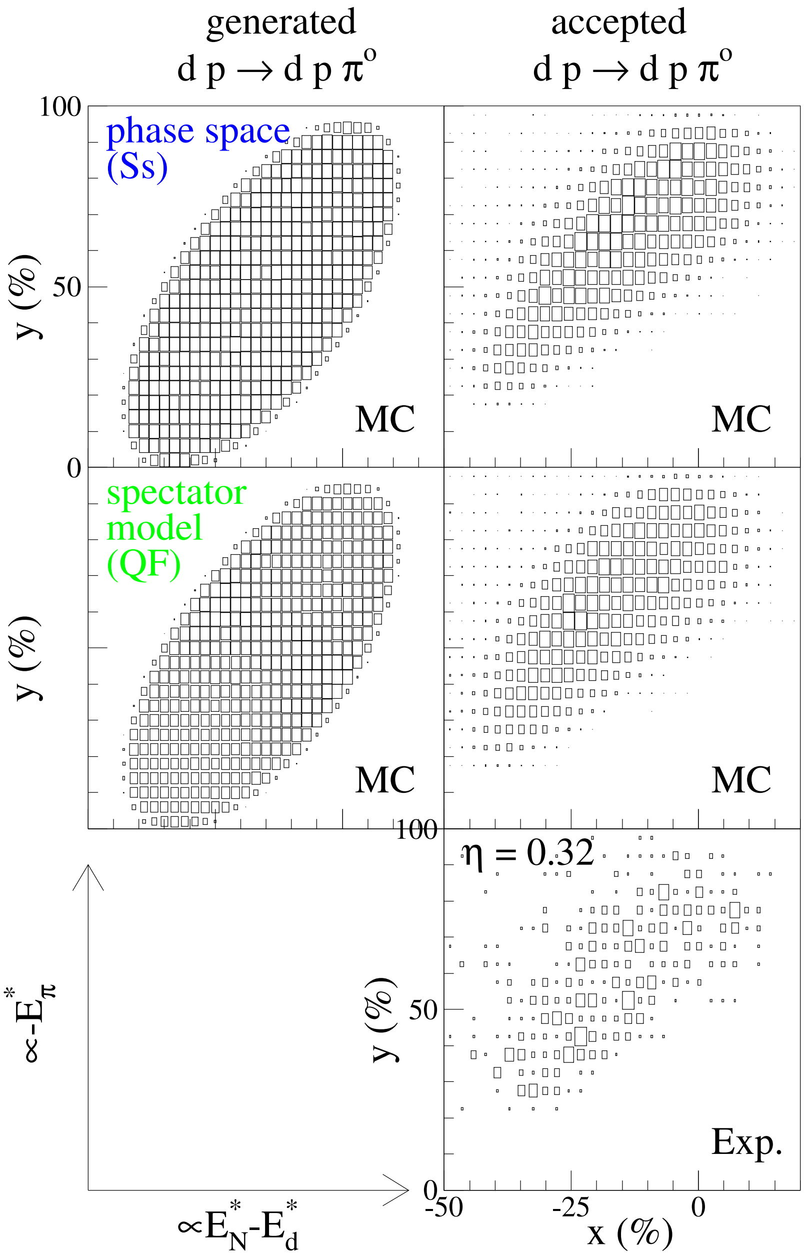

Figure 4.18: *The Dalitz plots at* T_d *=437 MeV* (η = 0.32)*. Only* $dp \rightarrow dp\pi^0$ *was within the detector acceptance at this energy. The detector acceptance was mainly reduced by the lower* 4^o *limit in* Θ *caused by the opening for the beam pipe. The differences in the phase space distributions of the different models vanish close to threshold.*

4.3.7 Summary of Errors

Statistical Errors

The number of experimentally observed events included in the analysis varied between 971 events for $dp \to dn\pi^+$ at T_d =492 MeV and 12480 events for $dp \to dp\pi^0$ (FDCFDCCDN) at $T_d = 559$ MeV. The statistical errors of $\delta_N = 1/\sqrt{N_{exp}}$ were therefore only in the order of 1 to 3 percent.

Systematical Errors

The systematical errors were more substantial.

For the luminosity determination they were assumed to be 15 percent for the September 1996 beam time and 5 percent for April 1997 (section 2.3). The *pd*-scattering reference data from [Roh 94] introduced another uncertainty in the order of 8 percent. The two errors were added quadratically and resulted in total errors for the luminosity in the order of 17 percent for the September 1996 data and 10 percent for April 1997.

The error in the efficiency of the deuteron identification δ_d was estimated to be 15 percent due to poorly known secondary reaction losses in the Forward Detector and uncertainties in the calibration of FHD3 (section 3.4.2). For the proton identification the systematical errors δ_p not reproduced by WMC were expected to be small (see e.g. [Häg 97]) and have been set to 1 percent. For the π^+ identification the efficiency of the delayed pulse routine was reproduced by WMC with an accuracy δ_{π^+} of better than 15 percent (section 3.4.3).

The errors caused by the extrapolation of the Monte Carlo results to regions of phase space not covered by the detector acceptance (δ_{accep}) were difficult to estimate. For $dp \to dp\pi^0$ the detector always covered most of the available phase space and therefore the error caused by uncertainties in the Monte Carlo model is assumed to be less than 10 percent. The previously described variations of the boundary conditions for the fitting procedures did not change the total cross sections for $dp \to dp\pi^0$ by more than that.

For $dp \to dn\pi^+$ the detector covered a much smaller fraction of phase space and therefore *no* reliable error estimate for the fractional contributions of the reaction models can be given. Of course it would be possible to assume isospin invariance and use the results obtained for $dp \to$-$dp\pi^0$ to describe the production mechanism for $dp \to dn\pi^+$ and calculate the cross sections accordingly. This is however only justified, if a pure quasifree production according to the spectator model can be assumed. Since the analysis has shown, that the quasifree spectator model accounts only for a part of the total cross section this approach has not been tried.

All given errors were assumed not to be correlated and have therefore been added quadratically.

4.3.8 Total Cross Sections for $dp \to dp\pi^0$ and $dp \to dn\pi^+$

According to the obtained model contributions it is now possible to calculate the total cross sections from equation 4.7. For prescaled events the prescaling factor P had do be applied. The numerical values are given in table 4.4 for $dp \to dp\pi^0$ and in table 4.5 for $dp \to dn\pi^+$ and are also plotted in figures 4.19 and 4.20.

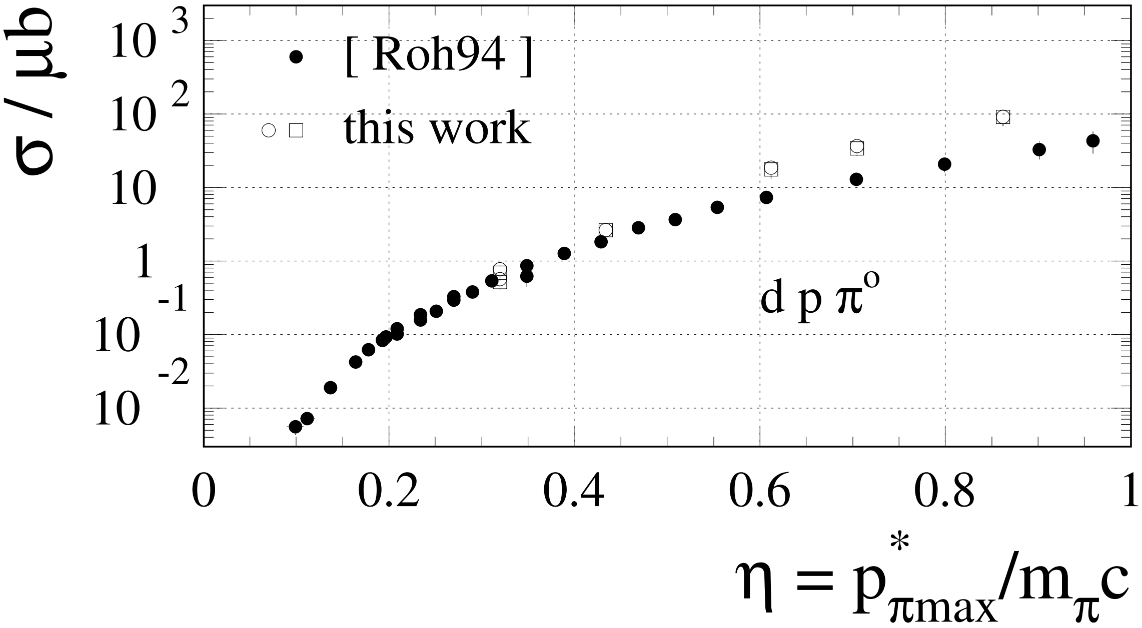

Figure 4.19: *The experimental total cross sections for* $dp \to dp\pi^0$ *. The closed circles (•) are the results from [Roh 94]. The open symbols are from this work. The open circles (○) are the results obtained with the FDCFDC analysis procedure and the open boxes (□) denote the results, if an additional* γ *hit was required in the Central Detector (FDCFDCCDN).*

T_d [MeV]	η	P	N_{exp}	N_{gen}	L $[10^{34}cm^2]$	δ_N [%]	δ_d [%]	δ_p [%]	δ_L [%]	δ_{accep} [%]	σ_{tot} [μb]
559.0^a	0.862	2^3	12480	193733	1.72	1	15	1	17	10	90 ± 22
514.8^a	0.705	2^3	2416	30161	0.71	2	15	1	10	10	34 ± 7
491.8^a	0.612	2^3	2634	34949	1.59	2	15	1	17	10	18 ± 4
454.7^a	0.434	2^1	1820	27962	2.14	2	15	1	10	10	2.6 ± 0.5
436.7^b	0.320	2^0	1747	13442	1.74	2	15	1	17	10	0.77 ± 0.19
436.7^b	0.320	2^0	1949	14531	2.57	2	15	1	10	10	0.57 ± 0.12

Table 4.4: *The experimental total cross sections for* $dp \to dp\pi^0$ *and the most important input parameters for their calculation. The estimated errors are also given. For* $dp \to dp\pi^0$ *two analysis procedures have been applied: (a) FDCFDCCDN and (b) FDCFDC.*

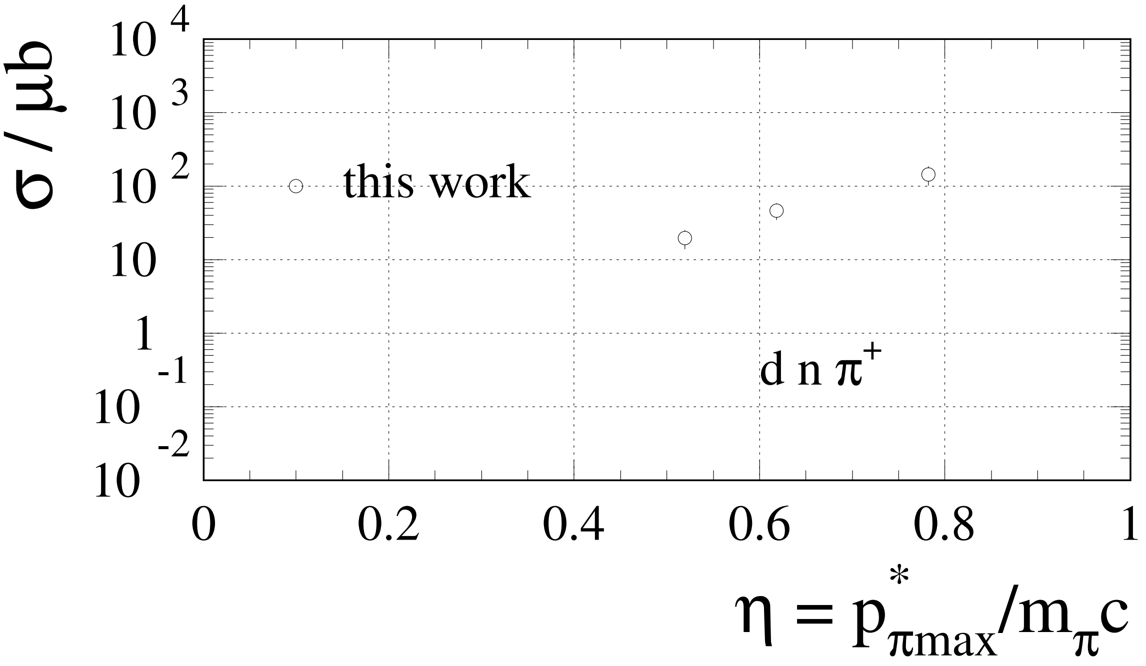

Figure 4.20: *The experimental total cross sections for* $dp \to dn\pi^+$

T_d [MeV]	η	P	N_{exp}	N_{gen}	L $[10^{34}cm^2]$	δ_N [%]	δ_d [%]	δ_{π^+} [%]	δ_L [%]	δ_{accep} [%]	σ_{tot} $[\mu b]$
559.0	0.782	2^3	9206	308250	1.72	1	15	15	17	-	144 ± 42
514.8	0.619	2^3	1274	41479	0.71	3	15	15	10	-	47 ± 12
491.8	0.519	2^3	971	38985	1.59	3	15	15	17	-	20 ± 6

Table 4.5: *The experimental total cross sections for* $dp \to dn\pi^+$ *and the most important input parameters for their calculation. The estimated errors are also given. The error caused by uncertainties in the model description due to the limited acceptance is* not *included.*

4.3.9 Comparison with Results from [Roh 94] and Predictions from [MN 93]

Figure 4.19 showed already, that the results obtained in this work do *not* agree with the previously published data from [Roh 94] at higher energies. At $\eta = 0.32$ and $\eta = 0.43$ there is no discrepancy within the error margins, but at higher energies the differences become significant. At $\eta = 0.86$ the calculated cross section is about a factor of 3 above the result from [Roh 94] and therefore in clear contradiction.

The discrepancy can be traced back to the acceptance of the Indiana experiment at higher energies shown in figure 1.8. The Indiana experiment had practically no acceptance for quasifree

$dp \rightarrow dp\pi^0$ production according to the spectator model from [MN 93] and as a consequence it has not been included in the model description used for the calculation of the total cross sections. For the coherent production mechanisms at values of $\eta > 0.5$ a small acceptance was obtained, but again with significant uncertainties in the model description.

Nevertheless agreement between the two experiments can easily be established, if the Indiana data is corrected for the unobserved quasifree contribution in the total cross sections. At $\eta = 0.86$ the results from this work yield a quasifree contribution of approximately 60 percent in the total cross section. Assuming that these 60 percent were not observable in the Indiana experiment one has to apply a correction factor of 2.5 to the Indiana data to obtain the real total cross sections. Indeed the application of this factor would eliminate most of the discrepancy and with similar corrections the results would agree within the errors at all energies !

At lower energies of $\eta < 0.5$ the quasifree contribution was found to be small anyway and therefore the results agree already without the correction.

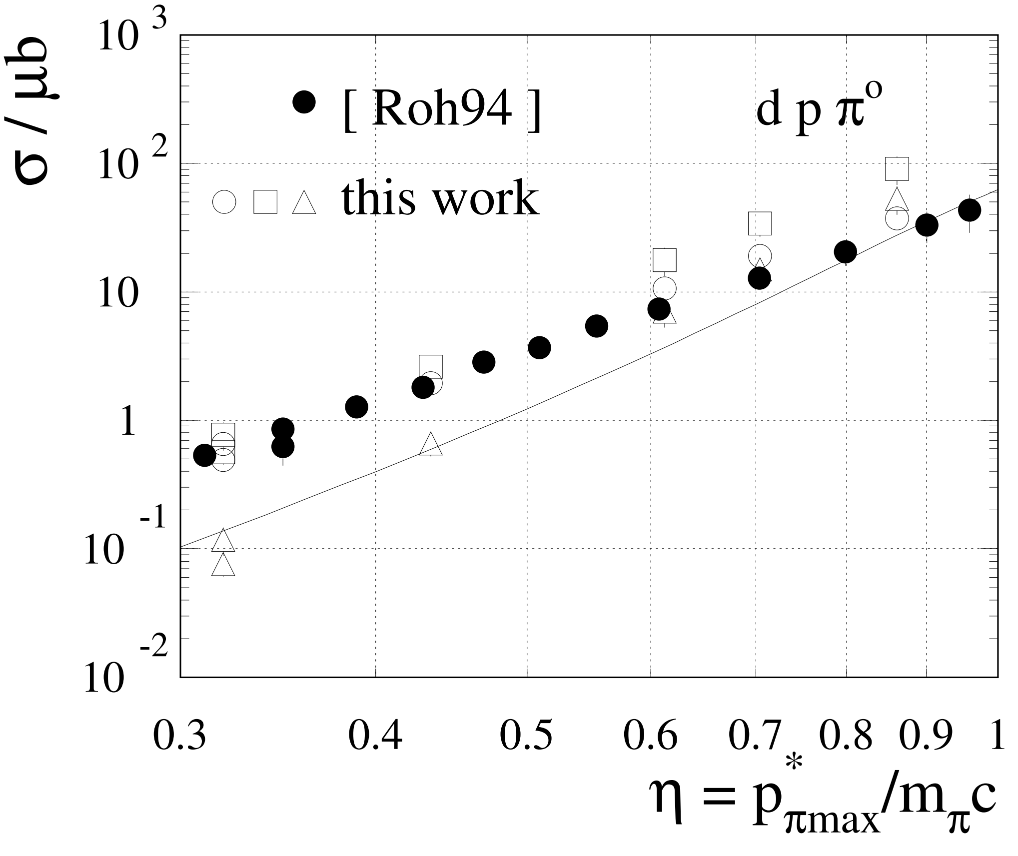

Figure 4.21: *The excitation functions of the total cross sections within the covered energy range. The filled symbols (•) are the results from [Roh 94] and the open symbols are the results from this experiment. The square symbols (□) give the total cross section for $dp \rightarrow dp\pi^o$. The contribution from quasi-free $pn \rightarrow d\pi^o$ is indicated by the open triangles (△) and the coherent pion production is shown as open circles (○). The line shows the calculated contribution from the quasi-free spectator model in [MN 93].*

This is also demonstrated in figure 4.21, where the total cross sections obtained in this work (□) are separated into a quasifree cross section (△) and the coherent cross section (○). The results from [Roh 94] are also included (●). Assuming that the Indiana experiment was essentially only sensitive to the coherent part full agreement is achieved.

It is also interesting to take a closer look at the absolute values of the quasifree contribution in the total cross section. The spectator model from [MN 93] was able to predict these cross sections and the prediction is shown in figure 4.21 as a solid line. Although the model fails to describe the total cross sections for $dp \to dp\pi^0$, it gives a quite good description of the excitation function for the quasifree interaction. The discrepancy between this calculation and our experimental results would then be attributed to the presence of the coherent interaction contribution.

4.3.10 The Influence of Final State Interaction

The last statement is at variance with [MN 93], who have also claimed, that the discrepancy in the total cross sections can be explained *without* assuming contributions from coherent processes, but solely with final state interaction.

Therefore they have included final state interaction in their spectator model as outlined in section 4.3.4. According to this model the final state interaction is treated as an additional factor ξ_{fsi} in the phase space integral (equation 4.10). It enhances the probability for smaller relative momenta in the *dp* center of mass system (except for very small relative momenta when Coulomb repulsion comes into play). The FSI-term has therefore an attractive effect.

For testing purposes, the FSI was included in the spectator model calculations of this work too. The attractive FSI effect would have the consequence, that in the lab system higher deuteron energies and lower proton energies are favored as shown in figure 4.22. Indeed could this at least partly explain the discrepancy between the spectator model and the experimental data observed for example in the proton and deuteron energy spectra in figure 4.3. Nevertheless, as shown in figure 4.22 an attractive final state interaction is *not* able to provide an additional transversal spectator momentum, necessary to force the proton to larger laboratory angles. These large proton angles can *only* be achieved, if the proton already participates in a momentum transfer before or during the pion production process and does not only act as a spectator.

The observation of protons under large laboratory angles is therefore a strong argument for the existence of coherent production mechanisms involving all three nucleons, because they can not be explained, assuming quasifree $pN \to d\pi$ production mechanisms from [MN 93], with or without final state interaction.

The inclusion of final state interaction in the spectator model did also *not* increase the contributions of the quasifree mechanism, if the fitting procedure was applied. The χ^2, however, was increased significantly at higher energies because now the characteristic peak at low deuteron energies could not be described with a good accuracy anymore. At $\eta = 0.86$ it changed from χ^2 =3.0 without inclusion of FSI to 8.3 with inclusion of FSI. At $\eta = 0.32$, however, the models converged and the differences in χ^2 became negligible (3.0 without FSI and 3.1 with FSI). Based on our data, the final state interaction seems therefore insufficient and inadequate to account for the discrepancy under discussion.

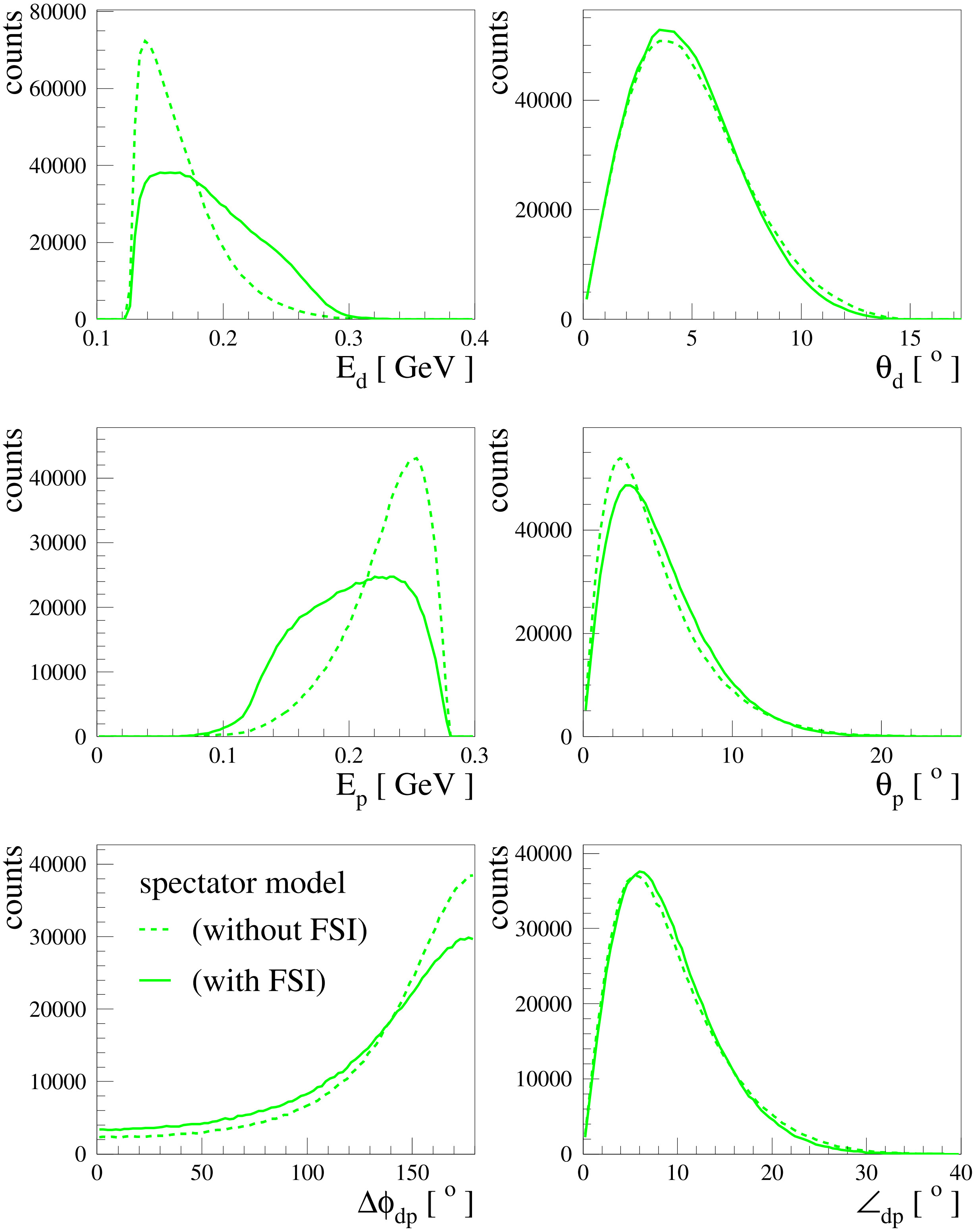

Figure 4.22: *Comparison of generated event distributions for* $dp \to dp\pi^0$ *at* $T_d = 559\,MeV$ *(*$\eta = 0.86$ *for the spectator model without (dashed line) and with Final State Interaction (solid line). The events cover the whole phase space and are not corrected for the detector acceptance.*

4.3.11 Summary

$dp \rightarrow dp\pi^0$ and $dp \rightarrow dn\pi^+$ have been examined in the energy region of $\eta = 0.32$ up to $\eta = 0.86$. The total cross sections for $dp \rightarrow dp\pi^0$ support previous results from [Roh 94] at values of $\eta < 0.5$, but are at variance at larger energies. The discrepancies can be resolved if a quasifree contribution according to the model of [MN 93] is added to the results in [Roh 94].

Quasifree pion production according to [MN 93] becomes dominant at values of $\eta > 0.8$ but does not explain the bulk of the spectra and total cross sections at lower energies. It is assumed that pion production mechanisms involving all three nucleons account for most of the total cross section at these energies. The nature of these processes can not be extracted in more detail.

4.4 Discussion of $dp \rightarrow ppp\pi^-$

This last pion production process under discussion is also the one with the worst quality of the experimental data. For $dp \rightarrow ppp\pi^-$ 672 events have been extracted at the beam energy of T_d=559 MeV ($\eta = 0.79$), 91 events at T_d=515 MeV ($\eta = 0.62$) and 39 events at T_d=492 MeV ($\eta = 0.52$). All data samples were extracted by identification of three protons as described in section 3.6.3 and may still include some background. Nevertheless an attempt has been made to examine this reaction and to *estimate* some cross sections.

The Motivation is twofold. In the past $pd \rightarrow ppp\pi^-$ has at least three times been the subject of examination. The purpose has always been to use the deuteron as a quasifree neutron target and to examine the assumed quasifree process $pn \rightarrow pp\pi^-$. [Dak 82] have measured total cross sections at proton beam energies of 500 - 1000 MeV ($2 < \eta < 4$) in a bubble chamber experiment. They were trying to find evidence for dibaryonic resonances, which were expected in a $np \rightarrow d' \rightarrow pp\pi^-$ channel. [Pon 89] have used a polarized proton beam of 400 MeV to extract analyzing powers and recently [Dun 98] have published three differential cross sections at T_p = 353, 403 and 440 MeV. In total the data base for $pn \rightarrow pp\pi^-$ is very poor compared to other channels; close to threshold exist no data at all (see figure 1.2).

Two arguments support a closer investigation of the $dp \rightarrow ppp\pi^-$ reaction.

- $pn \rightarrow pp\pi^-$ can be expressed in terms of the elementary cross sections as $\sigma_{pn\rightarrow pp\pi^-} = \frac{1}{2}\sigma_{11} + \sigma_{01}$. σ_{11} is well known from the examination of $pp \rightarrow pp\pi^o$, and a precise measurement of $pn \rightarrow pp\pi^-$ might therefore give insight in the σ_{01} cross section, which is not known close to threshold.

- $dp \rightarrow ppp\pi^-$ is a reaction with three protons in the final state. Since at least two of them must be emitted with parallel spins, the Pauli Principle might reduce the available phase space and therefore the cross sections close to threshold [Wil 99].

The data obtained in this experiment was not sufficient to answer these questions. They may, however, be of interest for future experiments to get an estimate of the total cross sections and reaction mechanisms.

Up to now no theoretical calculation for this reaction exists. Instead one can adopt the basic ideas of [MN 93] and apply a primitive spectator model, assuming that the proton of the initial deuteron acts as a spectator and the neutron and target proton undergo the quasifree $np \rightarrow pp\pi^-$ reaction as shown in figure 4.23. For this purpose the same routines have been

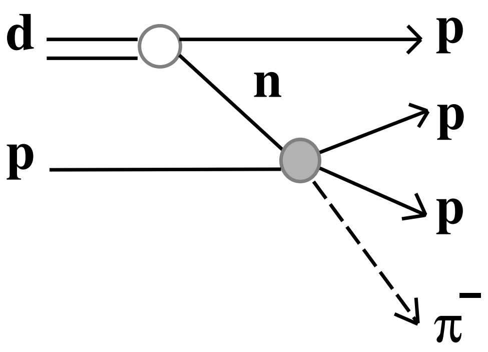

Figure 4.23: *Spectator model graph, the two vertices denote the deuteron wave function and the* $np \to pp\pi^-$ *reaction.*

applied as for the quasifree $dp \to dN\pi$ event generation. The $pN \to d\pi$ input cross section has been replaced by the one for $pn \to pp\pi^-$ that was estimated from isospin invariance:

$$\sigma_{tot(np\to pp\pi^-)}(\eta) \approx \frac{1}{2}\sigma_{tot(pp\to pp\pi^0)}(\eta) \tag{4.24}$$

using the parameterization from [Fäl 96]

$$\sigma_{tot(pp\to pp\pi^0)}(\eta) = D(\zeta\eta)^4 \left(1+\sqrt{1+\zeta^2\eta^2}\right)^{-2} \tag{4.25}$$

where $\zeta = 12.6$ is a numerical factor containing masses and binding energies. A pure phase space distribution has been assumed to approach the differential $pn \to pp\pi^-$ cross section.

The results from this spectator model have then been applied in combination with a pure phase space distribution to account for possible production processes involving all nucleons. For this reaction the fitting procedure was based on the proton energy and angular spectra as only input. Figure 4.24 shows the result of the fit at $T_d = 559\,\mathrm{MeV}$ ($\eta = 0.79$). Similar to the previous $dp \to dN\pi$ data, the spectra are not described by a pure phase space distribution. The enhancement of protons with less than 100 MeV kinetic energy in the lab system might originate from the $np \to pp\pi^-$ protons with an additional spectator proton distributed around 200 MeV. The significant dip around 150 MeV is not reproduced.

The angular distribution disagrees with a phase space distribution and favors the quasifree process. It is interesting to note, that at this energy the simple model yields again a quasifree contribution of roughly 60 percent, similar to the $dp \to dN\pi$ results. Beyond this overall agreement, the quality of the experimental data, in particular at the two lower energies prevents a more detailed investigation.

The results obtained can then be used to *estimate* the total cross sections for this reaction. They are shown in figure 4.25 and are about two orders of magnitude smaller then the ones for $dp \to dp\pi^o$. Errors are not included in the plot. They might be substantial due to the poor statistics, the unclear background conditions for this reaction and the lack of good models describing the fraction of events with one of the three protons lost in the beam pipe, resulting in possible systematic errors of the detector acceptance.

The only available total cross sections from [Dak 82] are also plotted for comparison. To describe the development of the total cross sections as a function of energy an η^5 and η^7 parameterization normalized to the data point at $T_d = 559\,\mathrm{MeV}$ ($\eta = 0.79$) is also given to guide the eye.

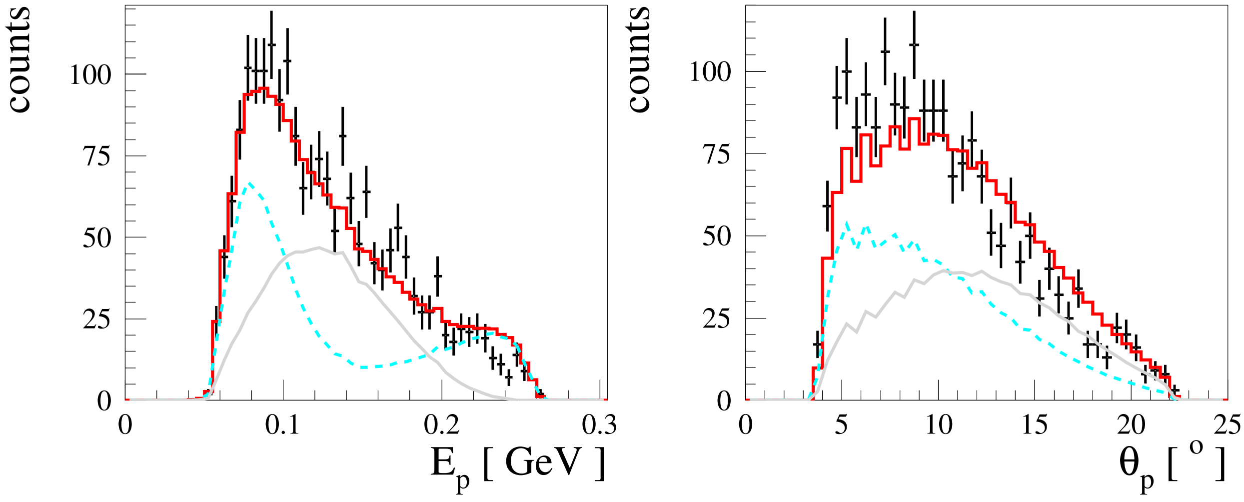

Figure 4.24: *Comparison of the experimental proton angular and energy distributions for* $dp \to ppp\pi^-$ *at* $T_d = 559\,MeV$ $(\eta = 0.79)$. *The dashed line is the spectator model contribution and the light solid line gives the contribution from a second process with an assumed phase space distribution. The dark solid line shows the sum obtained from the fitting procedure.*

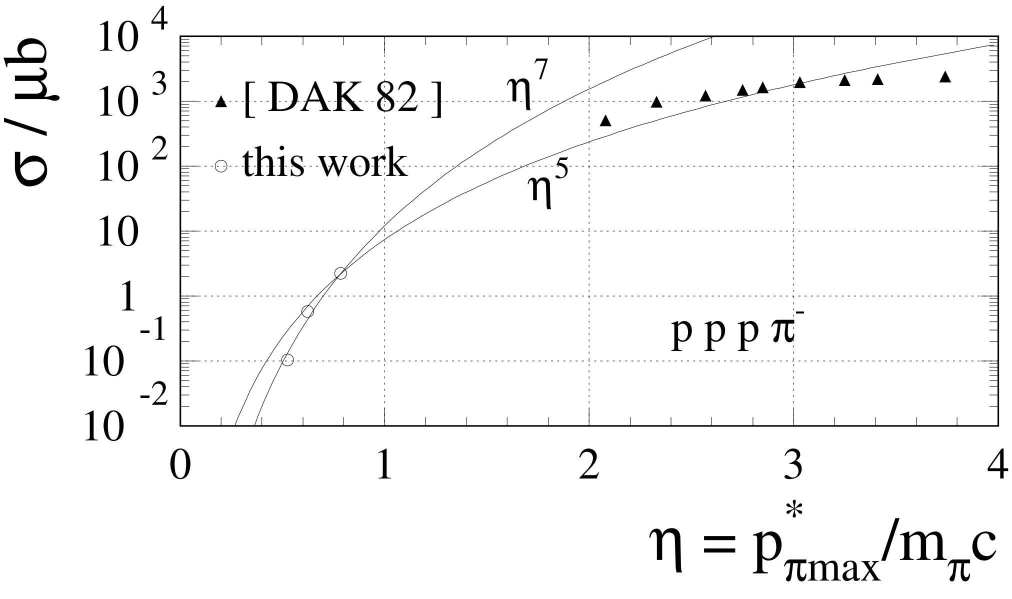

Figure 4.25: *Estimated total cross sections for* $dp \to ppp\pi^-$. *The reference data from [Dak 82] is also given.*

The energy dependence expected only from phase space, i.e. for a constant matrix element, is η^7. Effects of final state interaction between two protons as observed in e.g. $pp \to pp\pi^o$ could reduce this energy dependence in the near threshold region to η^5, while on the other hand the Pauli Principle might again introduce an aditional factor of η^2 [FW 98].

More experimental and theoretical effort is necessary to understand this reaction in the near threshold region.

4.5 Discussion of $dp \to dp\gamma$

As shown in section 3.6.5 the examination of the $dp \to dp\pi^0$ channel revealed also very clean data samples of deuteron proton Bremsstrahlung $dp \to dp\gamma$ with several thousand of overdetermined events. Although it has not been the purpose of this experiment to investigate the nucleon nucleus Bremsstrahlung, the events have been analysed too, to get an additional cross check for the $dp \to dp\pi^0$ results, which have been extracted with a very similar procedure. Since in principle there is no threshold for the Bremsstrahlungs-process, it is expected, that the production mechanisms and cross sections for this reaction do not change significantly within the energy range of $T_d = 440 - 560\,\mathrm{MeV}$. Therefore $dp \to dp\gamma$ seemed to be suited to be used as a monitor to indicate possible changes in the performance of the detector.

In addition the data may be of interest for themselves, because the $pd \to pd\gamma$ data base is poor and contradictory.

4.5.1 Overview on pd-Bremsstrahlung

In the past proton Bremsstrahlung on deuteron targets has been of some interest since it was regarded as an important step to understand Bremsstrahlungsprocesses observed in the interaction of nucleons with heavy nuclei (e.g. [Kwa 88]). In addition the deuteron was also regarded as a neutron target to examine the $pn \to pn\gamma$ reaction, which cross sections seem to be at least an order of magnitude larger than the ones for $pp \to pp\gamma$ ([Koe 67], [Bra 68], [Bil 98]).

First measurements have been published in the late sixties ([Edg 66], [Koe 67]) with contradicting results. [Edg 66] have used a proton beam of 140 MeV and only a γ-detector to identify Bremsstrahlungs events $pd \to X\gamma$ for which they have estimated a total cross section of $11\mu b$ with no more than $1\mu b$ originating from a $pn \to d\gamma$-'capture'-reaction. In clear contradiction [Koe 67] have published a value of $35 \pm 12\mu b$ for $pd \to X\gamma$ at $T_p = 197\,\mathrm{MeV}$ with a significant contribution from $pn \to d\gamma$.

The next investigations on pd-Bremsstrahlung have been published 20 years later. [Pin 90] reports a measurement of $pd \to X\gamma$ at $T_p = 200$ MeV ($\sigma_{tot} \approx 34\mu b$) and [Cla 92] have measured at $T_p = 145$ MeV ($\sigma_{tot} = 21 \pm 2\mu b$) and 195 MeV ($\sigma_{tot} = 34 \pm 4\mu b$), again only inclusive.

All these experiments suffer from the fact that they were not able to identify the outgoing charged particles. Therefore they were neither able to distinguish between $pd \to {}^3\mathrm{He}\gamma$, $pd \to pd\gamma$ or $pd \to ppn\gamma$ nor to measure above the pion-production threshold. Only in [Pic 87] an exclusive measurement of the radiative capture $pd \to {}^3\mathrm{He}\gamma$ below the pion production threshold has been reported by the IUCF. A recent experiment at $T_p = 190MeV$ seems to be able to distinguish protons and deuterons and has published preliminary differential cross sections [Kal 98].

While the experimental situation for these reactions is still poor the theoretical treatment of pd-Bremsstrahlung seems to be even worse. Up to now there exist no good calculations for this process [Kal 98] and only some comparisons with predictions for the free $pn \to pn\gamma$ have been shown (e.g. [Cla 92]).

4.5.2 Monte Carlo Description of $dp \to dp\gamma$

Since the results obtained within this experiment seem to be the first exclusive measurements of $dp \to dp\gamma$ above the pion production threshold with no theoretical predictions available, a phenomenological approach has been used to describe the experimental data with WMC .

In the spirit of the interaction $dp \to dp\pi^0$ it has been assumed that $dp \to dp\gamma$ is based upon two elementary processes, **(i) coherent Bremsstrahlung**, and a **(ii) quasifree process** $np \to d\gamma$ with an unaffected spectator proton. For the coherent Bremsstrahlung a simple three body phase space distribution has been used to generate the events.

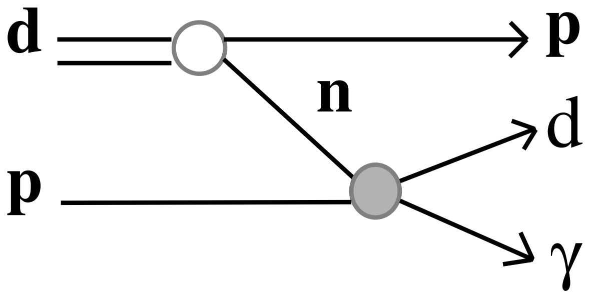

Figure 4.26: *Spectator model graph, the two vertices denote the deuteron wave function and the quasifree* $np \to d\gamma$ *reaction.*

For the quasifree process (figure 4.26) the spectator proton has been generated according to its momentum distribution in the deuteron. It was furtheron assumed, that the total $np \to d\gamma$ cross section is constant within the range of np center of mass energies, that can occur due to the momentum spread of the spectator proton. This seemed to be reasonable so far above the threshold. It was furtheron assumed that the $d\gamma$ angles are isotropic in the np cm-system. There exist measurements of $np \to d\gamma$ (compare e.g. [Nic 84]), which have shown some deviations of this assumption, but since they seemed to be small they have been neglected.

The generated events have then again been simulated with WMC and analysed with PWREC. Similar to $dp \to dp\pi^0$ the contribution of the two models has been determined with a best fit to the six experimental spectra shown in figure 4.27.

It is remarkable that this two parameter fit succeeds to describe the experimental data without any significant discrepancies, neither in the primary distributions shown in figure 4.27 nor looking at any derived spectra like e.g. invariant masses. There are some small differences within the deuteron and proton energy distributions, which may be due to simplified inclusion of the $np \to d\gamma$ cross sections in the spectator model.

Similar to the $dp \to dp\pi^o$ results the most significant deviations from the assumption of a pure quasifree production mechanism can be observed in the angular distributions of the assumed spectator proton, with a clear enhancement at larger angles.

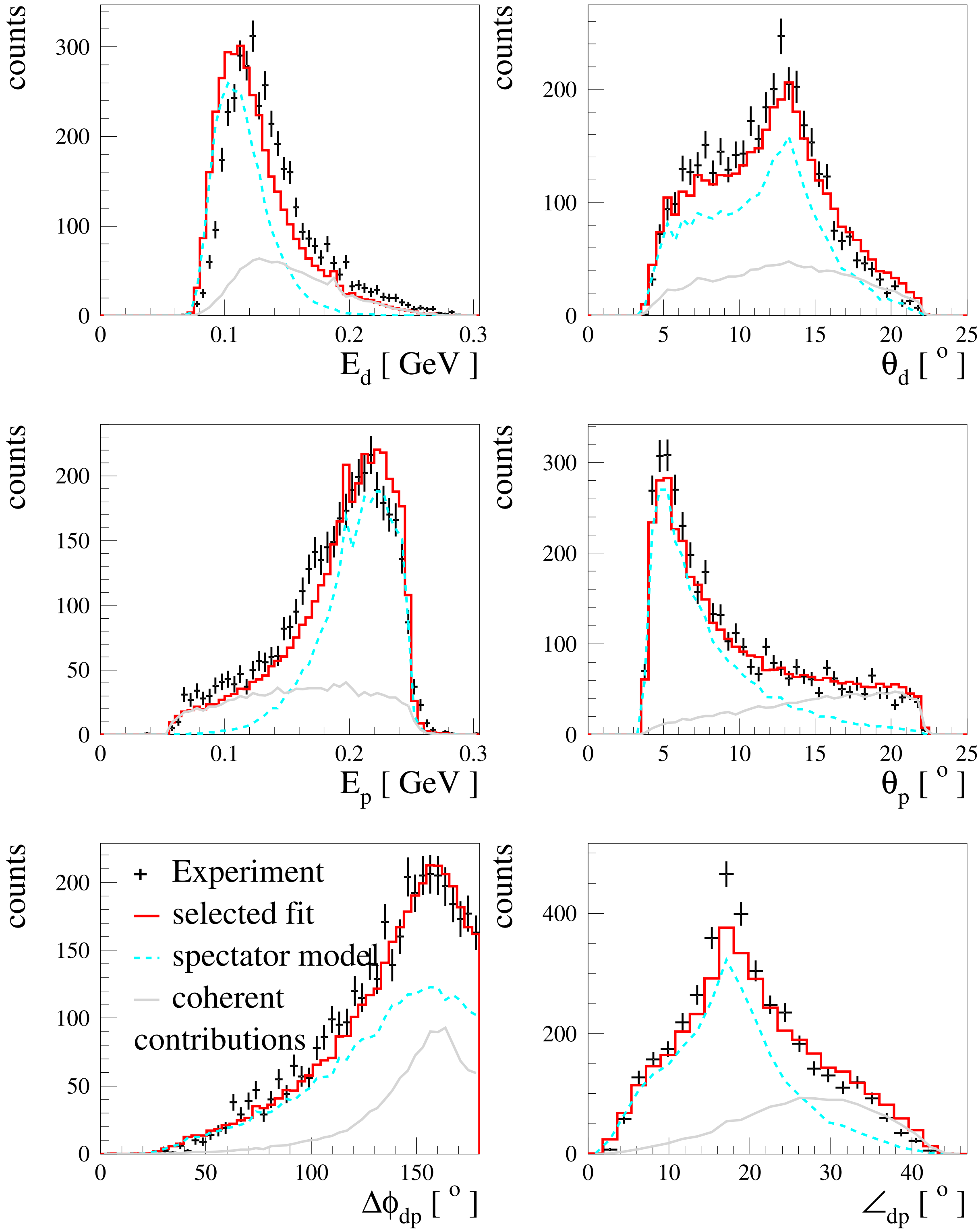

Figure 4.27: *Comparison of the experimental angular and energy distributions for* $dp \to dp\gamma$ *at* $T_d = 455\,MeV$ *with results obtained from the Monte Carlo simulation. Here only the spectator model and a pure three body phase space distribution have been used to describe the experimental data. The spectra at the other energies look very similar and are therefore not shown here. The cut-off at the proton energy of* $T_p \approx 250\,MeV$ *is caused by the use of FRH4 as a veto within the hardware-trigger.*

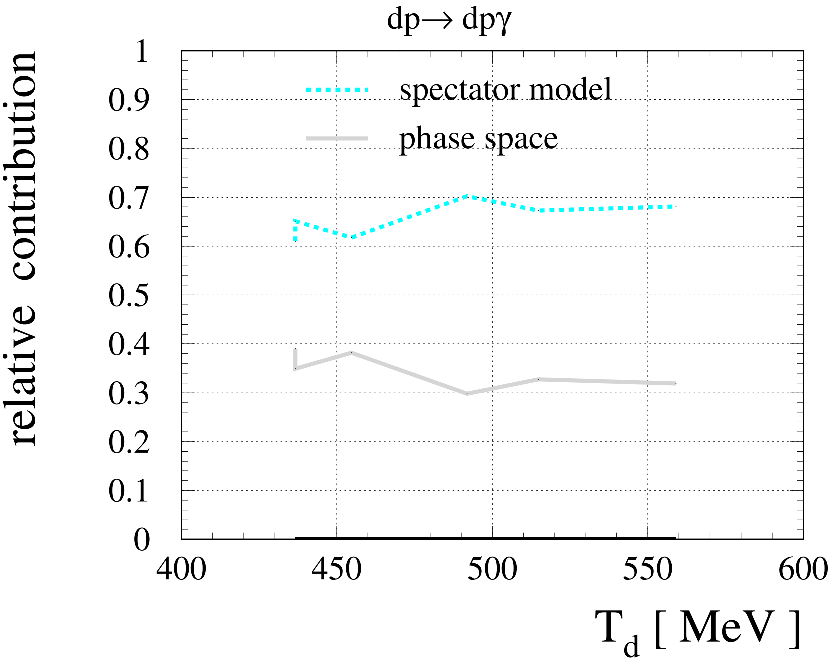

Figure 4.28: *Contribution of the two models to the total $dp \rightarrow dp\gamma$ distributions for different energies.*

The energy dependence of the two contributions is shown in figure 4.28. Over the whole measured energy range the quasifree production mechanism $np \rightarrow d\gamma$ accounts for approximately two thirds of the cross section. There seems to be a small systematical difference between the results from the September 96 and April 97 beam times, which can be due to uncertainties in the calibration, but it does not exceed a few percent.

4.5.3 Acceptance and Cross Sections

Prior to an interpretation of these results one has to take into account the acceptance of the detector. It was limited mainly by the Forward Detector, which results in a maximum opening angle between the deuteron and the proton. Therefore the detector was not sensitive to events with small E_γ, where the opening angle between the deuteron and proton had to be large, similar to elastic scattering. In addition the acceptance in phase space was reduced by the Central Detector, which covered only $\Theta_\gamma \approx 30^o - 90^o$ in the lab system.

This can be seen also in the Dalitz plots shown in figure 4.29, where the generated Monte Carlo events are compared with those, which were accepted with the PROMICE/WASA detector according to WMC. The Dalitz plots demonstrate, that the experimental results in figure 4.27 give a good description of the assumed quasifree production mechanism while they are not able to predict coherent Bremsstrahlung with low energetic γ's.

If one assumes, that the results shown in figure 4.28 are valid also for that part of phasespace, which is not covered by the detector, it is possible to *estimate* the total cross sections for this reaction.

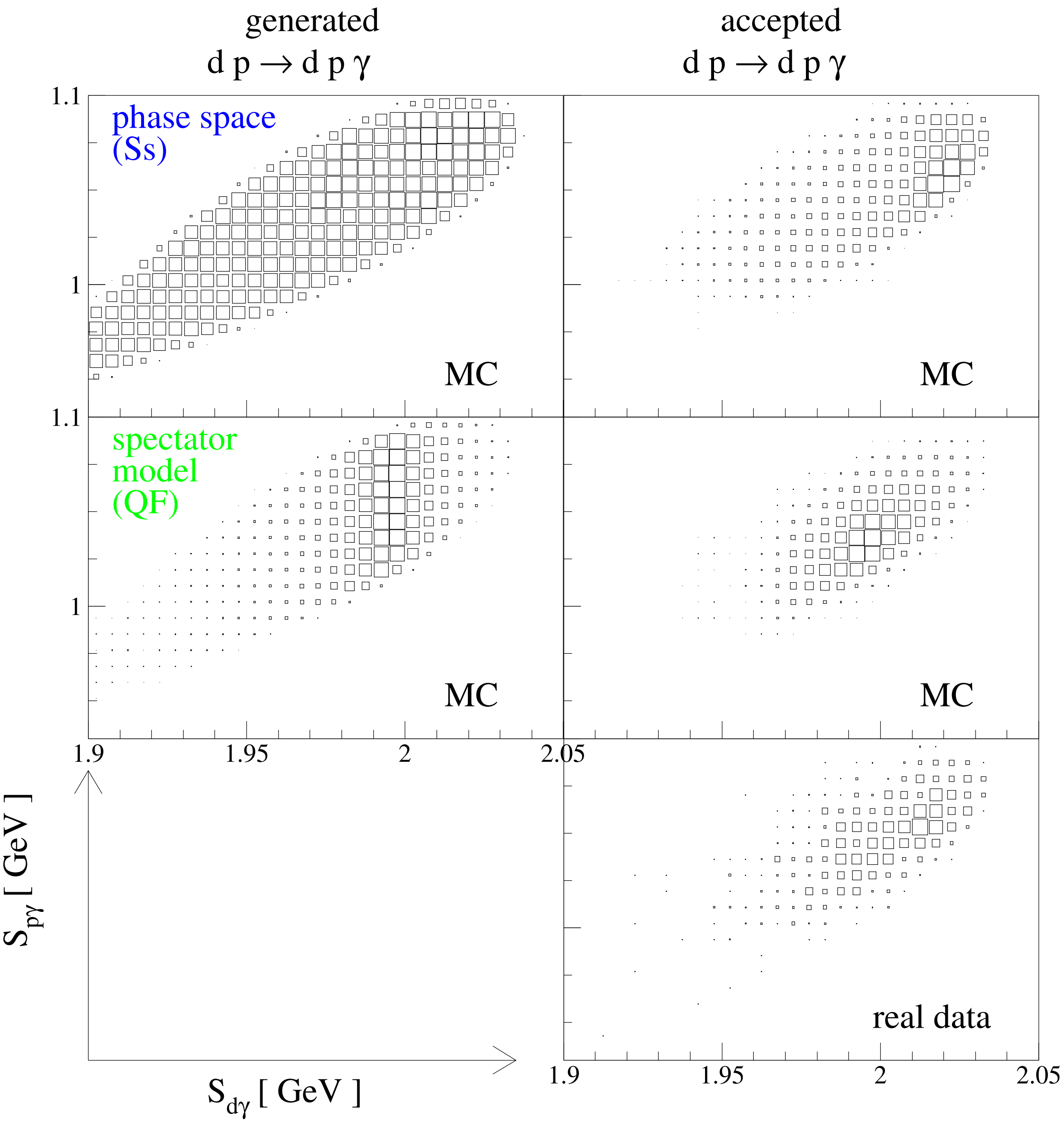

Figure 4.29: *Dalitz plots for $dp \to dp\gamma$ at $T_d = 492\,MeV$. The invariant mass within the $p\gamma$-system is plotted vs. the invariant mass within the $d\gamma$-system. The left column shows the whole set of generated events for the two models, while the right column includes the acceptance of the experiment. The detector has a favored acceptance for events with large γ-energies which can be seen within the first row, which contains the Monte Carlo (MC) data for a pure phase space distribution.*

The detector covers however a large fraction of those events which have been generated assuming the quasi-free production process, where the energy of the outgoing proton is more or less fixed due the deuteron wave function. This is shown in the second row while the third row contains the experimental data.

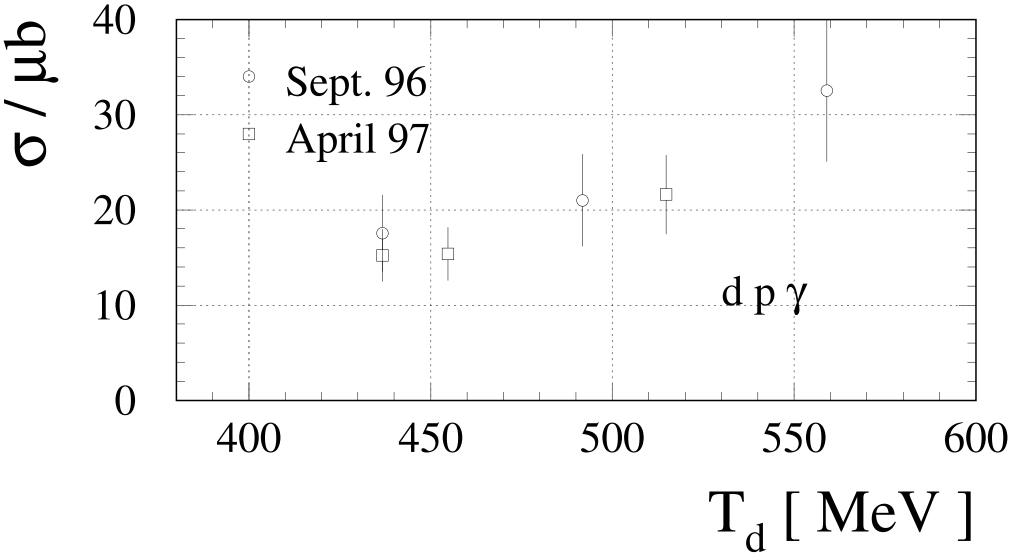

Figure 4.30: *The estimated total cross sections for $dp \to dp\gamma$ between $T_d = 437$ and $559\,MeV$. The plotted errors are only the statistical ones. The results from September 96 seem to overestimate the values from April 97 by up to approximately 15 percent.*

They are shown in figure 4.30. Within the observed energy range the total cross sections increase by a factor of 2 from 16 to 32 μb. This is not in particular disagreement with the results of approximately 34 μb, that have been published for proton projectiles corresponding to an energy of T_D =400 MeV ([Koe 67],[Pin 90],[Cla 92]) since these values were inclusive and contain also contributions from $dp \to {}^3\mathrm{He}\gamma$, $dp \to ppn\gamma$ or even $dp \to {}^3\mathrm{He}\pi^o$.

The estimated total cross sections for the quasifree $dp \to dp_s\gamma$ should also be comparable with previous results obtained for the $np \to d\gamma$ reaction for which a compilation of differential cross sections is given in [Nic 84]. Most of the data points shown there are calculated from results for the inverse photodisintegration process $\gamma d \to pn$, and the total cross sections within the energy region of $T_n = 190 - 290\,\mathrm{MeV}$ can be estimated to values in the order of 10 μb with an increase at higher energies.

This is in rough agreement with our results, at least at our lower energies. Assuming that two thirds of our total cross sections for $dp \to dp\gamma$ are caused by the quasi-free $np \to d\gamma$ process we get values between 10 and 20 μb for the $dp \to d\gamma p_{spec}$ process. A more detailed comparison is not meaningful, because the different results for photodisintegration are not in good agreement with each other either [Nic 84].

Returning to the $dp \to dp\gamma$ it seems as if there is a systematical difference in the order of up to 15 percent between the results we have obtained during the September 96 beamtime and those of April 97. A similar deviation can also be seen within the result for the $dp \to dp\pi^0$ cross section at $\eta = 0.32$ (figure 4.19). This can partly be explained by the deviations in the partial wave contributions shown in figure 4.28, but most of it is more likely due to a systematical error within the luminosity determination for September 96 (section 2.3).

Chapter 5

Conclusions and Outlook

5.1 Summary and Conclusions

Inelastic reactions channels with pion or photon production in deuteron proton collisions have been investigated in the energy range of T_d = 437 - 559 MeV with the PROMICE/WASA setup at the Cooler Synchrotron CELSIUS. The energy range extends from $\eta = 0.3$ near the three nucleon threshold up to the two nucleon threshold for pion production ($\eta \approx 0.85$). Special emphasis has been put on the examination of contributions of pure two nucleon interactions with the third nucleon acting as a spectator only. The selected energy range was of particular interest, because at the two nucleon threshold an assumed spectator nucleon can be emitted with zero spectator momentum in the initial deuteron rest frame. The inverse kinematics makes it nevertheless easily detectable.

For the main reaction of interest, $dp \rightarrow dp\pi^o$, a pure quasifree two nucleon interaction $np \rightarrow d\pi^o$ according to the spectator model from [MN 93] was found to be dominant close to the two nucleon threshold. However, the pure quasifree process failed to describe parts of the observed energy spectra and angular distributions of the proton and deuteron ejectiles. The inclusion of a final state interaction term in the spectator model did not improve the model description. The discrepancies have been solved by assuming so called coherent pion production mechanisms, where all three nucleons have to participate in the momentum transfer.

The measured total cross sections for $dp \rightarrow dp\pi^o$ agree with a previous IUCF experiment for $pd \rightarrow pd\pi^o$ ([Roh 93], [Roh 94]) at lower energies of $\eta < 0.5$. At higher energies of $0.5 < \eta < 0.9$ the results from [Roh 93] underestimate the values obtained in this experiment. Agreement can be achieved, if one assumes, that the IUCF experiment was not sensitive enough to the quasifree contributions to the total cross sections, because of the low spectator energy in the laboratory frame, and described only the coherent production mechanisms. A simultaneous measurement of the related reaction $dp \rightarrow dn\pi^+$ has yielded similar results for the relations between quasifree and coherent production mechanisms and thus supports the interpretation given.

In addition a first glance on the four body channel $dp \rightarrow ppp\pi^-$ has been shown. Again the observed spectra indicate, that a quasifree mechanism $np \rightarrow pp\pi^-$ contributes, but it fails to describe all of the data.

Finally the $dp \rightarrow dp\gamma$ reaction has been for the first time exclusively measured above the pion production threshold. The detector acceptance was limited to the areas of phase space favoring an assumed quasifree $np \rightarrow d\gamma$ process. The spectator model from [MN 93] has been applied accordingly and succeeds to describe about two thirds of the observed yield.

Altogether has this analysis shown, that the understanding of inelastic reactions in deuteron proton collisions is far from being complete.

The assumption of quasifree two nucleon interactions with a third spectator nucleon [MN 93] has been an important step to describe the reactions at energies, where these processes are kinematically possible, i.e. close to the two nucleon threshold.

However, other mechanisms exist, involving all nucleons, which give a significant rise of the cross sections close to threshold, compared to predictions from the spectator model. The detailed nature of these processes is not known yet.

5.2 Outlook

For a better understanding of three nucleon processes two ways of progress would be useful.

On the theoretical side more detailed calculations involving all three nucleons in the pion production process are needed. The addition of other quasifree two nucleon processes like $NN \rightarrow NN\pi$ or the inclusion of $pN \rightarrow pN$ scattering terms might be a next step. It would allow to develop models based upon known cross sections only. The models have to predict not only the total cross sections but also differential cross sections, i.e. angular and energy distributions or even polarization observables, if the spin structures are included. Without any doubt these calculations will not be trivial.

On the experimental side several supplementary measurements to improve the data base would be useful as well:

- For $dp \rightarrow dp\pi^o$ the experimental data base can only be improved in the near threshold region, if additional spin observables become accessible. At present the only place in the world to perform such a measurement is the IUCF accelerator with the PINTEX detector. Recently such an experiment has been proposed [Wel 99] to examine the two spin dependent total cross sections $\Delta\sigma_L/\sigma_{tot}$ and $\Delta\sigma_T/\sigma_{tot}$ ($\Delta\sigma$: spins opposite minus spins parallel for transverse (T) and longitudinal (L) polarisartion of the proton beam and deuteron target).

- The reaction $dp \rightarrow dn\pi^+$ is of the similar interest as $dp \rightarrow dp\pi^o$, but the experimental data is scarce. Assuming pure quasifree pion production the total cross section can be expected to be related to $dp \rightarrow dp\pi^o$ by an isospin factor of two and deviations from this assumption could give insight in the origin of the coherent production mechanisms. A more detailed investigation of this process requires a large angular acceptance for the π^+ detection to give reliable results for the total cross sections.

- The two body reactions $pd \rightarrow {}^3\mathrm{He}\pi^o$ and $pd \rightarrow {}^3\mathrm{H}\pi^+$ may be related to the unbound reactions $pd \rightarrow pd\pi^o$ and $pd \rightarrow nd\pi^+$ in the areas of phase space with small relative momenta of the outgoing nuclei. [Bou 96] and [Fäl 96] have estimated the effects. The investigation of these reactions will be continued for example by the GEM experiment at COSY.

- For the four body reaction $dp \rightarrow ppp\pi^-$ a closer investigation in the near threshold region requires an experiment with the ability to handle higher luminosities due to the comparatively small cross sections. To reject background events the identification of the π^- would be an excellent constraint.

- The 'Bremsstrahlung' reaction $dp \rightarrow dp\gamma$ has already been extracted with good statistics, but with a small acceptance in phase space. To learn more about the regions of phase space with small γ energies, a detector with a large acceptance for all outgoing particles is needed.

At present the WASA[1] detector (figure 5.1) is getting into opperation at the CELSIUS storage ring in Uppsala (Sweden) [TSL 98].

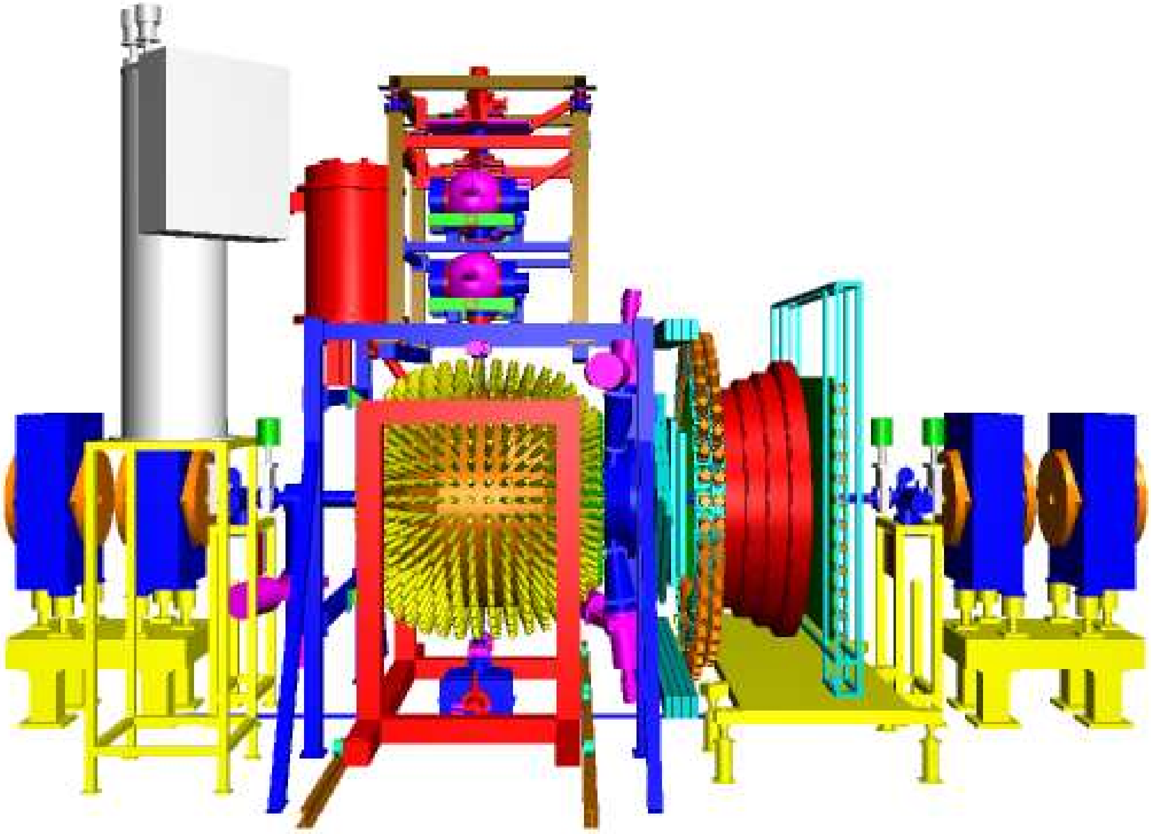

Figure 5.1: *Side view of the WASA detector.*

It is equipped with a pellet target allowing target densities of $10^{15} - 10^{16}$ atoms/cm^2 and corresponding luminosities in the order of 10^{32} cm^{-2}s^{-1}.

The detector will be a continuation of the PROMICE/WASA experiment described in this work, but with a significantly increased acceptence. Its new Central Detector with the ability to detect neutral and charged particles covers 96 percent of 4π; a value, which has to be compared with approximately 7 percent of the old PROMICE/WASA detector setup.

The new setup with its increased acceptance and luminosities should be able to improve the quality of the inelastic *dp*-reaction data sets significantly. For Spring 2000 a first run is forseen [Sco 99] aiming at the examination of $dp \to dp\gamma$, $dp \to dn\pi^+$ and $dp \to ppp\pi^-$.

It is expected, that the new WASA 4π detector with its increased acceptance will improve the quality of the data significantly within a limited amount of beam time.

---

[1] **W**ide **A**ngle **S**hower **A**pparatus

Appendix A

Detector Design Parameters

Scattering angular range	$4^o - 22^o$
(used within this analysis)	
Scattering angle resolution	$< 1^o$ (FWHM)
Hit time resolution	$< 3ns$ (FWHM)
Amount of sensitive material	$\approx 50g/cm^2$
radiation lengths	≈ 1
nuclear interaction lengths	≈ 0.6
Energy resolution for stopped protons	$\approx 3\%$ FWHM
Maximal kinetic energy for stopping	
protons	≈ 300 MeV
deuterons	≈ 400 MeV
π^+	≈ 170 MeV
Particle identification	E/dE technique, delayed pulse technique

Table A.1: *Design parameters of the Forward Detector [Häg 97].*

Name	# of elements	distance from target [cm]	radial extension [cm]	thickness [cm]	Scint. type	PM type
FWC	4 sectors		4 - 32	0.3	NE-102A	XP2102
FHD1	24 spirals		5 - 58	0.5	BC-404	EMI9954B
FHD2	24 spirals		5 - 58	0.5	BC-404	EMI9954B
FHD3	48 sectors		5 - 58	0.5	BC-404	EMI9954B
FRH1	24 sectors		4 - 54	11.0	BC-404	XP2412B
FRH2	24 sectors		4 - 59	11.0	BC-404	XP2412B
FRH3	24 sectors		4 - 65	11.0	BC-404	XP2412B
FRH4	24 sectors		4 - 72	11.0	BC-404	XP2412B
FVH	12 horizontal bars		6 - 82	2.0	BC-408	XP2262B

Table A.2: *Design parameters of the Forward Detector plastic scintillator counters [Dyr 97], [Cal].*

Sensitive area	$94cm \times 94cm$
Inner radius	$6cm$
Number of planes	8
Orientation	$4x$, $4y$
Number of straws per plane	$112(+2 \times 10)$
Straw diameter	$8mm$
Straw walls	$26\mu m$ aluminized mylar
Sense wires	$35\mu m$ stainless steel
high voltage	$\approx$ 2.15 kV
gas mixture	$50\% Ar$, $50\% CO_2$
resolution	$250\mu m$ RMS

Table A.3: *Parameters of the FPC Tracker [Dyr 97].*

Sizes:	
length	30 cm
front face	$\approx 4cm \times 4cm$
back face	$\approx 7.5cm \times 7.5cm$
Crystal wrapping:	70 μm Teflon 20 μm Mylar
longitudinal nonuniformity	$< 15\%$
PM-tube type	FEU-84-3
Resolution obtained for ^{137}Cs (670 keVγ)	$\approx$ 25% (FWHM)

Table A.4: *Parameters of the Central Detector CsI calorimeter elements [Häg 97],[Sch 95].*

Sizes of the 20 horizontal counters (CFLH + CFRH):	
length	33.0 cm
width	1.3 cm
thickness	4.5 mm
Sizes of the 28 vertical counters (CFLV + CFRV):	
length	28.6 cm
width	1.1 cm
thickness	4.5 mm
Scintillator type:	NE102
PM-tube type	RCA S83001EA1 Hamamatsu R 647-1

Table A.5: *Design parameters of the Central Detector plastic scintillator counters [Tur 99],[Cal].*

References

[Ada 92] D. Adams et. al., *Der tiefere Sinn des Labenz*, Rogner & Bernhard,(1992).

[Arv 74] J. Arvieux, *Phase Shift Analysis of Elastic Proton-Deuteron Scattering Cross Sections and* ^{3}*He Excited States*, Nuclear Physics A221 (1974) 253-268.

[Bab 74] I. A. Babalola et. al., *A study of final state deuteron events in 1.825 GeV/c pd interactions*, Nuclear Physics B78 (1974) 561-575.

[Bec 76] F. D. Beccheti *et al.*, *Response of plastic scintillator detectors to heavy ions* Nucl. Instr. Meth. **138**, 93, 1976.

[Bet 97] A. M. Betsch, *Studies of the Charged Single Pion production in Proton-Proton Collision at CELSIUS* Diplomarbeit, Universität Tübingen, 1995.

[Bil 98] R. Bilger et. al., *Proton Proton Bremsstrahlung at 797 MeV/c*, Physics Letters B 429 (1998) 195-200.

[Bir 64] J. B. Birks, *The theory and practise of scintillation counting*, Macmillan, New York, 1964.

[BK 73] E. Byckling and K. Kajantie, *Particle Kinematics*, John Wiley & Sons, London, 1973.

[Bon 95] A. Bondar et. al., *The* $pp \to pp\pi^o$ *reaction near the kinematical threshold*, Physics Letters B 356 (1995) 8-12.

[Bou 88] A. Boudard et. al., *The* T_20 *of the* $\vec{d}p \to^3 He\pi^o$ *reaction at threshold and* π *absorption on a pair of nucleons*, Physics Letters B 214 (1988) 6-9.

[Bou 96] A. Boudard et. al., *Triplet np final state interaction at large momentum transfers*, Physics Letters B 389 (1996) 440-444.

[Bra 68] F.P. Brady et. al., *Neutron-Proton Bremsstrahlung at 208 MeV*, Physical Review Letters Volume 20, Number 14, p.750ff, 1968.

[Bro 95] W. B. U. Brodowski, *Design und Aufbau einer Vetowand für den WASA/PROMICE-Detektor am CELSIUS-Speicherring und erste Messungen der Reaktion* $pp \to pp\pi^+\pi^-$ Diplomarbeit, Universität Tübingen, 1995.

[Bro 99] W. Brodowski, PhD thesis, Universität Tübingen. Not published yet.

[Byk 73] E. Byckling, K. Kajantie, *Particle Kinematics*, John Wiley & Sons, ISBN 0 471 12885 6.

[Cal 92] H. Calen, *Overview of the WASA-PROMICE Offline Programs*, Users guide to the WASA-PROMICE Offline Programs, (internal report TSL, Uppsala, updated continuously).

[Cal] H. Calen et. al., *Alignment Informations for the WASA-PROMICE Offline Programs*, (extracted from the alignment data base).

[Cal 93] H. Calen, M. Waters, *Calibration of the Forward Detector*, PW memo May 1993, (internal report TSL, Uppsala).

[Cam 87] J. M. Cameron et. al., *Differential cross section and analyzing powers for the* $pd \rightarrow^3 He\pi^o$ *reaction in the* Δ*-resonance region*, Nuclear Physics A472 (1987) 718-732.

[Car 78] J. Caroll et al., *A study of the reaction* $pd \rightarrow {}^3\mathrm{He}\pi^0$ *in the resonance region* Nuclear Physics A305 (1978) 502-508

[CERN 93] CERN Program Library Short Writeups (1993) *Catalog of Program packages and entries.*

[CERN 93a] CERN Program Library Long Writeup W5013(1993) *GEANT Detector Description and Simulation Tool.*

[CERN 93b] CERN Program Library Long Writeup I101(1993) *EPIO User's Guide.*

[CERN 93c] CERN Program Library Short Writeup W515(1993) *GENBOD.*

[CERN 93d] CERN Program Library Short Writeup W505(1993) *FOWL.*

[CERN 93e] CERN Program Library Long Writeup Q121(1993) *PAW.*

[CERN 94a] CERN Program Library Long Writeup W506(1994) *MINUIT.*

[CERN 95b] CERN Program Library Long Writeup Y250(1995) *HBOOK Reference Manual.*

[CERN Val] CERN DD-Division OC-group, VALET-PLUS User's Guide.

[Cla 92] J. Clayton et. al., *Proton-deuteron bremsstrahlung at 145 and 195 MeV*, Physical Review C Volume 45, Number 4, p.1810ff, 1992 .

[Coh 96] T. D. Cohen et. al., $pp \rightarrow pp\pi^o$ *reaction near threshold: A chiral power counting approach*, Physical Review C Volume 53, Number 6, p.2661ff, 1996 .

[Cra 70] R. L. Craun and D. L. Smith, *Analysis of response data for several organic scintillators*, Nuclear Instruments and Methods 80 (1970), p.239-244.

[Cre 60] A. V. Crewe et. al., *Charge Independence in the Reactions* $p + d \rightarrow^3 He + \pi^o$ *and* $p + d \rightarrow^3 H + \pi^+$ *at 450 MeV* Physical Review Volume 118, Number 4, p.1091ff, 1960 .

[Dae 95] W.W. Daehnick et. al., *Differential Cross Sections for* $pp \rightarrow pn\pi^+$ *near Threshold* Physical Review Letters Volume 74, Number 15, p.2913ff, 1995.

[Dak 82] Dakhno et. al., *Measurement of the total cross sections for the reaction* $pn \rightarrow pp\pi^-$ *in the dibaryon-resonance energy region (500 - 1000 MeV)* Sov. J. Nucl. Phys. 36(1), July 1982.

[Dro 96] M. Drochner et. al., *Total and Differential Cross Sections of* $pp \rightarrow \pi^+d$ *Reactions Down to 275 keV above Threshold* Physical Review Letters Volume 77, Number 3, p.454ff, 1996.

[Duc 78] Duck et. al., $pd \rightarrow nd\pi^+$ *reaction mechanisms* Physical Review C Volume 18, Number 2, p.887ff, 1978.

[Dun 60] A. F. Dunaitsev, Yu. D. Prokoshkin, *The* $pn \rightarrow pn\pi^o$ *reaction in the energy range from threshold to 665 MeV* Soviet Physics JETP Volume 11, Number 3, p.540ff, 1960.

[Dun 98] Duncan et. al., *Differential Cross Section of the* $pn \rightarrow pp(^1S_0)\pi^-$ *Reaction Extracted from* $pd \rightarrow ppp\pi^-$ Physical Review Letters Volume 80, Number 20, p.4390ff, 1998.

[Dyr 97] J. Dyring, *Detailed Studies of the Reaction* $pp \rightarrow pp\eta$ *using a Straw Chamber Tracking Device* Uppsala Dissertations from the Fac. of Sci. and Techn. **14**.

[Edg 66] J.A.Edgington and B.Rose, *Nuclear Bremsstrahlung from 140 MeV Protons*, Nuclear Physics 89, p.523ff, 1966.

[Eks 97] C. Ekström, *Internal Targets* TSL-Note 97-32, March 1997

[Fes 85] H. Fesefeldt, *The Simulation of Hadronic Showers - Physics and Applications -* CERN Reprint PITHA 85/02.

[Fäl 96] G. Fäldt, C. Wilkin, *Bound state and continuum production in large momentum transfer reactions* Physics Letters B 382 (1996) 209-213.

[Fla 98] Flammang et. al., *Analyzing powers and cross sections of* $pp \rightarrow pn\pi^+$ *near Threshold* Physical Review C Volume 58, Number 2, p.916ff, 1998.

[Fra 80] J. Franz et. al., *Study of the reaction* $n + d \rightarrow ^3 He + \pi^-$ *from 400 to 580 MeV* Physics Letters 93B (1980) 284 ff..

[FW 98] G. Fäldt, C. Wilkin, *Private Communication*

[Glö 96] W. Glöckle et. al. , *The three-nucleon continuum: achievements, challenges and applications* Physics Reports 274 (1996) 107-285.

[Gre98] J. Greiff, *A short description of a least-*χ^2*-fit-procedure using MINUIT* Internal Report 1998 (TSL, Uppsala)

[Goo 60] T. J. Gooding and H. G. Pugh, *The response of plastic scintillators to high enery particles*, Nuclear Instruments and Methods 7 (1960), p.189-192.

[Gus94] L. Gustavson et. al. , *A Data Acquisition System for the Wide Angle Shower Apparatus* IEEE Trans. Nucl. Sci., 41 (1994) 1155

[Häg 97] S. Häggström, *Production of η-mesons in Proton-Neutron Collisions* Uppsala Dissertations from the Fac. of Sci. and Techn. **13**.

[Hal 53] R. W. Hales and B. J. Moyer, *Atomic Number Dependence of Neutral Meson Yield from Proton Bombardment* Physical Review Volume 89, Number 5, p.1047ff, 1953 .

[Han 95] C. Hanhardt et. al., *The reaction* $pp \rightarrow pp\pi^o$ *near threshold* Physics Letters B358 (1995) 21-26.

[Han 98] C. Hanhardt *Pion Produktion in Proton-Proton-Stößen* Bericht des Forschungszentrums Jülich, 3476, 1998

[Har 60] D. Harting et. al., *Experiment on Charge Independence in Interaction of nucleons and pions* Physical Review Volume 119, Number 5, p.1716ff, 1960 .

[Har 97] J.G. Hardie et. al., *Kinematically complete measurement of* $pp \rightarrow pn\pi^+$ *near Threshold* Physical Review C Volume 56, Number 1, p.20ff, 1997.

[Hei 96] P. Heimberg et. al., *Measurement of the* $\vec{p}p \rightarrow d\pi^+$ *Cross Section and Analyzing Power at Threshold* Physical Review Letters Volume 77, Number 6, p.1012ff, 1996.

[Her 95] E. Hernandez and E. Oset, *Off shell* πN *amplitude and the* $pp \rightarrow pp\pi^o$ *reaction near threshold* Physics Letters B350 (1995) 158-162.

[Hog 77] K. R. Hogstrom, *Pion production from the* $pd \rightarrow d\pi N$ *reaction at 585 MeV* , PhD thesis, Rice University, Houston, Texas, 1977.

[Hog 78] K. R. Hogstrom et. al., *Pion production from the* $pd \rightarrow d\pi^+ n$ *reaction at 585 MeV* , Physical Review C Volume 17, Number 1, p.259ff, 1978.

[Hol 92] S. Holm, *Proc. 13th Int. Conf. on Cyclotrons and their Applications,* Vancouver, Canada, July 6-10, 1992, 106.

[Hor 94] C. J. Horowitz et. al., *Role of heavy-meson exchange in pion production near threshold*, Physical Review C Volume 49, Number 3, p.1337ff, 1994.

[Hut 91] D. A. Hutcheon et. al., *Measurements of* $NN \rightarrow d\pi^o$ *very near threshold*, Nucl. Phys. A535,618-636, 1991.

[Joh 99] J. Johansson, PhD thesis, Uppsala University. Not published yet

[Joha 99] T. Johanson, PANIC99 Conference Contribution / private communication.

[Kal 98] N. Kalantar-Nayestanski, *Results of Recent Bremsstrahlung Measurements on Few-Body Systems at KVI*, Reprint from Nucl. Phys. A631,242c-261c, 1998.

[Koc 97] I. Koch, *Luminositätsmessung des Experimentes* $dp \rightarrow dp\pi^o$ *mit Hilfe von Halbleiterdetektoren* Diplomarbeit, Universität Hamburg, 1997.

[Koe 67] P.F. Koehler et. al., *Neutron-Proton Bremsstrahlung at 197 MeV*, Physical Review Letters Volume 18, Number 21, p.933ff, 1967.

[Kol 66] D.S. Koltun and A. Reitan, *Production and Absorption of S-Wave Pions at Low Energy by Two Nucleons*, Physical Review Volume 141, Number 4, p.1413ff, 1966.

[Kup 95] A. Kupsc, *Deuteron nuclear losses in plastic scintillator* PW Memo 1995,(internal report TSL, Uppsala).

[Kur 95] G. R. Kurz, π^+/π^-*-Identifikation in Szintillationszählern* Diplomarbeit, Universität Tübingen, 1995.

[Kuz 93] A. Kuzmin, *The PW CsI hodoscopes calibration* PW Memo 1993,(internal report TSL, Uppsala).

[Kwa 88] M. Kwato et. al., *Nuclear Bremsstrahlung Production in Proton-Nucleus Reactions at 72 MeV*, Physics Letters B Volume 207, Number 3, p.269ff, 1988.

[Lee 93] T. S. Lee and D. O. Riska, *Short Range Exchange Contributions to the Cross Section for* $pp \rightarrow pp\pi^o$ *near Threshold*, Physical Review Letters Volume 70, Number 15, p.2237ff, 1993.

[Leo 87] W. R. Leo, *Techniques for Nuclear and Particle Physics Experiments*, Springer, Berlin, 1987.

[Lo79] J.W. Lo et. al., *Pion production in the reaction* $d(p;d,\pi)n$ *at 800 MeV with a spectator neutron*, Physical Review C Volume 20, Number 4, p.1479ff, 1979.

[Low81] J.W. Low et. al., *Angular distribution of the reaction* $pd \rightarrow^3 He\pi^o$ *at 800 MeV* , Physical Review C Volume 23, Number 4, p.1656ff, 1981.

[Mac 87] R. Machleidt et. al. , Phys. Rep. 149, 66 (1987)

[Mal 91] F. Malek et. al., *Photon spectrum of the neutron-proton bremsstrahlung at 170 MeV*, Physics Letters B Volume 266 (1991) 255-258.

[Mey 90] H. O. Meyer et. al., *Total Cross Section for* $p + p \rightarrow p + p + \pi^o$*near Threshold Measured with the Indiana Cooler*, Physics Review Letters Volume 65 Number 23 (1990) 2846ff..

[Mey 92] H. O. Meyer et. al., *Total cross section for* $p + p \rightarrow p + p\pi^o$ *close to threshold*, Nuclear Physics A539 (1992) 633-661.

[Mey 98] H. O. Meyer, *Nuclear Physics with Light-Ion Storage Rings*, Annu. Rev. Nucl. Part. Sci. 1997. 47:235-71

[Mey 98b] H. O. Meyer, *Meson Production in Nucleon-Nucleon collisions near threshold*, Proc. 8th Int. Conf. on the Structure of Baryons, Bonn, 22-26. Sept. 1998

[Mey 98c] H. O. Meyer et. al., *Dependence of* $\vec{p}\vec{p} \rightarrow pp\pi^o$ *near Threshold on the Spin of the Colliding Nucleons*, Physical Review Letters Volume 81, Number 15, p.3096ff, 1998.

[MN 93] H. O. Meyer and J. A. Niskanen, *Quasifree pion production in the three nucleon system*, Physical Review C Volume 47, Number 6, p.2474ff, 1993.

[Mil 91] G. A. Miller and P. A. Sauer, *Total cross section for* $p + p \rightarrow p + p + \pi^o$ *near threshold*, Physical Review C Volume 44, Number 5, p.R1725ff, 1991.

[Mör 95] A. Mörtsell, *Neutral Pion Production in Proton-Proton Collisions Close to the Kinematical Threshold* Uppsala Dissertations from the Fac. of Sci. and Techn. **6**.

[Nik96] V. N. Nikulin et. al., *The* $\vec{d}p \rightarrow^3 He\pi^o$*reaction near threshold*, Physical Review C Volume 54, Number 4, p.1732ff, 1996.

[Nic 84] G. Nicklas et. al., *Neutron-Proton Radiative Capture at Medium Energies*, Physics Letters Volume 141B, number 3,4 (1984) 170-172.

[Nis 92] J. A. Niskanen, *Energy dependence of the* $pp \rightarrow (pp)_{S-wave}\pi^o$ *total cross section*, Physics Letters B289 (1992)227-232.

[Nis 95] J. A. Niskanen, *Comment on 'Role of heavy meson exchange in near threshold* $NN \rightarrow d\pi$*'*, Physical Review C, Volume 53, Number 1, p.526ff, 1996.

[Oer 67] W. T. H. van Oers and J. D. Seagrave, *The Neutron Deuteron Scattering Length*, Physics Letters B24 (1967) 562-565.

[Occ 47] G. P. S. Occhialini et. al, Nature **159**, 186,694 (1947).

[Par 96] B. Y. Park et. al., *Chiral perturbation approach to* $pp \rightarrow pp\pi^o$ *reaction near threshold*, Physical Review C Volume 53, Number 4, p.1519ff, 1996 .

[PDG 94] Particle Data Group, Phys. Rev. **D50**, 11 (1994).

[Pic 87] M. A. Pickar et. al., *Proton radiative capture by deuterium between 100 and 200 MeV*, Physical Review C Volume 35, Number 1, p.37ff, 1987.

[Pic 92] M. A. Pickar et. al., *Near-threshold proton-induced neutral pion production from deuterium*, Physical Review C Volume 46, Number 2, p.397ff, 1992.

[Pin 89] J.A. Pinston et. al., *Nuclear Bremsstrahlung Production in Proton-Nucleus Reactions at 168 and 200 MeV*, Physics Letters B Volume 218, Number 2, p.128ff, 1989.

[Pin 90] J.A. Pinston et. al., *Proton-deuterium Bremsstrahlung at 200 MeV*, Physics Letters B Volume 249, Number 3,4, p.402ff, 1990.

[Pon 89] C. Ponting et. al., *Analyzing-Power Measurement in* $pn \rightarrow \pi^- pp(^1S_0)$*: Pion Absorption by Quark Clusters*, Physical Review Letters Volume 63, Number 17, p.1792ff, 1989.

[Pro 57] Iu. D. Prokoshkin, A. A. Tiapkin, π^o *Meson Production in pp and pn Collisions in the 390-660 MeV Energy Region* Soviet Physics JETP Volume 5, Number 4, p.618ff, 1957.

[Rei 97] D. Reistad, *Performance and Perspectives on CELSIUS* TSL-Note 97-31, March 1997

[Roh 93] H. Rohdjeß et.al., *Total Cross Section for* $dp \rightarrow dp\pi^o$ *Close to Threshold* Physical Review Letters 70(1993)2864.

[Roh 94] H. Rohdjeß, *Pion Production in pd Reactions Close to Threshold* PhD thesis, Univ. of Hamburg, 1994.

[Roh 98] H. Rohdjeß et. al., *Elastic pd scattering with 200 - 300 MeV protons*, Physical Review C Volume 57, Number 5, p.2111ff, 1998.

[Ros 54] A. H. Rosenfeld, Physical Review 96, 139 (1954).

[Sat 97] T. Sato et. al., *Chiral perturbation theory and the* $pp \rightarrow pp\pi^o$ *reaction near threshold*, Physical Review C Volume 56, Number 3, p.1246ff, 1997 .

[Sch 95] U. Schubert, *The Reaction* $pp \rightarrow pp\eta$ *Close to Threshold* Uppsala Dissertations from the Fac. of Sci. and Techn. **5**.

[Sco 95] W. Scobel, *Production of* π^o *from* $dp \rightarrow dp\pi^o$ *at CELSIUS with deuteron projectiles* Proposal to the TSL.

[Sco 99] W. Scobel, *Investigation of inelastic dp reactions at WASA/CELSIUS with deuteron projectiles* Proposal to the TSL, accepted in April 1999.

[Sed 93] M. Sedlacek et al., *Proc. Workshop on Beam Cooling and Related Topics* Montreux, switzerland Oct. 1993, CERN 04-03, 235.

[Sil 85] B. H. Silverman et al., *Cross section measurements of* $pd \rightarrow {}^3\mathrm{He}\pi^0$ *and* $pd \rightarrow {}^3\mathrm{H}\pi^+$ *at intermediate energies.* Nuclear Physics A444 (1985) 621-636

[Sti 85] T. Stiehler et. al., *A measurement of the total cross section of the reaction* $n + p \rightarrow d + \gamma$ *at* $E_n = 25MeV$, Physics Letters 151B number 3,4, p.185ff, 1985.

[TSL 95] The Svedberg Laboratory, *Progress-Report 1994-1995*

[TSL 98] The Svedberg Laboratory, *Progress-Report 1996-1997*

[Tur 99] A. Turowiecki, *private communication*

[Ver 82] B. J. VerWest, R. A. Arndt, *NN single pion production cross section below 1500 MeV* Physical Review C Volume 25, Number 4, p.25ff, 1982.

[Wat 92] M. Waters, *The light output efficiency of the Jülich trigger hodoscope* PW-memo November 1992, (internal report TSL, Uppsala)

[Wat 93b] M. Waters, *Some considerations about quenching effects* PW-memo September 1993, (internal report TSL, Uppsala)

[Wat 51] K. M. Watson and K. A. Brueckner, *The Analysis of* π *Meson Production in Nucleon-Nucleus Collisions* Physical Review, Volume 83, Number 1, p. 1 ff., 1951

[Wat 52] K. M. Watson, *The Effect of Final State Inross Sections* Physical Review, Volume 88, Number 5, p. 1163-1171, 1952

[Wel 99] A. Wellinghausen, *Private Communication*

[Wil 99] C. Wilkin, *Private Communication*

[Yuk 35] H. Yukawa, Proc. Phys. Math. Soc. Jpn 17, 48 (1935)

[Zab 94] J. Zabierowski, Nucl. Inst. and Meth. A383(1994) 577.

[Zlo 93] J. Zlomanczuk, *Energy Calibration of the WASA-PROMICE Forward Detector* PW Memo 1995, (internal report TSL, Uppsala).

[Zlo 96] J. Zlomanczuk, Private communication

Acknowledgments

I would like to thank Prof. Dr. Wolfgang Scobel for all the support and suggestions, which he gave to me throughout all stages of this work. In particular I am grateful for the freedom I had throughout the data analysis.

I would like to thank all other people who have participated in this experiment. The results in this work would not have been possible without the support of the TSL and all members of the PROMICE/WASA collaboration. In particular I am grateful to Dag Reistad and his crew for preparing and providing a stable beam in CELSIUS; to Curt Ekström and Carl Johan Fridén for an excellent working target system; to Vladimir Dunin for the silicon detectors; to all people who have participated in the experimental runs of the PROMICE/WASA detector and in particular to Wolfram Brodowski, Hans Calén, Göran Fäldt, Kjell Fransson, Stina Häggström, Jan Johanson, Arne Johansson, Tord Johansson, Alfons Khoukaz, Andrzej Kupść, Jens Pätzold, Petter Sundberg, Colin Wilkin and Jozef Złomańczuk for theoretical and practical assistance throughout the data analysis.

I also like to thank Heiko Rohdjeß for his assistance in the preparation of the experiment and his advices afterwards.

In particular I like to thank Inken Koch for her extensive work on the luminosity detectors and her patience.

Wolfgang Gärtner and the members of the mechanical workshop in Hamburg have (as usual) done an excellent job, preparing the vacuum test facility for the silicon detectors. The same can of course be said about the members of the electronics workshop, who have prepared the (pre-)amplifiers used in this experiment.

The work was always accompanied by the members of the EDDA collaboration in Hamburg, who gave me the possibility to participate also in another experiment and who always provided a friendly working atmosphere, shared computer expertise and the necessary supply of coffee, which was well appreciated.

Finally I like to thank all other people in Hamburg and Uppsala, who made the past nearly four years an enjoyable and successful time.

Ich versichere, diese Arbeit selbständig angefertigt und keine anderen als die angegebenen Hilfsmittel verwendet zu haben.

Jan Greiff Hamburg, im August 1999